Life Cycle and Techno-Economic Assessments of Photocatalytic Hydrogen Production

by

Jayranjan Omranjan Maurya

A thesis submitted in partial fulfillment of the requirements for the degree of

Master of Science

in

ENGINEERING MANAGEMENT

Department of Mechanical Engineering

University of Alberta

Abstract

Hydrogen (H_2) can play a critical role in global greenhouse gas (GHG) mitigation. Photoelectrochemical water splitting using solar radiation is a promising H_2 technology. Titanium dioxide (TiO_2)- and carbon nitride (g-C_3N_4)-based photocatalysts are the most widely used photocatalytic materials because of their activity and abundance. Several attempts have been made to improve the photocatalytic performance of these materials in terms of their activity level, life span, response to visible radiation, and stability. However, the environmental impacts of these modifications are often not included in existing studies. This research, therefore, develops a bottom-up cradle-to-grave life cycle assessment (LCA) framework to evaluate the environmental performance by comparing GHGs and energy payback time (EPBT). A framework was also developed to conduct a techno-economic assessment (TEA) to estimate the economic feasibility by calculating the levelized cost of hydrogen (LCOH) of four alternative pathways: TiO_2 nanorods (TNR), fluorine-doped carbon nitride quantum dots embedded with TiO_2 (CNF: TNR/TiO_2), g-C3N4, and a g-C_3N_4/BiOI composite. Unlike most studies that focus only on certain stages, such as laboratory-scale photocatalytic fabrication, this study includes utility-scale cell production, assembly, operation, and end-of-life to give a more precise environmental performance estimate. The results show that g-C_3N_4/BiOI has the lowest GHG footprint (0.43 kg CO_2 eq per kg of H_2) and CNF: TNR/TiO_2 has the lowest energy payback time (0.4 years). In every pathway, energy use in material extraction processes makes up the largest GHG contribution, between 83% and 89%. Photoelectrochemical water splitting is highly feasible for adaptation as a mainstream H_2 production pathway in the future.

The TEA results show that TNR has the lowest cost, 4.9 $/kg of H_2. The H_2 cost ranges from 4.9 to 7.8 $/kg of H_2. In all four pathways, the largest contribution is from capital investment and labour costs; together they make up around 75% of the total cost. Material costs account for 13% to 29% of the overall cost. Photoelectrochemical water splitting has significant feasibility for adaptation as a mainstream H_2 production pathway in the future.

Sensitivity and uncertainty analyses were performed to identify the key input parameters that have significant impacts on the GHG emissions and the LCOH, as well as to obtain a range of results (through Monte Carlo simulation). Sensitivity analysis showed that cell life span, solar insolation, and silver extraction are key inputs impacting the GHG emissions, whereas panel manufacturing cost and solar insolation have a significant impact on the LCOH. The GHG emissions values are $1.4^{+0.4}_{-0.55}$, $0.89^{+0.16}_{-0.24}$, $1.96^{+0.24}_{-0.26}$, and $0.49^{+0.21}_{-0.11}$ kg of CO_2 eq per kg of H_2 produced for TNR, CNF: TNR, g-C_3N_4-S, and BiOI/g-C_3N_4-S, respectively. The LCOH values are $4.9^{+0.75}_{-0.70}$, $5.7^{+0.45}_{-0.65}$, $5.8^{+0.55}_{-1.15}$, and $7.8^{+0.45}_{-0.95}$ $ per kg of H_2 produced for TNR, CNF: TNR, g-C_3N_4-S, and BiOI/g-C_3N_4-S, respectively.

Photoelectrochemical water splitting is still in the initial stage of development and hence materials are still being developed. In addition, the technology is not yet economically feasible at a mass production level. Technological limitations such as uncertainty in the life span of the cell and low solar insolation in some locations limit the applicability of the technology. However, with current research on the development of earth-abundant, stable, and active photocatalyst materials, it is expected that the technology will be adopted in the near future for H_2 production. In summary,

photocatalytic H_2 production has immense potential to be adopted for large-scale commercialization shortly.

Preface

This thesis is an original work by Jayranjan Omranjan Maurya under the supervision of Dr. Amit Kumar. The majority of this work will be submitted for publication in peer-reviewed journals. The details are as follows:

Chapter 2 of this thesis, “Life cycle assessment of earth-abundant photocatalysts for enhanced photocatalytic hydrogen production,” coauthored by Jayranjan Omranjan Maurya, Eskinder Gemechu, and Amit Kumar, will be submitted to a peer-reviewed journal for publication.

Chapter 3 of this thesis, “The techno-economic assessment of alternative materials for hydrogen production via photoelectrochemical water splitting,” by Jayranjan Omranjan Maurya, Eskinder Gemechu, and Amit Kumar, will be submitted to a peer-reviewed journal for publication.

I was responsible for defining the problem, data collection, data analysis, model development, and manuscript composition. Eskinder Gemechu reviewed the research, provided feedback, and corrected the journal papers. Amit Kumar was the supervisory author and provided supervision on problem formulation, results, and manuscript edits.

Acknowledgements

I am grateful for the financial support provided by the NSERC/Cenovus/Alberta Innovates Associate Industrial Research Chair in Energy and Environmental Systems Engineering and the Cenovus Energy Endowed Chair in Environmental Engineering. Many thanks to the Future Energy Systems research effort at the University of Alberta, which made this research possible in part through the Canada First Research Excellence Fund (CFREF).

Dr. Amit Kumar, my supervisor, deserves my heartfelt gratitude for his guidance, mentorship, and support during my research. His guidance, insight, and constant feedback were crucial. I'd also like to express my gratitude to Dr. Eskinder Gemechu for his prompt responses, knowledge sharing, and unwavering support, all of which helped me to complete my research. I want to express my gratitude to Astrid Blodgett for editing my papers.

I highly appreciate the assistance of Dr. Abayomi Olufemi Oni for his timely review and feedback on my journal papers. I am thankful to the members of the Sustainable Energy Research Group for their useful inputs and helpful conversations throughout my research. I'd like to express my gratitude to my friends for accompanying me on this adventure. I am appreciative of the professional development opportunities provided by the University of Alberta Sustainability Scholar programme and Adaptation Resilience Training (ART) programme, as well as the Mechanical Engineering Graduate Students Association.

Finally, I would like to acknowledge my parents for their overwhelming support and for believing in me. I would not be the same person without their love and encouragement.

Table of Contents

List of Tables

List of Figures

List of Abbreviations

ATR	Autothermal reforming
BiOI/g-C_3N_4-S	Pristine bismuth iodide-doped carbon nitride sheets
CCS	Carbon capture and storage
CED	Cumulative energy demand
CNF: TNR	Fluorine-doped carbon nitride quantum dots embedded with TiO2
CO_2	Carbon dioxide
DOE	Department of Energy
EG	Ethylene glycol
EI	Energy intensity
EPBT	Energy payback time
eV	Electron volt
FTO	Fluorine-doped tin oxide
GaAs	Gallium arsenide
g-C_3N4	Carbon nitride
g-C_3N_4/BiOI	Carbon nitride sheet bismuth iodide composite
GHG	Greenhouse gas
H_2	Hydrogen
KOH	Potassium hydroxide
LCA	Life cycle assessment

LCOH	Levelised cost of hydrogen
MW	Megawatt
Na_2SO_4	Sodium sulphate
NGD	Natural gas decomposition
PEC	Photoelectrochemical
PTFE	Teflon polytetrafluoroethylene
PV	Photovoltaic
PVC	Polyvinyl chloride
RUST	Regression, Uncertainty, and Sensitivity Tool
S2F	Solar to fuel
SAG	Semi-autogenous grinding
SMR	Steam methane reforming
TEA	Techno-economic assessment
TiO_2	Titanium dioxide
TNR	Titanium dioxide nanorods

Chapter 1: Introduction

1.1 Background

With the population increasing, global energy demand increases. Specifically, in the last forty years, global energy demand has increased 100 percent [1]. Currently, most energy is produced using fossil fuels including coal, natural gas, and crude oil [2]. There are two important constraints in fossil fuel-based energy production. First, fossil fuels deplete at a higher rate than their rate of deposition [3]. Second, burning fossil fuels generates a significant amount of greenhouse gas (GHG) emissions, which leads to global warming [4]. Hence, there is a need to decarbonize the global economy. The current challenge is in adopting processes for this transition that are technically feasible, environmentally friendly and economically viable [5].

Decarbonization requires large-scale energy transformation [6]. This can be in the form of energy efficiency improvement, carbon capture and storage, renewable energy use, and switching to zero-emission energy carriers such as renewable electricity or hydrogen [7, 8]. Of these, hydrogen can play a key role in mitigating GHG emissions because of its properties such as clean combustion and high energy density [8, 9]. Given these properties, hydrogen demand is expected to increase tenfold between 2015 and 2050 [8, 9].

Hydrogen can be produced from several pathways. The most common is steam methane reforming (SMR), autothermal reforming (ATR) and coal gasification, which make up more than 90% of the current supply [10, 11]. These pathways use fossil fuels as the primary feedstock and hence have high life cycle GHG emissions [9-11]. The life cycle GHG emissions of SMR and ATR could be lowered through carbon capture, use, and storage (CCUS) technologies [12, 13]. Hydrogen from

renewable sources such as solar and wind is of great interest and carries immense potential because of its low life cycle GHG emissions [14].

The major renewable source-based hydrogen production pathways are solar electrolysis, wind electrolysis, and photoelectrochemical water splitting. Solar energy is abundantly available compared to any other source of renewable energy [15]. Photocatalysis is the splitting of water into hydrogen and oxygen under solar insolation. The decomposition of water occurs on a photosensitive material surface known as a photocatalyst [16]. There are two types of photocatalysis: photocatalytic water splitting and photoelectrochemical water splitting. Photocatalytic water splitting is the decomposition of water on a photocatalytic particle surface suspended in water due to an incident ray. It is not a catalytic reaction as water splitting is an endothermic (uphill) reaction. Hydrogen and oxygen are produced simultaneously, as both oxidation and reduction of water occur on the same solid surface of the photocatalyst. Due to this, there is a competition between the recombination of separated charges and the use of these charges to decompose water molecules. As the surface area is low, the recombination rate is very high in photocatalytic water splitting and hence overall yield is quite low. Photoelectrochemical water splitting is the phenomenon of water splitting into two different photoactive electrodes. These should meet the band gap requirements to carry out both halves of the redox reaction for water splitting. The valence bonds of the semiconductor material should be more positive than water oxidation potential and the conduction bands of these semiconductors should be more negative than proton reduction potential. Due to these restrictions, an external bias is applied to assist the separation and migration of photoexcited electrons and holes. This study considers photoelectrochemical water splitting without bias as the system for evaluation. Figure 1.1 shows the pictorial differences in the functionalities of these two pathways.

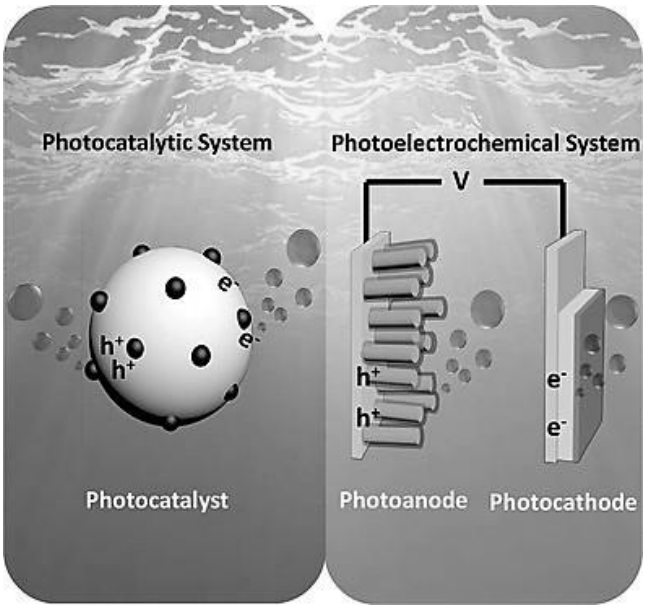

Figure 1.1: Photocatalytic and photoelectrochemical water splitting (adapted from *[16]*)

The performance of photoelectrochemical water splitting technology depends on several factors such as the materials used to produce the photocatalysts, the wavelength of light, and the duration of exposure. Photocatalytic hydrogen technology is currently in the development phase and because of the uncertainty in the performance of various photocatalysts under different conditions including solar insolation, the technology still needs considerable research [17].

Research on photocatalytic water splitting was reported as early as 1972 when Fujishima and Honda used titanium dioxide (TiO_2) semiconductors to dissociate water into hydrogen and oxygen [18]. After that, a range of photocatalysts was designed and tested [19]. Many materials and technological modifications have been tested to optimize hydrogen production and provide a support base for a wide range of applications of the water-splitting pathway. The aim is to increase the photoresponse of the photocatalyst while considering limitations in operations such as charge recombination, low stability, and limited response to only ultraviolet radiations. These setbacks

inhibit the adoption of the technology for the mass-scale production of hydrogen and increased market penetration.

A few studies on photocatalyst design and efficiency improvements have been published [17]. At present, more focus is laid on the development of active, stable, earth-abundant and visible range photo responsive photocatalytic materials [20]. These properties can provide an optimized scenario for the adoption of the technology for mass-scale production of hydrogen in the future [20]. Juan et al. provide perspectives on efficiency improvements including factors that can affect the activity and efficiency of the overall system [21]. Besides occurring abundantly in nature, TiO_2 is the most studied photocatalyst because of its many benefits, such as high photochemical stability, low production cost, and non-toxicity for applications [22, 23]. TiO_2 has a bandgap of 3.2 eV, which limits its applicability under visible light, and a high charge recombination rate, which decreases its activity [22, 24]. This is an applicability challenge for other naturally occurring photocatalysts as well. When coupled with semiconductors of visible light range, the resultant heterojunction now has a lower bandgap than before and is, therefore, able to harvest a broader spectrum of sunlight.

Of the low-energy bandgap semiconductors, graphitic carbon nitride (g-C_3N_4) has recently attracted attention [25]. Being a non-metallic photocatalyst, g-C_3N_4 is a visible light-responsive and low-cost semiconductor with high thermal and chemical stability [26, 27]. g-C_3N_4 has some limitations, such as small active sites for interfacial (photon) reaction and a low surface area, which lead to the moderate oxidation reaction of water to produce protons (H^+) and low charge mobility that disrupts the delocalization of electrons [26]. Coupling g-C_3N_4 with TiO_2 to generate a type II heterojunction could enhance hydrogen production under visible irradiation [28]. As with any new and upcoming technology, it is important to carefully determine the economic, environmental, and social implications of photoelectrochemical water splitting at its initial stage of development [5].

Understanding a technology's environmental and economic performances through LCA and TEA models can immensely help understand the improvement scope of technology while also highlighting its future potential [29]. LCA is an internationally standardized [30, 31] and widely used approach to evaluate the environmental performance of a product system, taking into account its full life cycle from material extraction to the end of life [32, 33]. TEA considers both the technical and economic aspects of technology to evaluate the cost implications of a system and allows comparison with other technologies that perform the same activities [34]. The overarching goal of this thesis is to provide LCA and TEA frameworks that can be used to systematically evaluate the environmental and economic viability of a photoelectrochemical water splitting-based energy system.

1.1.1 Literature review

A detailed literature review of LCA and TEA studies of photoelectrochemical water splitting was carried out as a part of this thesis to identify the key knowledge gaps. The LCA studies conducted in the past examine the multiple environmental impacts associated with photocatalyst use but include only certain life cycle stages [35-40]. For example, Clemens et al. compared two photocatalytic solar-to-fuel concepts for methanol/methane (hydrogen fuel) production with conventional technologies for hydrogen generation [36]. They observed that photocatalytic hydrogen produced resulted in 31% fewer GHG emissions than conventional technologies such as SMR [36]. Sathre et al. developed a hypothetical model for mass-scale hydrogen production through photoelectrochemical water splitting [37]. The model helped me understand the process and requirements to shift from laboratory-scale to mass-scale photocatalytic hydrogen generation. However, the study focused only on the cell fabrication and operation stages. Stages such as

material extraction and panel assembly that can contribute significantly to net energy demand and GHG emissions were not included. Zhai et al. assessed the net primary energy balance of a solar-driven photoelectrochemical cell [35]. With the understanding of high energy demand fabrication step processes, alternative steps could be researched to reduce energy demand and potential GHG emissions. Both Sathre et. al. and Zhai et. al. considered gallium arsenide (GaAs) as a photocatalyst. GaAs have better activity than most photocatalytic materials, but both gallium and arsenic are rare [38], and most photoactive materials are obtained from rare earth elements or compounds [39]. In summary, most LCA studies focus on improving the photocatalyst material, evaluating and comparing the photocatalyst performance, and optimizing the fabrication process so that the overall pathway will result in the least environmental impact.

The sizing or scaling of the technology from the laboratory to pilot project or mass-scale hydrogen production is another knowledge gap. Sathre et al. linearly scaled their model for the mass production of hydrogen [37]. The scaling might not be linear, and Chaudhari et al. found that with an increase in cell production, energy consumption and hence GHG emissions may not follow a linear relationship [41]. Given the few studies on scaling the technology, there are significant gaps in material selection, full life cycle stage accountability, implementation of scaling effect for mass hydrogen production, and reliable methods of estimating GHG emissions. This study, therefore, aims to address these literature gaps by developing a bottom-up LCA framework to evaluate the environmental performance of large-scale photocatalytic hydrogen production using alternative materials.

There are a few TEA studies on photocatalytic hydrogen production [42-46]. Goto et al. designed a prototype for hydrogen production and attempted to reduce the panel production cost by reducing panel thickness [43]. Grube et al. examined photocatalytic hydrogen production pathways along

with other technologies for the year 2025 [44]. They observed that the levelized cost of hydrogen (LCOH) production in all cases was significantly higher than the US Department of Energy (DOE) target for the year 2020. James et al. carried out a detailed TEA of several photoelectrochemical systems for large-scale hydrogen production that considered photocell design and auxiliary equipment and assumed a constant-performing system [46]. However, with time the performance of photocells reduces because of irregularities and degradations in a photocatalyst. Also, different materials can have a range of hydrogen production rates. Hence, it is important to consider the change in photocatalyst materials as they can significantly affect the cost of hydrogen production.

Current TEA studies show that there are many gaps in the technology, giving avenues for improvement. No study considered the effect of improving the change of photocatalytic material on the cost of hydrogen production. With improvements in the performance of the various photocatalytic materials, changes are needed in the fabrication steps. These changes affect the overall cost of hydrogen production for scaled quantities. Existing studies do not consider the fabrication steps for the photocatalytic material. Hence, this study aims to address these literature gaps by developing a complete TEA framework to evaluate the economic feasibility of large-scale photocatalytic hydrogen production using alternate materials.

1.2 Research gaps

The following knowledge gaps were identified:

- The LCAs in the literature do not include all the life cycle stages of the photocatalyst, in particular, the material production and fabrication stages.

- Some of the fundamental materials such as titanium and silver required to make a photocatalyst or photocell are scarce and precious metals and add considerably to the energy and costs of the system. Moreover, they must be recycled and repurposed. There is very little information in the literature in this area.
- There is no well-established method in place to scale up laboratory data to a wide scale. Nor is there data on the scale factors of the cost components that go into the total cost. These criteria help more accurately estimate photocatalytic cell expenses, and a comprehensive study has yet to be completed.
- Since photoelectrochemical water splitting technology is still at a low readiness level (TRL), its performance depends on several factors, and hence a reliable system is needed to measure the uncertainty and sensitivity of the inputs to the output of the system.
- There are very few LCA studies done in Canada on photoelectrochemical water splitting technology, especially on how the available solar insolation would affect its performance.

1.3 Research objectives

The study develops a bottom-up LCA and TEA framework to estimate the environmental and economic performances of photoelectrochemical water splitting, respectively.

The specific objectives are to:

- Scale-up photocatalytic hydrogen production from laboratory data to mass production to evaluate the environmental and economic implications;
- Determine the life cycle GHG emissions per kg of H_2 generated and identify materials and processes with high GHG emissions contributions;

- Determine the cost values of the performance indicators of the technology (the minimum sustainable price [(MSP] [$/W] and the levelized cost of hydrogen [$/Kg of H_2]);
- Develop scale factors to establish the relationship between the production capacity and the overall module costs;
- Perform sensitivity and uncertainty analyses to identify parameters highly sensitive to the output results and also to provide the probable range of values for each environmental and economic indicator.

1.4 Scope and limitations of the thesis

This study employs an LCA approach to evaluate the environmental performance in terms of GHG emissions and energy payback time (EPBT) of four photocatalysts for photoelectrochemical water splitting to produce hydrogen. LCA includes detailing material and energy consumption from the raw material extraction stage to the end of life when degraded components are dismantled and discarded while others are recycled and reused. This thesis provides a TEA for cost estimation based on a production pathway that incorporates inputs from the LCA results.

This study has the following limitations:

- The study is limited to Alberta; the electricity mix, solar insolation levels, and cost figures analyzed are all unique to this Canadian province. However, by making minimal adjustments to the input datasets, the framework can be extended to other jurisdictions.
- Presently a wide range of photocatalysts is available and many are under development. This study considered only four photocatalysts. Including more photocatalysts can provide better results and a larger dataset to compare hydrogen production in future.

- For the environmental assessment, the study is limited to GHG emissions as a key environmental metric. Another impact such as water footprint is not addressed. Assessment of this impact can help understand the overall performance of the pathway better.
- The cost of the photocatalytic system was calculated assuming 5 tonnes of hydrogen per day production throughput. The results were expanded to six additional data points, with a focus on each cost component up to 30 tonnes per day, and cost curves for larger capacities were developed. The scale factors were created with economies of scale in mind. The operations management philosophy is concerned with scale diseconomies after a certain point in production; this was not taken into account in our study. Also, inflation and other economic factors are assumed to be constant; however, they are liable to change. This is a limitation if inflation changes more than expected.

1.5 Organization of the thesis

This thesis is in paper format and is organized to have four chapters. Each chapter is independent and can be read separately. Some information might be repeated in different chapters. This chapter, the introduction, presents the overall background of the thesis. Chapters 2 and 3 will be submitted to journals for publication.

Chapter 2 presents a bottom-up approach to the LCA of earth-abundant photocatalysts for mass-scale production of hydrogen. The chapter also covers the aim and scope of the LCA, inventory analysis particular to the functional unit, and the process for calculating the key energy performance indicators. The second section of the chapter discusses the GHG emissions, net energy ratio, and energy payback time associated with this technology.

Chapter 3 discusses the development of the TEA model of the photocatalyst for the mass-scale production of hydrogen. This chapter presents an economic feasibility assessment through the development of a techno-economic assessment model and the development of economies of scale. The analysis includes an evaluation of the LCOH and MSP. Finally, the chapter gives cost estimates for photoelectrochemical water splitting based on the TEA. The photocatalytic hydrogen production pathway is the same as that in Chapter 2. In addition, scale factors for various cost components' cost curves are developed to anticipate the price of photocatalytic panels, as well as a way to calculate the LCOE.

Chapter 4 presents the key conclusions of this research, from the environmental and economic performance perspectives of photoelectrochemical water splitting. Recommendations for future work are also made.

Chapter 2

Life cycle assessment of earth-abundant photocatalysts for enhanced photocatalytic hydrogen production

2.1 Introduction

Fossil fuel-based energy accounted for 81% of global primary energy in 2018 [47] and was responsible for 60% of CO_2 emissions [48, 49]. To limit the adverse impacts of climate change, the global CO_2 level needs to be reduced to 45% below the 2010 level by 2030 and to "net zero" by 2050 [50]. These targets require large-scale energy transformation [6]. Energy efficiency improvements, carbon capture and storage, and renewable energy use are among the alternative pathways to deep decarbonization of the global energy system [51, 52]. Hydrogen has a key role in achieving net-zero emission targets [6, 52]. Because of its clean combustion and high energy density, the demand for hydrogen as a fuel and an energy career is expected to increase 10 times between 2015 and 2050 [52, 53].

More than 95% of hydrogen is produced with fossil fuel as a feedstock [53], mainly via steam methane reforming (SMR). Underground coal gasification and oil-based hydrogen production pathways are also common [54]. Only 4% of global hydrogen is from renewable sources [55]. Fossil fuel-based hydrogen has relatively high greenhouse gas (GHG) emissions compared with hydrogen from renewable pathways [35, 56], and this has led to the development of novel pathways for hydrogen production such as electrolysis using wind energy and the use of solar energy for water splitting [57]. The latter is the least explored. As solar energy has the most potential among all renewable sources, technologies related to it are likely to be more technologically feasible in future [58].

Photocatalysis is the splitting of water into hydrogen and oxygen under solar irradiation. The decomposition of water occurs on a photosensitive material surface known as the photocatalyst, the performance of which depends on multiple factors such as constituent elements, the wavelength of light, and duration of exposure. Photocatalytic hydrogen technology is currently in the development phase. Many materials and technological modifications have been tested to optimize hydrogen production and provide a support base for a wide range of applications of the water-splitting pathway. Research on photoelectrochemical water splitting was reported as early as 1972 when Fujishima and Honda used titanium dioxide (TiO_2) semiconductors to dissociate water into hydrogen and oxygen [18]. After that, many types of photocatalysts were developed [19]. The current research in photoelectrochemical water splitting revolves around the development of earth-abundant, active, and stable photocatalytic materials that can provide the best-case possibility of mass hydrogen production using solar energy [20]. TiO_2 is the most studied photocatalyst because of its many benefits, such as high photochemical stability, low cost, and non-toxicity [22, 23]. TiO_2 has a bandgap of 3.2 eV , which limits its applicability under visible light, and a high charge recombination rate, which decreases its activity [22, 24]. When coupled with semiconductors of visible light range, TiO_2 could have a narrow bandgap that enhances photocatalytic activity by increasing charge separation. Of the low-energy bandgap semiconductors, graphitic carbon nitride (g-C_3N_4) has attracted attention [25]. g-C_3N_4 is a visible light-responsive and low-cost semiconductor with high thermal and chemical stability [26, 27]. g-C_3N_4 has some limitations, such as small active sites for interfacial (photon) reaction and low surface area, which lead to the moderate oxidation reaction of water to produce protons (H^+) and low charge mobility that disrupts the delocalization of electrons [26]. Coupling g-C_3N_4 with TiO_2

to generate a type II heterojunction by doping with fluorine and phosphorus could allow us to obtain enhanced hydrogen production under visible irradiation [28].

Photoelectrochemical water splitting technology is a recent development, and its environmental performance evaluation has not been done. There are few published studies on photocatalyst development and efficiency improvement. Major limitations exist in the vaguely covered environmental performance of the materials for the photocatalysts. In-depth studies related to renewable hydrogen generation pathways through water splitting include solar thermolysis [59] [60], wind electrolysis [57, 61], and nuclear-based Cu-Cl cycles [62]. These technologies are more mature than photocatalytic hydrogen production. The GHG emissions values range from 0.56 to 4.5 kg CO_2-eq per kg of H_2 in the studies [57, 59-61].

Clemens et al. evaluated and compared the environmental prospects of two photocatalytic solar-to-fuel (S2F) concepts with conventional technologies for power generation and methanol/methane (hydrogen fuel) production [36]. Photocatalytic hydrogen (fuel) production resulted in 31% fewer GHG emissions than steam methane reforming. The study did not consider the performance of photocatalytic materials nor evaluate in detail the overall life cycle emissions. Sathre et al. developed a hypothetical model for mass-scale hydrogen production through photoelectrochemical water splitting [37]. The model helps to understand the requirements to shift to mass-scale photocatalytic hydrogen generation. However, the study focuses on the cell fabrication and operation stages. Stages such as material extraction and panel assembly can contribute significantly to net energy demand and GHG emissions and so should be included in the study's system boundary. Further examination that includes primary energy and related GHG emissions for material extraction could provide a deeper understanding of the technology. Zhai et al. assessed the net primary energy balance of a solar-driven photo-electrochemical cell and

covered in-depth the primary energy requirements for cell fabrication [35]. However, the study does not provide information on material extraction or GHG emissions. Both studies considered gallium arsenide (GaAs) as a photocatalyst. GaAs have better activity than most photocatalytic materials, but both gallium and arsenic are rare [63], and most photoactive materials are obtained from rare earth elements or compounds [39]. Moreover, cerium-based titanium dioxide (TiO_2) produces significantly more hydrogen than raw TiO_2 [39]. For the technology to be adopted on a commercial scale, a large volume of such rare earth elements is needed, and using them will generate more GHG emissions than using the relatively available earth-abundant photocatalytic material because there are more unit operations and energy-intensive processes in the extraction of rare earth elements [40]. The increased GHG emissions and the scarcity of photocatalytic materials will lead to both technological and environmental constraints for large-scale applications. A trade-off of higher hydrogen yield is higher GHG emissions. Current studies do not justify the abundance of photocatalytic material with higher activity. Clemens et al., for instance, did not emphasize the life cycle stages of cell fabrication, assembly, and material extraction in their study [36]. Both Sathre et al. [37] and Zhai et al. [35] included cell fabrication and assembly in their studies, but not material extraction. The existing literature, therefore, has significant gaps in material selection, full life cycle stage accountability, implementation of scaling effect for mass hydrogen production, and reliable methods of estimating GHG emissions. This study aims at addressing these gaps in the literature.

Sathre et al. linearly scaled the model for the mass production of hydrogen [37]. Chaudhari et al. found that with an increase in cell production, energy consumption and hence GHG emissions may not follow a linear relationship [41]. All of these studies evaluate net primary energy requirements and thus do not follow a detailed bottom-up approach. The studies cited above also lack any in-

depth, data-based analysis as most of them use generic values of photocatalyst performance. Hence, the environmental performance assessment cannot be relied upon with certainty for a specific location. Given this uncertainty, studies that can justify the appropriate range of hydrogen production and GHG emissions based on input parameters are needed. There is a scarcity of information on a complete LCA of mass-scaled photocatalytic hydrogen generation-specific. The study location is also important as the technology will be used in a region with solar irradiation availability. Hence, a proper environmental evaluation framework is needed to gauge the performance of hydrogen pathways, especially the materials for photocatalytic hydrogen production.

This study, therefore, aims to address the above-mentioned literature gaps by developing a bottom-up LCA framework to evaluate the environmental performance of large-scale photocatalytic hydrogen production using alternative materials. The specific objectives are to:

- Develop data-intensive spreadsheet-based models to develop data for scaling-up photocatalytic cell fabrication from laboratory data to mass production.
- Assess hydrogen production system performance for four pathways: titanium nanorods (TNRs), TNRs embedded with fluorine-doped carbon nitride quantum dots (CNFQDs) (CNF: TNR), carbon nitride sheets (g-C_3N_4-S), and pristine bismuth iodide-doped carbon nitride sheets (BiOI/g-C_3N_4-S).
- Quantify the material and energy interactions in material extraction, cell fabrication, operations, and end of life.
- Conduct LCA of photocatalysts.
- Identify materials and processes with high energy demand and GHG emissions.
- Identify environmental trade-offs among alternative photocatalyst materials.

- Conduct sensitivity and uncertainty analyses to understand the impact of input parameters on life cycle GHG emissions from different pathways.

2.2 Method

Figure 1 shows the methodological framework used in this study. It includes the goal and scope definition, the system design for cell fabrication based on laboratory information, scaling cell fabrication to mass production, hydrogen production facility setup and operation, inventory analysis, energy and GHG assessment, and result interpretation. Each stage is discussed in this section.

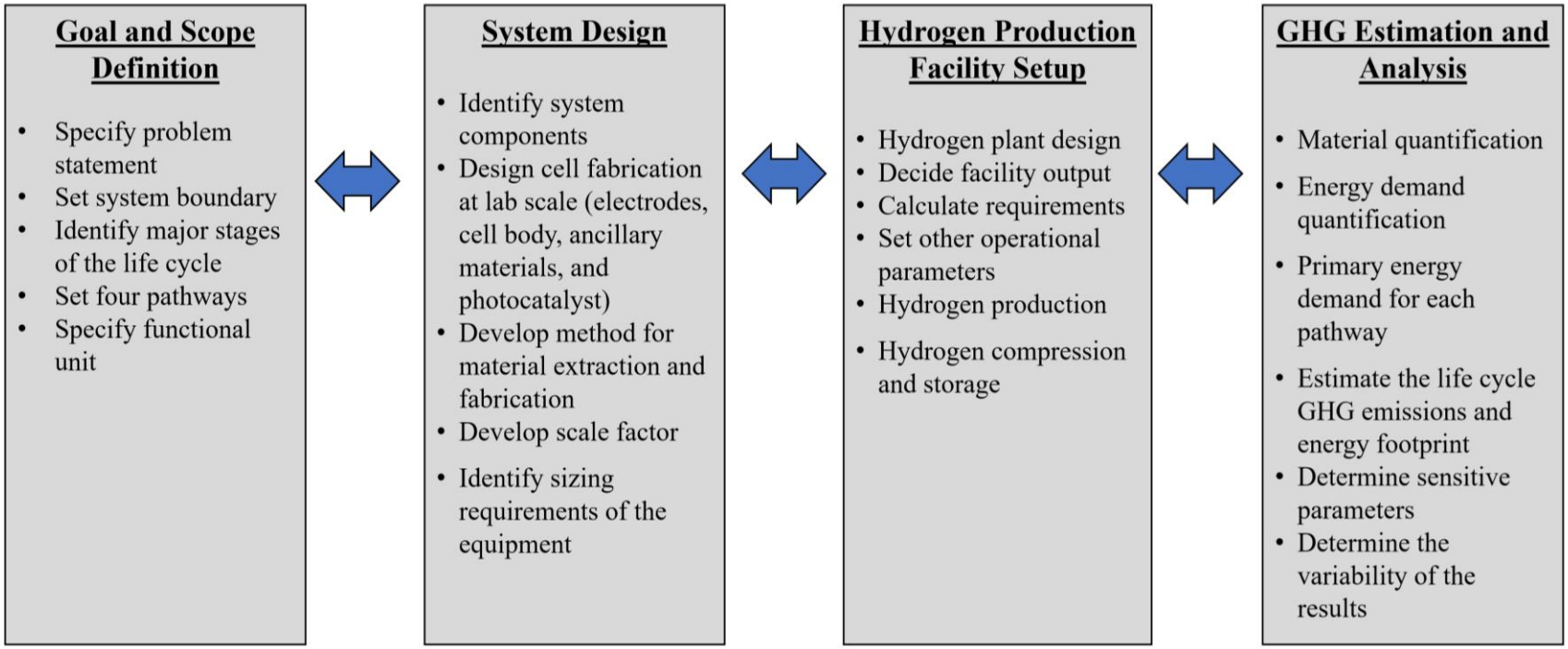

Figure 2.1: Framework of the study

2.2.1 Goal and scope definition

The primary goal of this study is to develop a framework and apply the LCA methodology to evaluate the environmental performance of photoelectrochemical water splitting. The study focuses on hydrogen production system performance through four pathways, each using a unique photocatalyst. The photocatalysts considered are titanium nanorods (TNRs), TNRs embedded with fluorine-doped carbon nitride quantum dots (CNFQDs) (CNF: TNR), carbon nitride sheets (g-C_3N_4-S), and pristine bismuth iodide-doped carbon nitride sheets (BiOI/g-C_3N_4-S). These photocatalysts were chosen because of their abundance, stability in operation, life span, and activity. With these parameters, it will be possible in future to scale up to a commercial-scale hydrogen production facility without technological or economic constraints. Table 1 summarizes the key features of the four photocatalysts considered. The functional unit of the system is 1 kg hydrogen production.

Table 2.1: Summary of the key properties of the four photocatalysts considered in the study

Photocatalysts	Key features	Limitations	Reference
Titanium dioxide nanorods (TNRs)	• Most widely tested photocatalyst • High activity, improved surface area, high solar-to-thermal efficiency (STH)	• High charge recombination • Only ultraviolet response	[64]

Photocatalysts	Key features	Limitations	Reference
Fluorine-doped carbon nitride quantum dots (CNFQDs) and embedded TiO_2 nanorods (CNF: TNR)	• Novel photocatalyst • Modified using carbon nitride to improve its performance	• Limited activity compared to rare metal-based photocatalysts	[64]
Carbon nitride (g-C_3N_4)	• Non-metallic earth-abundant photocatalyst • Composed mostly of chemicals and uses carbon for the formation • High photocatalytic activity	• Small surface area • High charge recombination	[65]
g-C_3N_4-S/BiOI composites (g-C_3N_4-S/BiOI)	• BiOI has a large surface area for redox reaction • Carbon nitride doped with BiOI • Improved active surface area • Lower recombination	• BiOI is rare primarily because of lower bismuth concentration in nature.	[65]

One more alternative for the above photocatalysts would have been P-doped carbon nitride quantum dots. This can be synthesized when phosphorus, P-doping and size quantization is used to produce highly active CNPQDs. CNPQDs have excellent photocatalytic activity and can be

synthesized by a facile and solid-state thermal condensation polymerization reaction method. This study focuses on CNFQDs due to the scarcity of information available in the public domain [28].

Currently, the information on the environmental performance of photoelectrochemical water splitting technology is limited to the intermittent stages [35], hence, complete, environmentally sound pathway development and evaluation are needed. It is important to identify the environmental benefits and trade-offs of photoelectrochemical water splitting to properly compare the technology with other green technologies such as wind electrolysis and solar thermolysis [57,60]. There are trade-offs concerning activity and stability, hydrogen yield, response to wavelength, etc. As this study is expected to provide the environmental performance of an earth-abundant, active, and stable photocatalytic material-based pathway, the results can be used to understand the opportunities and limitations in terms of GHG emissions and energy payback time. Moreover, the results of this research are expected to help researchers in this field understand the technology's critical environmental concerns and develop photocatalytic materials with improved performance. The information might also help policymakers to frame long-term policies favouring commercialization and mass-scale hydrogen production through photoelectrochemical water splitting.

Photoelectrochemical water splitting decomposes water molecules on a photocatalyst using solar energy [66]. Electrons are excited through the absorption of specific solar wavelengths stimulating the redox reaction that splits water molecules into oxygen and hydrogen [66]. For this to occur, a specific potential needs to be reached to fill the energy bandgap between the ground state and the excited state of the electrons [67]. Only certain materials, more specifically, photocatalytic cells, can provide the required response to visible sunlight for water splitting. The main components of a photocatalytic cell are the cathode, anode, electrolyte, cell body, and water as a feedstock [68].

This study considers four photocatalysts to evaluate hydrogen production under similar conditions and ultimately gauge the associated life cycle GHG performance of each pathway.

Figure 2.2 shows the defined system boundary. The main stages included in the analysis are material extraction and production, component fabrication and hydrogen production (operation), and end-of-life. Each stage is discussed in detail below.

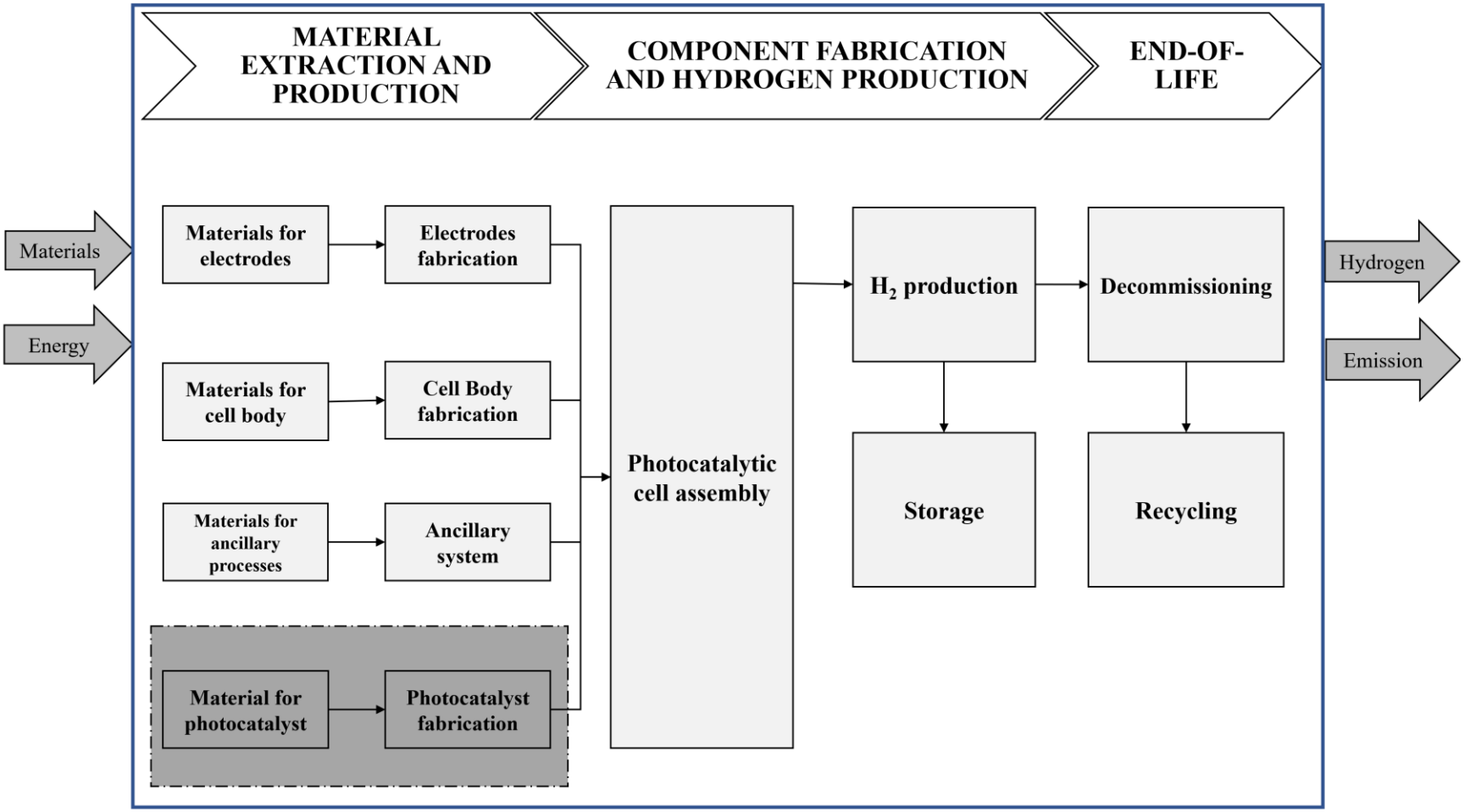

Figure 2.2: System boundary

2.2.1.1 Material Extraction

Material extraction refers to the extraction of basic elements for photocatalytic cells such as material for electrodes, cell body ancillary processes, and photocatalysts. Platinum and silver are the most used photocathodes and counter electrodes, respectively [69, 70]. Platinum is used as a cathode because of its stability, long life span, and activity under a vast range of operating conditions. Platinum is mined, extracted, and refined from ore, and the related primary energy is quantified in this study. Platinum is also used as a powder or for sheets or rods and acts as an electrode in fabrication steps [71, 72]. We used platinum rods in this study. Polyvinyl chloride (PVC) acts as a lightweight, high transmittance material for the proper operation of the photocatalytic cell [35]. Ancillary materials include electrolytes and a separating membrane (Teflon polytetrafluoroethylene [PTFE]). Electrolytes assist in the transfer of electrons between electrodes to carry out redox reactions. The selection of the electrolytes is based on the photoanode (photocatalyst). Potassium hydroxide (KOH) and sodium sulphate (Na_2SO_4) were considered [73]. A perforated membrane is required to separate the cathode and anode of the cell. A PTFE membrane helps in transferring the electrons from the anode to the cathode while separating the other materials [74]. The other key aspect of component preparation is photocatalysis chemical synthesis. All of these materials syntheses are based on the procedure followed by Kabir et al. and Alam et al. [64, 65]. Energy and emissions related to material extraction for the electrodes, ancillaries and cell body are the same for each pathway because we want to compare the performance of photocatalytic materials with similar materials and physical parameters. Differences in performance are controlled by the photocatalyst material. The lab-scale photocatalytic cell setup provides the basic structure for scaling up the system. However, for mass production of hydrogen, larger photocatalytic cells are needed. The scaling of the material amount

requirement is linear with the increase in size from 10 x 10 x 7.5 x 0.2 cm (where 0.2 cm is the thickness of the hollow cuboidal cell) to 1 x 1 x 0.02 m [37]. The material requirement for extraction is then estimated for every case based on the activity of one photocatalytic cell and cell size increase. This amount is then multiplied by the number of cells required to produce 5 tonnes of hydrogen per day. This number of cells differs for each case as the activity of every photocatalyst is different and hence hydrogen production by each cell in every case will differ. For example, TNRs will need around 130,000 cells to produce 5 tonnes of H_2 per day, but CNF: TNR will need only 36,000 cells. The number of cells is obtained by dividing the 5 tonnes by the amount of hydrogen produced by one photocatalytic cell per day. The amount of hydrogen produced for each photocatalyst is different and is shown in section A9 of the appendix. This difference in the number of cells required impacts the material requirements and is controlled by the performance of the photocatalyst in every case, as explained earlier. Hence, it is important to analyze the synthesis of photocatalyst material for every case. This analysis is described in the next section.

2.2.1.2 Photocatalyst synthesis

We derived the synthesis of photocatalysts from Kabir et al. [64] for TNRs and CNF: TNR and from Alam et al. [65] for carbon nitride sheets (g-C_3N_4-S) and BiOI/g-C_3N_4-S. TNRs and their derivatives are among the most widely used photocatalyst materials because of their abundance, high activity, and stability under normal conditions [75]. However, TNRs respond most to ultraviolet radiation and hence improvements are needed to increase the response to other wavelengths. TNRs were developed to improve the surface area of the photocatalyst, which further enhances photocatalytic activity [76]. The growth of TNRs of various lengths and sizes was studied by Wang et al. [77], who grew them on a fluorine-doped tin oxide (FTO)-coated glass slide,

titanium (iv)-n butoxide, acetone, methanol, and de-ionized water by the process of sonication [77]. The TNRs were then deposited on an FTO by spin-casting using HCl and diluted titanium (IV) isopropoxide followed by calcination. Finally, an array of TNRs was grown hydrothermally using hydrochloric acid and glacial acetic acid in an autoclave [78-80].

CNF: TNR is a modified version of TNRs in which carbon nitride quantum dots are embedded on TNRs. The resulting heterojunction improves the activity of the photocatalyst by reducing charge recombination [81]. Also, the addition of carbon nitride quantum dots allows visible range response of the photocatalyst [81]. The first step in growing titanium nanorods on FTO glass substrate is the same for TNRs and CNF: TNR. After the preparation of TNRs, following the method described above, fluorine-doped carbon nitride quantum dots (CNFQDs) were produced using the methods developed by Lu et al. and Wang et al. [27, 82]. It is necessary to produce CNFQDs and TNRs before embedding them to make CNF: TNR. The CNFQDs were synthesized by the solid-phase thermal reaction of urea, citric acid, and ammonium fluoride using a centrifuge and then entrapping the obtained CNFQD in TNRs by hydrothermal growth over FTO glass, as for TNRs [64]. The flowchart of synthesis of TNR and CNF: TNR photocatalysts are shown in A1.

Carbon nitride sheets (g-C_3N_4-S) are non-metallic photocatalysts synthesized for visible range response. They have high photocatalytic activity and are formed with carbon [83]. However, they have a small surface area on their own and a high charge recombination rate that limits their activities. Hence, they are often doped with other compounds to overcome these limitations [84]. Carbon nitride sheets were among the photocatalysts studied by Alam et al. [65]. In this study, carbon nitride sheets (g-C_3N_4-S) and pristine g-C_3N_4/BiOI were considered. Dicyandiamide is the main precursor. (With NH_4Cl and dicyandiamide in an alumina crucible and a lid, dicyandiamide

was thermally polycondensed by the authors to yield bulk g-C_3N_4. The water in the mixture was evaporated after the crucible was heated in a tube furnace with planned heating (where the rate of heating and cooling are pre-defined) to suspend the g-C_3N_4-S.) [65].

Pristine bismuth iodide-doped carbon nitride sheets (BiOI/g-C_3N_4-S) are a modified version of carbon nitride sheets. A BiOI has a large surface area and hence the rate of redox reaction taking place on its surface improves [77]. A BiOI also helps reduce recombination [77]. However, the lesser availability of bismuth in the compound can lead to higher extraction emissions, energy, and costs. As precursors, g-C_3N_4-S and Bi $(NO)_3.5H_2O$ are combined and then dissolved in ethylene glycol (EG) and ultrasonically homogenized to achieve a homogenous solution. Separately, a stoichiometric amount of KI was dissolved in ethanol and ultrasonically processed until the solution was clear [65]. Under vigorous stirring, the KI solution was added dropwise to the solution containing Bi $(NO)_3.5H_2O$ and g-C_3N_4-S. The blended solution was then heated for 17 hours in a Teflon-lined stainless-steel autoclave to obtain the photocatalyst. The flowchart showing the synthesis of g-C3N4-S and g-C3N4/BiOI photocatalysts is in A2 of the appendix.

2.2.1.3 Photocatalytic cell assembly

After the raw materials are extracted and produced, the components are assembled to make photocatalytic cells, which are used to build panels. The panel structure's basic frame and support are composed of steel, and the top is covered with PVC for alignment. The design and material data of the panel were taken from Sathre et al. [37]. The cell size is assumed to be 1 m x 1 m x 2.2 cm. A panel is composed of 14 cells. The number of panels is determined based on the productivity and amount of hydrogen required.

A lab-scale photocatalytic cell setup provides the basic structure used to scale up the system. However, for mass production of hydrogen, larger photocatalytic cells are needed. According to

Sathre et al., the scaling of the material amount required is linear with the increase in size from 10 x 10 x 7.5 x 0.2 cm (where 0.2 cm is the thickness of the hollow cuboidal cell) to 1 x 1 x 0.02 m [37]. The material required for extraction is estimated for every case based on the activity of one photocatalytic cell and the cell size increase. For scaling up, it is important to know the size of the equipment available to perform the same task on a large scale [85]. For every laboratory process, a range of equipment was chosen with a broad capacity range. The equipment for each unit operation and its available capacity in the current market is shown in section B5 of the appendix, with other details such as energy consumption, land footprint, and vendor. A curve was plotted between equipment capacity and power consumption. The list of equipment shows that most equipment functions best in the range of 500-1500 cells per day. In this study, a capacity of 5000 cells per day is assumed. For every pathway, the photocatalytic cell fabrication process had the highest residence time and lowest capacity among all processes. So, cell fabrication was identified as critical, and this process largely determines the production capacity. For example, in the case of TNR cell fabrication, the annealing process is the longest (4 hours) in the cycle, hence fabrication capacity is determined based on the optimized output from this process. The critical path is determined for all the cases to understand the optimization required for scaling up to maximum capacity. In the supplementary sheet, section A3 of the appendix shows the process design and fabrication layout for all four considered cases.

2.2.1.4 Operations and hydrogen production

The operations stage here refers to the production of hydrogen in the field in an array of panels erected in the direction of solar irradiation. Every panel has a set of 14 photocatalytic cells and every panel is connected through pipes for the transfer of water and a mixture of hydrogen and oxygen, using water pumps, vacuum pumps, and compressors. The arrangement of panels and

design of the facility is adapted from the study conducted by Sathre et al. [37]. Water pumps are used to maintain the supply of water to the panels, and vacuum pumps are needed to transfer the collected mixture of hydrogen and oxygen to the compressor, after which it is compressed and later hydrogen is stored in storage tanks [37]. The input supply of water for photocatalysis was municipal water taken from a municipality, treated, and deionized at the site before supplying it to the field operating system. In this study, we have used a municipality in Alberta, a western Canadian province. Water is continuously circulated through the system and refilled as it decomposes into hydrogen and oxygen. Hydrogen production through photoelectrochemical water splitting from the facility is 5 tonnes of hydrogen per day. This capacity is based on the size of the panel-producing facility and present-day equipment, which are most effective at this capacity of hydrogen production. For this, all the related equipment was scaled as discussed in the previous section. Overall production capacity is expected to decrease 5% every year [37]. Hydrogen will be produced as described in section 2.1. Then, for each pathway, a facility will be set up to operate the photocatalytic cell panels to produce hydrogen as output.

2.2.1.5 End of life

After a cell comes to the end of its life, it is decommissioned. The components are either recycled or landfilled. The recycled component GHG emissions are deducted from total GHG emissions as these components will reduce the demand for virgin material in the subsequent cycle. Following the National Energy Technology Laboratory's method of assessing the life cycle of an energy system, we assumed that decommissioning requires 10% of the energy used for the initial construction of the photocatalytic cells [86].

2.2.2 Inventory analysis

The inventory analysis considers materials and energy inputs for each unit operation in the system boundary. In general, photocatalytic cells are quite stable and can function from 5 to 15 years [35]. Here, the life span of the cell was assumed to be 5 years. Thus, the facility will need two-panel replacements over the considered life span. The arrangements of photocatalytic cell components such as photocathode (photocatalyst), photoanode, and electrolyte are described in the literature [35]. The materials data for these components were adapted from Kabir et al., Alam et al. and Thakur et al. respectively [64, 65, 80]. The cumulative energy demand (CED) for the individual photocatalyst was calculated to understand the energy required to produce photocatalytic cell components. Energy intensities (EI) were obtained from Wernet et al. and GREET [87, 88].

2.2.2.1 Inventory for material extraction

The main framework for photocatalytic cell design was derived from Zhai et al. [35] and includes material for the photocathode, photoanode, electrolyte, and cell body fabrication. The electrodes used are platinum and silver. The size of the electrodes is based on the size of the cell (10 x 10 x 7.5 x 0.2 cm, where 0.2 cm is the thickness of the hollow cuboidal cell). Here, small electrodes were used and these were obtained commercially [89]. These electrodes are 0.5 mm in diameter and 32 mm in length [89]. These dimensions, along with the volume of the electrode, multiplied by the density, give the mass of electrodes required. For the cell body, a 10 x 5 x 5 cm hollow cube with a thickness of 0.5 mm is assumed. This cell is made of PVC, which provides structure to the cell and support to other components. A small amount of PVC is required to cover the electrodes. As electrodes are around 10% of the cell volume, PVC for coating is assumed to be PVC for the cell body. This value gives the overall volume of PVC required per cell, which, when multiplied by the density, gives mass requirements. For ancillary materials, a small amount (5 g) of PTFE

(Teflon polytetrafluoroethylene) membrane is required for semi-permeable separation. The water volume is the same as the cell volume. For electrolytes, the volumes were adapted from the photocatalyst synthesis as discussed in the next paragraph. These masses were then multiplied with the energy intensities of each material to give primary energy demand per cell unit.

Photocatalysts were prepared according to the fabrication steps described in the previous section. Electrolytes were used according to the capacity of the cell and specifications from Kabir et al. and Alam et al. [64, 65]. The extraction stage is similar for each pathway, and the materials for inventory and required energy demand are listed in Table 2. The table shows the raw material and energy required to produce one unit of a photocatalytic cell for all four pathways.

Table 2.2: Material extraction inventory

Process	***Material***	***Amount (Gram/Unit Cell)***	***Energy Unit (MJ/Gram)***	***Comments/Source***
Material for electrodes [89]	Pt	0.13	1.03	Used commercially available electrode from CH Instruments [89]
	Ag	0.08	10.69	Used commercially available electrode from CH Instruments [89]
Material for cell body [35]	PVC body	0.51	0.06	Cell size: 10 x 10 x 0.2 cm Multiply with density to get mass

Process	***Material***	***Amount (Gram/Unit Cell)***	***Energy Unit (MJ/Gram)***	***Comments/Source***
	PVC coat	0.05	0.06	Used for coating electrodes; assumed 10% of PVC for body
Ancillary materials [64, 65]	PTFE	5	0.11	Assumed based on cell size
	Water	100	0.00001	Assumed based on cell size
	KOH	60.5	0.03	Adapted from Kabir et al. [64]
	Na_2SO_4	50	0.001	
Photocatalyst material [64, 65]	$Ti(C_4H_9O)_4$	0.85	0.07	
	CH_3COOH	2.62	0.03	
	FTO	11.14	0.02	Adapted from Zhai et al., Kabir et al., and Alam et. al [35, 64, 65]
	CH_4N_2O	3.6	0.03	Adapted from Kabir et al. [64]
	NH_4F	0.3	0.03	
	$C_6H_8O_7$	1.94	0.04	
	$C_2H_4N_4$	2	0.06	Adapted from Alam et al. [65]
	NH4Cl	10	0.04	
	$Bi(NO_3)_3$	0.35	0.09	
	$C_2H_6O_2$	22.26	0.04	

Process	*Material*	*Amount (Gram/Unit Cell)*	*Energy Unit (MJ/Gram)*	*Comments/Source*
	KI	10	0.08	

Every photocatalyst has a different activity for the same intensity (average wavelength) of solar insolation. Hence, to produce 5 tonnes of hydrogen, the number of photocatalytic cell panels required will be different. For example, TNRs have an output density of 0.3 mA/cm^2 [64]. This means that for a heterojunction of 75% of 1 m x 1 m of the photocatalytic cell, 42.8g of H_2 is produced [37, 64]. For 5 tonnes of hydrogen, therefore, around 130,000 cells are needed. For this scaling of cells from lab to field, every case will need many materials for the electrodes, cell bodies, ancillary processes, and photocatalysts. As explained previously, the amount of material will differ from case to case. For example, for TNRs, 7 tonnes of platinum is required, whereas for CNF: TNR, 1.94 tonnes of platinum is needed to produce 5 tonnes of H_2. This difference in material requirement will result in different net energy demands and GHG emissions. For each case, the material and energy demand inventory for extraction and component production of photocatalytic cells is shown in section A4 of the appendix.

2.2.2.2 Inventory for component fabrication and photocatalytic cell assembly

The material and energy inventory for the fabrication stage of photocatalysts mainly includes the panel fabrication and assembly processes and major equipment at the facility. Because these processes are scaled up for 5 tonnes of hydrogen production, for each process the equipment is scaled to satisfy the production requirement of 5000 cells per day from the facility. The processing capacity is determined by the working volume of the equipment, which is divided by the volume

of one cell to obtain the number of cells that can be processed at once, or in one cycle. The energy required to operate the equipment is then quantified for one cycle. The equipment should be of a sufficiently high capacity to process 1000 cells combined in one or more cycles per day. Hence, a list of different equipment sizes was compiled and equipment was chosen based on the number of cells that need to be processed. This framework can be extended for other ranges, such as 5000 cells per day up to 20000 cells per day. For simplicity, this study considers the equipment needed to produce 5000 cells in every case and calculates the energy demand for every process. After the cell components are produced and assembled, they are aligned to produce panels. Each panel requires 340 kg of steel and 207 kg of PVC cover on top of every panel [37]. This corresponds to 12592.6 MJ energy demand per panel. This value is derived from the 2019 GREET model's energy intensity set for parameters related to Alberta grid electricity and natural gas use in the extraction and production of steel and PVC [90, 91]. The energy demand is multiplied by the number of panels required in each case. The panel assembly process is manual and hence no energy or GHG emissions are noted. The sections A6, A7 and A8 of the appendix provide detailed information on the material for cell production, fabrication process inventory, and panel assembly, respectively.

2.2.2.3 Inventory for operation and hydrogen production

In the photocatalytic cell, an electrochemical reaction takes place, which is a redox reaction. In oxidation, half the water oxidizes to oxygen, whereas in reduction, half the water reduces to hydrogen. These reactions result in the flow of electrons, which causes a current. It is difficult to measure the exact amount of hydrogen produced and separate it from the mixture of hydrogen and oxygen produced simultaneously. Hence, the produced current is measured for some time and is converted to the mass of hydrogen produced. For the pathways studied here, the intensity of the current has already been measured on a laboratory scale [64, 65]. This study uses these results and

adjusts them in the conditions for Alberta for all considered pathways. For the laboratory setup, the input light energy is through a solar simulator (AM 1.5G). Alberta's average annual insolation is 4500 MJ/m^2 or 150 W/m^2 [92]. Its average insolation intensity is, therefore, 212 times that of a solar simulator. We assumed that only 30% of solar irradiation can be harnessed by photocatalytic cells and hence, after multiplying (30% by 212), we get the multiplier of 63.5. This multiplier is used to gauge the production of hydrogen from large cells for mass production. The results are in line with the results obtained in similar studies [93, 94]. A small deviation in the results is due to differences in process energy considerations, electricity mix, and physical parameters such as solar insolation. The detailed calculation for hydrogen production is shown in section A8 of the appendix.

After assembly and setup, the facility is assumed to operate for 15 years (the life span of the facility [37]). The operation stage also includes supplies such as water pumps, vacuum pumps, and compressors, the number of which is based on the capacity or horsepower of the equipment. Table 3 shows the equipment, compressors, vacuum pumps, and de-ionization plant units needed for the workload considered. The energy requirement (electricity) to operate each piece of equipment was estimated. The number of each piece of equipment was estimated based on the capacity and number of panels required. We assumed one water pump can supply water to 2000 panels, based on the water contained in the panels and the amount of water that needs to be replenished after water splitting every hour, and the number of water pumps was calculated by dividing the number of panels by 2000. The number of water pumps is equal to the number of vacuum pumps as both handle the same mass of materials. Compressors have a smaller load as their work is to compress the hydrogen and not move the gases through the field. Hence, the number of compressors is assumed to be half of the number of vacuum pumps. The main feedstock is de-ionized water. After

initial filling, 5 tonnes of hydrogen are produced every day, which means around 45 tonnes of water is decomposed every day, which should be replenished in the system. Two tonnes of water per hour are filtered from a municipal supply and de-ionized in the de-ionization unit every 24 hours. A capacity of 2 tonnes per hour was selected based on the requirement to treat 45 tonnes of water effectively. The supply system consists of two parallel lines connecting the facility: the hydrogen and oxygen line, and the water lines. Water is continuously circulated in the system and refilled as it decomposes into hydrogen and oxygen. The produced hydrogen and oxygen mixture is collected, and hydrogen is separated and stored for upstream applications. The continuous operation of the equipment uses primary energy in the form of electricity. This demand is divided by the total hydrogen production to obtain energy demand for the operations stage for every case.

Table 2.3: Equipment inventory for operations

Equipment	**Capacity (in HP)**	**TNR**	**CNF: TNR**	**g-C_3N_4-S**	**g-C_3N_4 /BiOI**	**Comments & References**
Pump	50	5	2	4	2	For water supply to panels. Power rating and capacity are derived from Stewart [95]
Vacuum pump	35	5	2	4	2	For movement of oxygen and hydrogen from panels. Power rating and capacity are derived from Stewart [95]

Equipment	Capacity (in HP)	TNR	CNF: TNR	g-C_3N_4-S	g-C_3N_4 /BiOI	Comments & References
Compressor	30	3	3	3	2	For compression of collected H_2. Power rating and capacity are derived from Acklands Grainger [96]
De-ionization unit	5	1	1	1	1	Capacity: 2 tonnes per hour. Equipment specification from Alibaba.com [97].
Energy demand (in MJ/Kg of H_2) For 15 years of operation	-	1.1	0.6	0.9	0.5	All equipment has a life span of 15 years Purchasing.com [98].

2.2.3 Energy and environmental impact estimate

The inventory data of each pathway was translated by the authors into GHG emissions and energy payback time (EPBT). This estimate shows that the approach used is focused on both energy and environmental matrices.

The energy payback time (EPBT) measures the time in years the system or process requires to recover the energy used to produce an item, in this case, the photocatalytic cell [99]. Equation 1 shows the EPBT for the photocatalytic system's assumed output energy in the form of hydrogen

fuel. The materials used in the module preparation and local solar insolation are the key factors that affect the EPBT of the system.

$$EPBT = \frac{\mathrm{E}_{tot}}{E_{out}} \quad (1)$$

E_{tot} refers to the total embedded energy consumed in the entire life cycle of the photocatalytic cell system from raw material extraction to final disposal, recycling, or reuse. E_{out} is the annual energy production capacity of the system, found by converting the mass of hydrogen produced to energy.

The life cycle GHG emissions are calculated by summing all the emissions associated with each raw material and energy used to produce the photocatalytic cell. For the system, each component's GHG emissions are estimated separately. For example, we use platinum as one of the electrodes. Extraction, fabrication, and production of all the components are assumed to be carried out in Alberta, Canada, except for the extraction of platinum, which is assumed to be from South Africa because of the abundance of platinum ore in that region [100]. For all the remaining processes, electrical energy is assumed to be from the Alberta grid and the associated emissions are quantified accordingly [101]. Process energy for every material (such as Pt, Ag, KOH, etc.) is broken down into respective input fuels and each fuel amount is multiplied by emission factors to get the associated GHG emissions. The solar-to-thermal conversion efficiency is assumed to be 25% (i.e., only 25% of the light falling on the heterojunction area is used to carry out the reaction) [35]. Also, we assumed a 5% annual depreciation in the performance of the photocatalytic cell based on constant physical parameters [37]. The photocatalysts are assumed to be stable for 5 years and replaced after that [64, 65]. We used a GHG emissions factor of 0.55 kg CO_2 eq/kWh for the year 2020 [101]. This factor is expected to change in time with changes in the electricity mix. Other primary energy sources used are natural gas, diesel, coal, and petroleum. The emissions factors for

natural gas, diesel, and coal are 68, 95, and 100 g CO_2 eq per MJ, respectively [102, 103]. For petroleum, the value is assumed to be 3146 g CO_2 eq per litre [102, 103].

2.2.4 Sensitivity and uncertainty analyses

Sensitivity analysis is used to identify the key input parameters to which the output of the system is sensitive. For such input parameters, small changes or errors can result in significant deviations in the output. In this study, the Morris statistical method was used to perform sensitivity analysis on the model. Because the number of inputs is high, this method is more suitable than other available methods [104]. Complexity is higher in studies with a high number of inputs, and this is because a deeper analysis is required to identify the impact of many parameters on the output. The results give the most sensitive parameters. Uncertainty analysis is done with these sensitive parameters. Uncertainty of insignificant parameters has negligible value and shows negligible deviation from the actual results, hence only a few parameters (the most sensitive) are considered. For uncertainty analysis, we used the Monte Carlo simulations because of their ability to analyze multiple inputs and are among the most reliable methodologies for uncertainty analysis [104].

For this study, the GHG emissions and amount of hydrogen produced from a single photocatalytic cell are the outputs of interest. Some key inputs that govern these outputs are the materials for the photocatalyst, ancillary materials, materials for the electrodes, materials for the cell body, and the fabrication process. Solar insolation, the life span of the cell, and degradation percentage also affect the overall results.

There are three main reasons to conduct sensitivity and uncertainty analyses. First, many values were adopted from published sources and vary significantly. Second, during a particular phase, such as the calculation of energy and material requirement for material extraction or fabrication of

the photocatalytic cell, an undetected error may be introduced. Third, the input values adopted can be from a range of time frames and while they are correct for those instances, other time frames are used in this study. Currently, the life span of a photocatalytic cell is uncertain. In this study, the range of 5-15 years was considered based on values reported in the literature [37]. The solar insolation region is assumed to be Alberta. The range of 3400-5000 MJ/m^2/year was taken from the Agricultural Land Resource Atlas of Alberta [92]. For the other parameters, values were evaluated and developed for each pathway. To determine the impact of errors, the uncertainty range considered in this study is ±20% for each parameter [105]. We assumed a uniform distribution of data in carrying out the analysis. The sensitivity and uncertainty analysis uses the Regression, Uncertainty, and Sensitivity Tool (RUST) developed by Di Lullo et al. [106].

2.3 Results and discussion

2.3.1 GHG Emissions

Figure 3 shows the life cycle GHG emissions for all four cases. CNF: TNR and BiOI/g-C_3N_4-S show the lowest GHG emissions, 0.91 and 0.43 kg of CO_2 eq per kg of H_2 produced, respectively. The low GHG emissions values are due to their high response to solar radiation, which results in higher hydrogen yields. The activity of the system is the measure of the number of electrons the photocatalyst material generates to carry out the redox reaction of the water splitting. A higher activity level means a higher rate of reaction, hence increased hydrogen production. Activity is measured in terms of current density, that is, the number of electrons released by the photocatalyst per second. The current densities are adapted from Alam et al. and Kabir et al. [64, 65]. The current density or activity of the CNF: TNR was three times higher than that of the CNF. Adding CNFQDs to the TNR increases the activity, but it also increases the material and energy required to produce CNFQDs and the associated GHG emissions. However, the hydrogen yield outweighs the GHG

emissions. The GHG emissions from the additional material requirements increase by only 10%. Similarly, the addition of BiOI increases the g-C_3N_4-S yield in the BiOI/g-C3N4-S case more than the GHG emissions that were added because of the production of BiOI. Hence, for higher activity among materials, life cycle GHG emissions are reduced. TNR and g-C_3N_4-S result in higher life cycle GHG emissions, 1.49 and 2.08 kg of CO_2 eq per kg of H_2 produced, respectively. The material extraction stage contributes significantly to GHGs in all cases, from 83% (TNR) to 89% (g-C_3N_4-S).

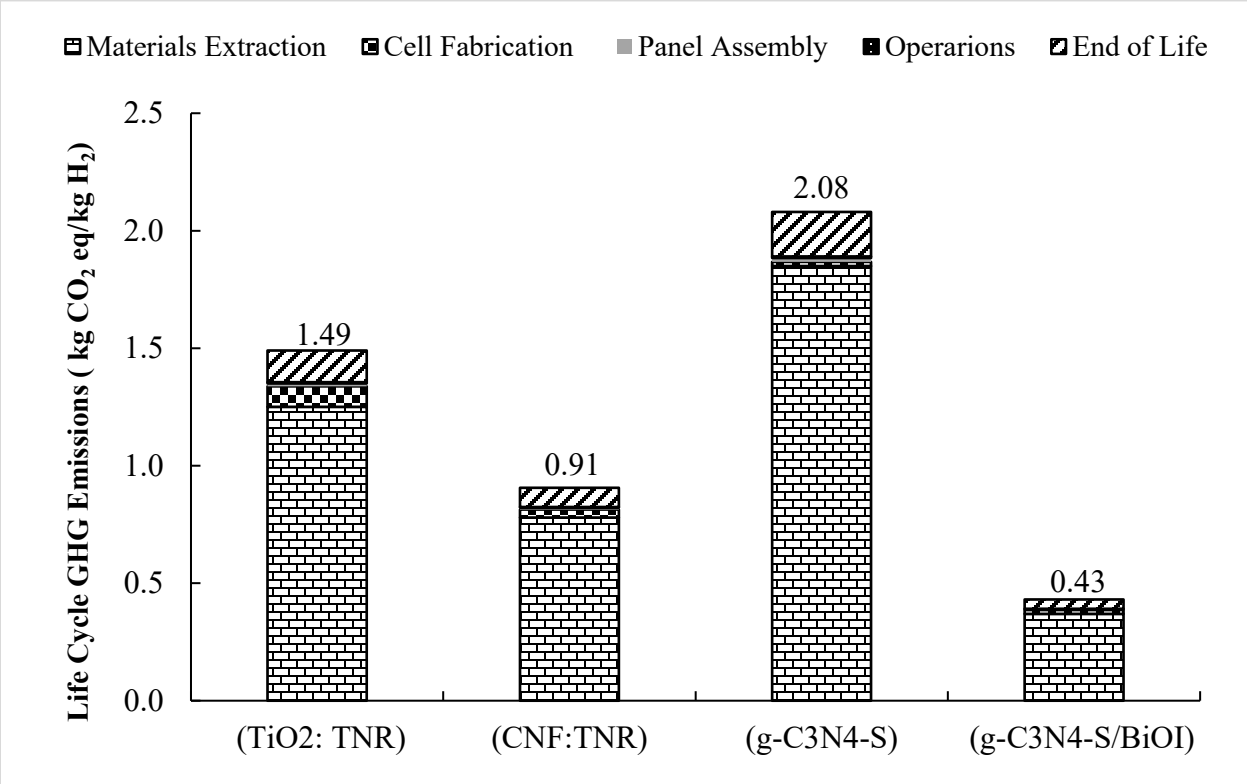

Figure 2.3: Life cycle GHG emissions of hydrogen production pathways via water splitting

Figure 4 shows the elemental contribution of GHG emissions associated with material extraction. The extraction of silver (Ag) and the production of potassium hydroxide (KOH) were the

components with the greatest GHG impact in every pathway. The extraction and production of silver are highly energy-intensive [87, 88]. Key processes include blasting, ore extraction, and ore processing. Semi-autogenous grinding (SAG) mills are responsible for 52% of the total energy required per tonne of processing and ball mills account for 84% of the total energy required per tonne [107]. Even though the silver requirement is low (0.6 grams per kg of H_2 produced), the GHG emission intensity of silver extraction and processing is the highest among the materials on the inventory list. Silver extraction to refining accounts for 99.86 g CO_2 eq per kg on the Alberta grid. For KOH, it is observed that the number of precursors is more. Calcium hydroxide and potassium carbonate are the main elements in the production of CaO (quick lime) from $CaCO_3$ (limestone), the process of which is thermal decomposition and requires high energy for the process [87, 88]. Primary energy demand accumulates considerably in the production of KOH, as noted in the literature [87, 88]. KOH is required as an electrolyte and accounts for 109 g CO_2 eq per kg of KOH produced. KOH requires 14.7 kg per kg of H_2 production. This shows that both Ag and KOH are emissions-intense materials and hence further improvements are needed in their use. Other materials for Ag and KOH with smaller GHG emissions and comparable performance will improve the technology.

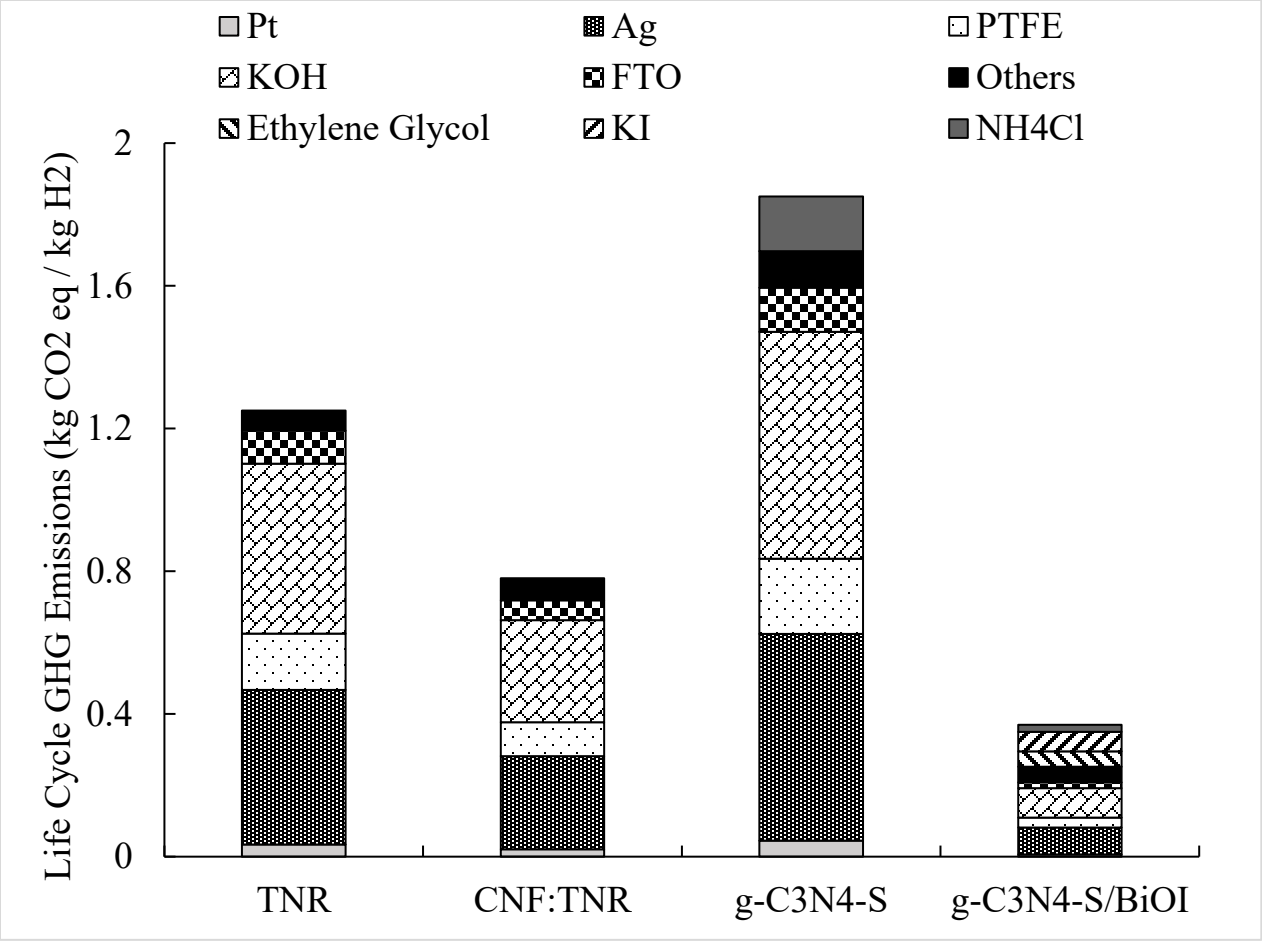

Figure 2.4: Elemental contribution to material extraction

The operation stage also shows GHG contributions in the range of (0.3% to 0.7%) in almost all pathways. The emissions in the operation stages are mainly due to energy demand from water pumps, compressors, and vacuum pumps. The range in GHG emissions among pathways is a result of the different amounts of equipment required to deliver the same amount of hydrogen over the life span of the plant. The vacuum pump and water pump contribute more than 80% in all the cases, as shown in Figure 2.5. Compressors are needed only for the compression of hydrogen in the field, whereas pumps are required to circulate water and gases from one place to another all over the field and hence require more power for operations. As electricity is the main energy source for operations, the electricity grid mix is relevant. Alberta's current electricity mix is dominated

by fossil fuels, hence every unit of electricity consumed will contribute more GHG emissions than the other locations which have partial or complete dependence on renewables. Thus, GHG emissions from operations vary significantly by jurisdiction due to differences in contributions from primary fuels.

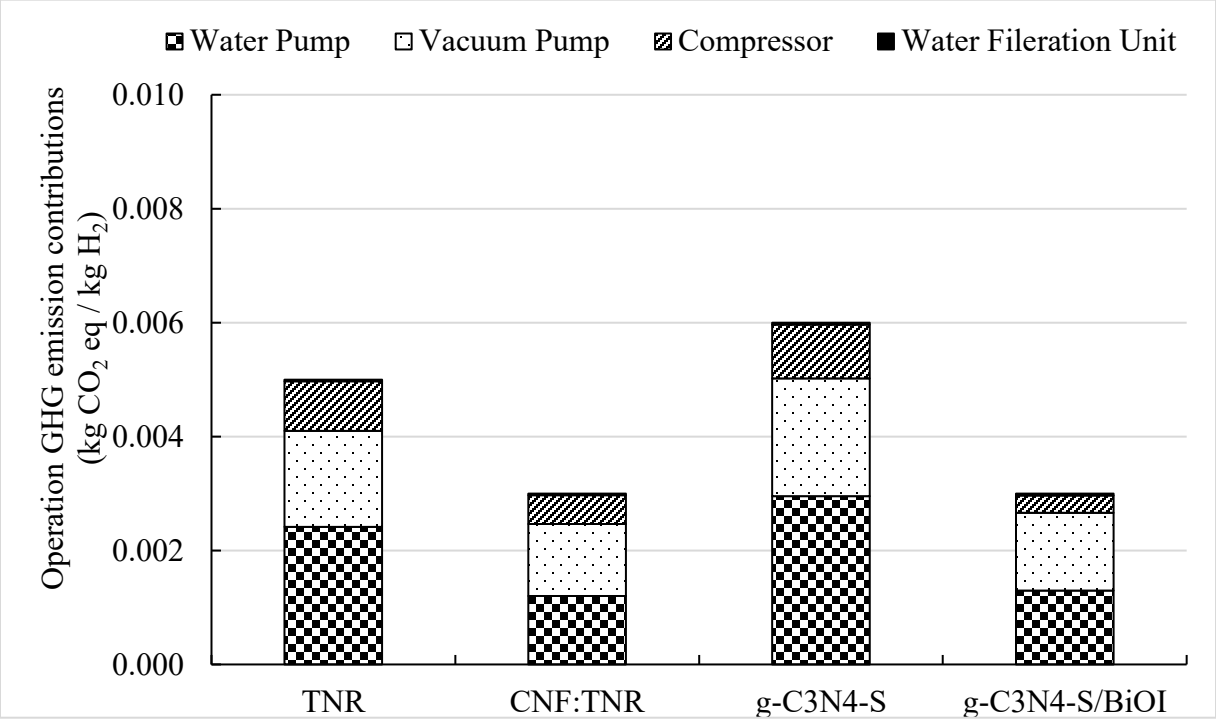

Figure 2.5: Operation GHG emission contributions

Stages such as cell fabrication, panel assembly, and end of life contribute insignificantly to emissions. Water filtration has a low energy requirement compared to other processes, hence its relative contribution is negligible. Cell fabrication has a considerable contribution in the g-C_3N_4-S case, 4% of the total GHG emissions. This is because one of the key processes in the fabrication steps, annealing, takes five hours to complete one cycle. Annealing is both highly energy-intensive and operates longer per cycle than other unit operations, thus contributing to significant primary

energy demand and GHG emissions. However, with technological progress, new methods may be adopted to improve the performance of the cell fabrication process.

2.3.2 GHG Emission comparison with other hydrogen production technologies

In the present literature, multiple studies on hydrogen production pathways are available. However, it makes sense to compare hydrogen production technologies under similar physical conditions and assumptions. Recently, Oni et. al. conducted a detailed analysis of life cycle GHG emissions from grey and blue hydrogen production pathways [108]. The considered technologies for grey hydrogen are steam methane reforming (SMR), autothermal reforming (ATR), and natural gas decomposition (NGD). For blue hydrogen, carbon capture (CC) was incorporated into these technologies to observe the change in life cycle GHG emissions from these pathways. SMR had two types of CC: SMR-52% (with 52% CC rate) and SMR-85% (with 85% CC rate). It was observed that ATR had the lowest life cycle GHG emissions of 3.91 kg CO_2 eq/kg H_2, and conventional SMR had the highest emissions value of 11.35 kg CO_2 eq/kg H_2 when CC is not considered. The life cycle GHG emissions for SMR are reduced to 8.20 and 6.66 kg CO_2 eq/kg H_2 when CC rates of 52% and 85% are considered, respectively. ATR-CC and NGD-CC offer GHG emissions as low as 3.91 and 4.54 kg CO_2 eq/kg H_2, respectively [108]. The contributions to these emissions came from on-site emissions, electricity emissions and upstream natural gas emissions. Among these, electricity emissions are of great concern as the electricity mix impacts the overall emissions significantly. Here, the Alberta electricity grid is the electricity source, which has a relatively high emission factor. So, as compared to other geographical locations, the values are a little higher. The electricity-based emissions can be lowered by utilizing electricity from a

combined power plant or renewable power source. Also, opting for low carbon-intensive feedstocks could help further reduce the emissions.

Renewable technologies such as wind electrolysis have significantly lower GHG emissions of 0.68-0.9 kg CO_2 eq per kg of H_2 produced [109]. Most of the GHG emissions are due to energy and material requirements in the setup of the turbine and the compression and storage of hydrogen. Another renewable technology is solar PV electrolysis, wherein electricity generated from photovoltaic panels is used to carry out the electrolysis of water. Due to high uncertainty and variation in solar irradiation availability and performance range of PV panels, the performance range of solar PV electrolysis is 2.1 to 6.5 kg CO_2 eq per kg of H_2 produced [109]. These results establish a base for future commercialization and provide competitive advantages over established conventional technologies.

Our analysis shows that the GHG emissions range for photoelectrochemical water splitting is in the range of 0.44 – 2.08 kg CO_2 eq/kg H_2. Although photoelectrochemical water splitting technology provides promising results from an environmental perspective, the technology is yet to be developed because of existing limitations. At present, most projects are at the laboratory scale and hence mass scale projects are unrealized and it is difficult to immediately shift to producing high volumes of hydrogen. Different photocatalytic materials produce different ranges of hydrogen, and hence the selection and activity of photocatalytic materials to compete with conventional technologies are the key barriers to the development and deployment of water splitting. Research to improve the performance of photocatalytic materials and develop new photocatalysts with greater stability and activity is underway. Because the technology is in the early stage, it costs considerably more than SMR [57]. This limits future penetration opportunities

and more research are required to make the technology economically feasible for mass-scale hydrogen production.

2.3.3 Energy payback time (EPBT)

The EPBT calculated ranges from 0.4 to 1.35 years, as shown in Figure 2.6. The lower value of EPBT corresponds to the high energy of hydrogen and lower GHG emissions. So, the amount of hydrogen produced corresponds to a higher value of energy than any other energy form. Most pathways can cover the input energy in around a year, which is optimistic for renewable energy technology. CNF: TNR has the lowest energy payback time; it will recover the energy used to produce photocatalytic cells, operations, and end of life in around 3 months. Because of high hydrogen production per photocatalytic cell and low material requirement in CNF: TNR, more hydrogen is produced per unit time, which helps recover the energy sooner. This result also provides leverage to select alternative materials with relatively little higher energy demand, with a trade-off of improved productivity.

The lower EPBT of photoelectrochemical water splitting shows that the technology has immense potential in terms of the payback period. Similar hydrogen production technology includes wind electrolysis, solar PV panels, and SMR. Conventional technologies such as SMR and coal gasification have an EPBT of 3 years and 2.5 years, respectively, whereas, for wind electrolysis and solar PV panels, the payback time is 0.9 and 1.05 years, respectively [110-112]. Hence, the EPBT of the photocatalytic hydrogen generation pathway is in line with similar renewable technologies. Therefore, future adaptation is possible for mass-scale production of hydrogen, and further developments could improve the performance of the technology.

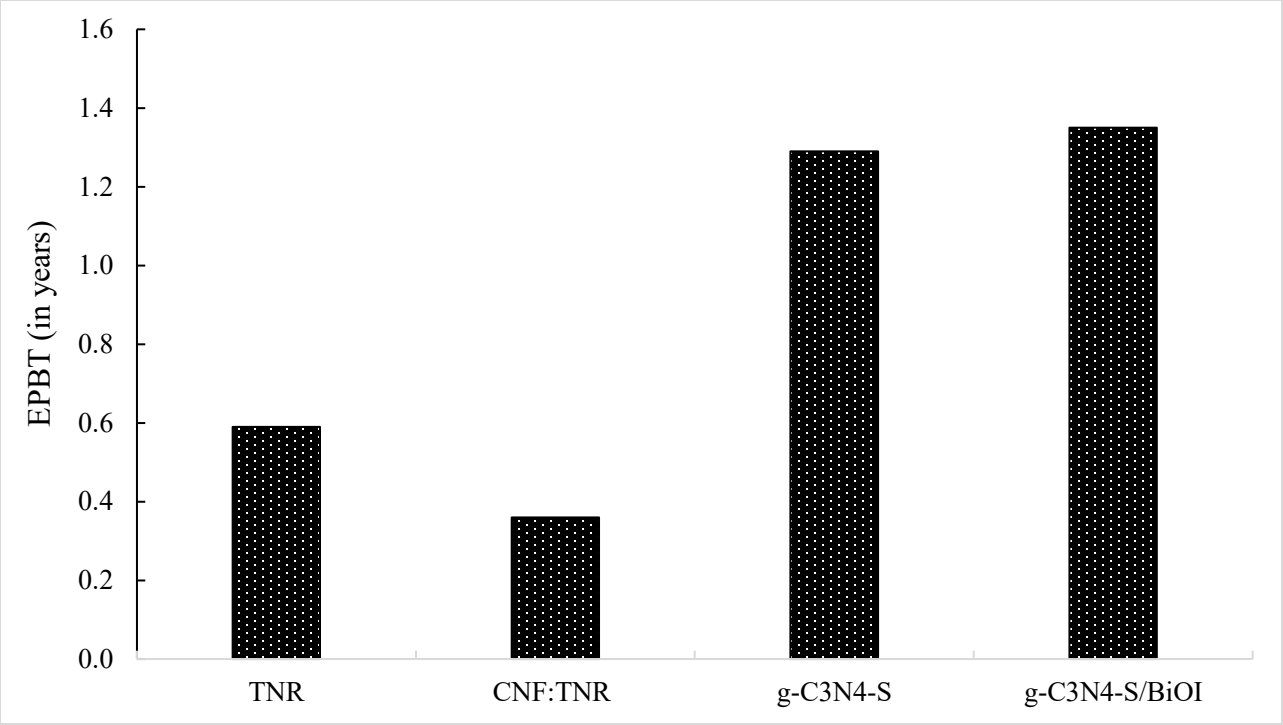

Figure 2.6: Energy payback time for photocatalytic hydrogen production

2.3.4 Sensitivity and uncertainty analyses results

Figure 2.7 presents the combined sensitivity analysis results. It shows the inputs that most affect the output. The X-axis is the Morris mean and depicts the variations in the outputs based on the change in inputs from minimum to maximum values. The Y-axis is Morris's standard deviation; it shows the magnitude of deviation of output for every change in input parameters. Further details on the morris mean can be found in an earlier publication [106]. The parameters plotted on the top right corner are the most sensitive. All four pathways show the same sensitivity because most of the elements are common to them. Hence, a common plot is shown. The life cycle GHG emissions are most sensitive to the life span of the cell, insolation, amount of silver used, energy required for cell fabrication, and volume of potassium hydroxide. Cell life span has a direct impact on the

output because with the increase in the life span, overall hydrogen production increases, thereby reducing the overall GHG emissions per unit of hydrogen production. This study considered the life span of the cell to be 15 years, which is the most likely life span of a photocatalytic cell, as shown in recent studies [35, 37]. Similarly, the output from photocatalytic cells varies proportionally with the insolation available. So, more availability of solar energy will contribute to an increase in hydrogen production. For materials, silver and KOH are sensitive as their manufacturing stages have more precursors with high primary energy demands. Silver production has considerable energy demand in the ore processing stage, specifically in SAG milling. Also, the ore concentration stage is energy-intensive. These stages make silver highly sensitive to the energy demand for photocatalytic hydrogen production. Similarly, KOH has precursors in the form of quicklime, which in turn is produced from the thermal decomposition of slaked lime. This is one of the key processes and has high energy demand. Hence, above discussed parameters such as insolation, and materials such as KOH directly impact the overall GHG emissions.

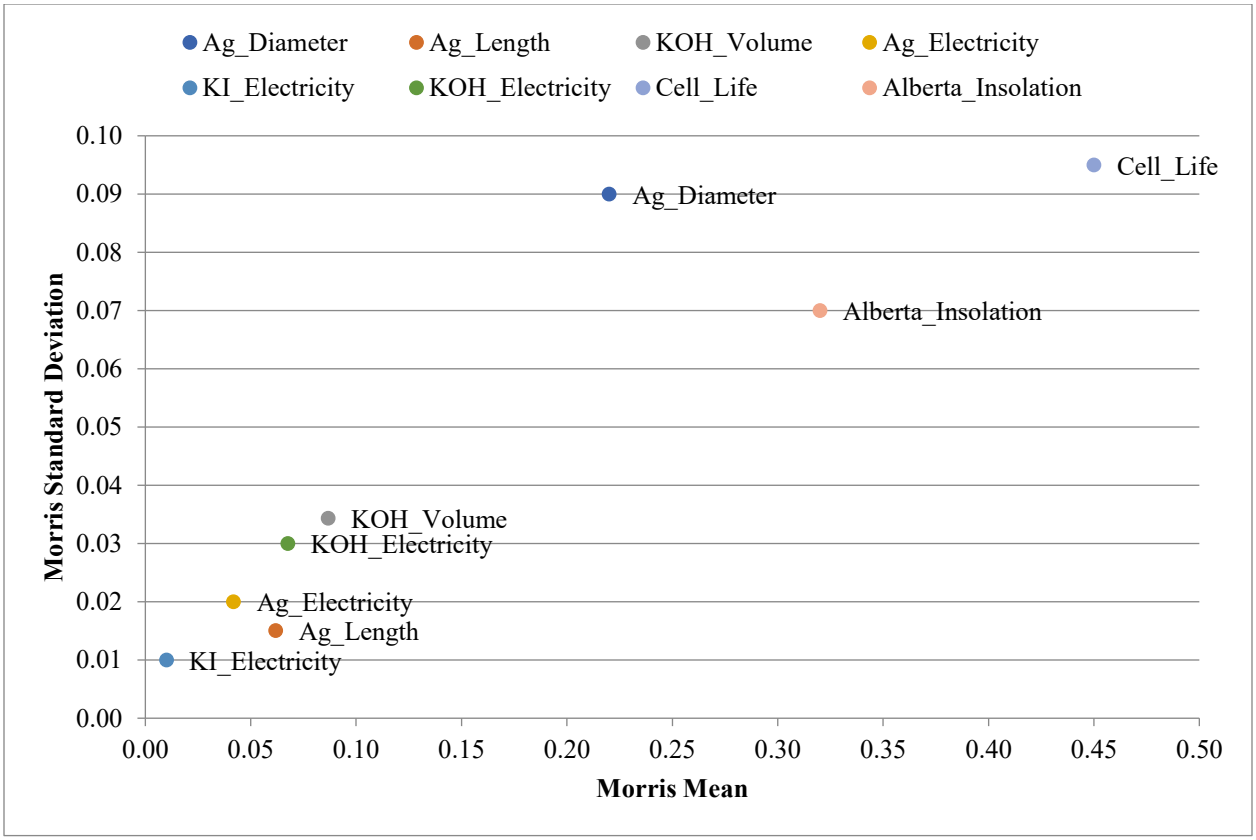

Figure 2.7: Sensitivity analysis for all pathways

Sensitivity analysis showed that cell life span, Alberta's insolation, Ag extraction, and KOH production are key inputs in the analysis. Hence, any error in these parameters can increase deviations in overall GHG emissions. To understand the range of error and the limits of these results, we conducted an uncertainty analysis using the RUST model developed by Di Lullo et al. [106] and a Monte Carlo simulation. With a uniform distribution of the inputs, minimum and maximum values were specified and then a randomly selected input from this range was selected and iterated 500 times to obtain the final distribution.

The results of the uncertainty analysis are shown in Figure 8. The GHG emissions values are $1.4^{+0.4}_{-0.55}$, $0.89^{+0.16}_{-0.24}$, $1.96^{+0.24}_{-0.26}$, and $0.49^{+0.21}_{-0.11}$ kg of CO_2 eq per kg of H_2 produced for TNR, CNF: TNR, g-C_3N_4-S, and BiOI/g-C_3N_4-S, respectively. The most uncertainty was caused by the life

span of the cell. The higher range in the GHG emissions for the TNR is because more photocatalytic cells are required to produce the same amount of hydrogen compared to CNF: TNR. Since more Ag and KOH are required, the mean GHG emissions are more than CNF: TNRs. Also, as Ag and KOH are key sensitive parameters, the sensitivity and uncertainty analysis results in a higher range of GHG emissions. Similarly, g-C_3N_4-S has a higher mean GHG value and a larger range than g-C_3N_4/BiOI. Existing research is focused on developing more reliable material production and improving the life span of the cell. Certainty in parameters will improve the quality of the results to a great extent in future. With a location change, the insolation

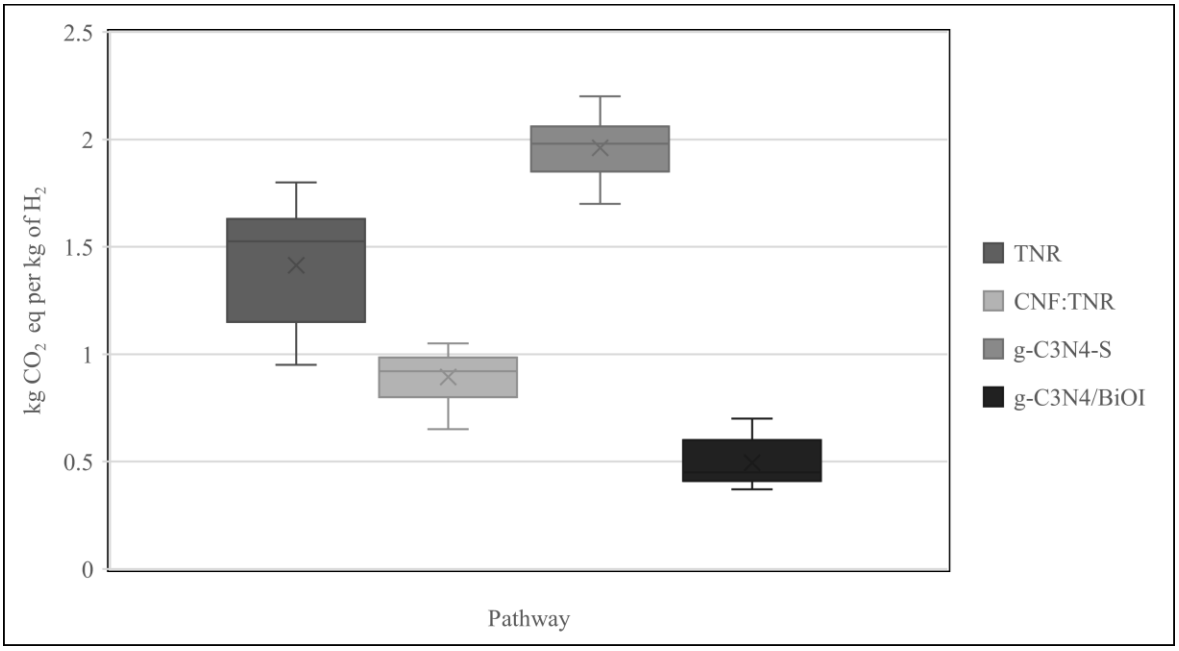

Figure 2.8: Uncertainty analysis results

also change, and the output from the model will change accordingly. These results show that the model can be adapted to many geographical locations and produce consistent results.

2.4 Conclusion

To mitigate the adverse effects of climate change, a transformation of the global energy system is required from fossil fuels to renewable energy sources. Hydrogen is a green technology alternative that can play an important role in decarbonizing energy systems. Photoelectrochemical water splitting-based hydrogen production is a promising pathway that can mitigate GHG emissions to a large extent. Since its inception, the technology has developed significantly and the overall photoconversion efficiency of photocatalysts has improved. Because the technology is still in the early stages, however, few environmental assessments are available to assess the performance of photocatalytic materials. The main purpose of this study was to assess the environmental performance of photocatalytic materials. A bottom-up life cycle assessment was performed to estimate the GHG emissions and EPBT of the energy system. Over time, different materials are expected to be tested, and the environmental and technological performance of the overall system is expected to improve considerably. Improvement depends on the type of photocatalytic materials used and related processes involved. It is important to understand the role of the photocatalytic material from an environmental perspective as the aim of the technology is to mitigate GHG emissions through alternate pathways.

For output of 5 tonnes per day, we estimated GHG emissions in kg of CO_2 eq per kg of H_2 in the range of 0.5-1.95 in four pathways. This result shows that with photoelectrochemical water splitting, hydrogen production can considerably lower GHG emissions compared to conventional means such as SMR and coal gasification. CNF: TNR shows the lowest GHG emissions, 0.38 kg of CO_2 eq per kg of H_2. This is because the photocatalyst CNF: TNR has the greatest activity among the pathways. The EPBT ranges from 0.4 to 1.35 years, which shows that this technology

can be easily adapted as a mainstream pathway if life span and efficiency are improved. These benefits will help in the transition towards the decarbonization of the economy.

In every pathway, potassium hydroxide electrolytes and silver electrodes emit the most GHG emissions. The material extraction stage contributes the most, at 83-89% of the total GHG emissions. Alternate materials can considerably improve the carbon footprint of the pathways and in future be modelled so that their advantages and trade-offs with similar materials can be compared. Hence, the framework presented in this study will help develop hydrogen production pathways. It also provides a method to evaluate the environmental performance of similar hydrogen systems.

Sensitivity and uncertainty analyses were performed to understand the impact of input parameters on the output of the system. We found that GHG emissions differ because of differences in the life span of photocatalytic cells. We also found that the extraction of KOH had a great impact on GHG emissions. With sensitivity and uncertainty analyses, the reliability of the results increases, and results can be used to develop new policies for photoelectrochemical water splitting technology. In summary, photocatalytic hydrogen production has immense potential for large-scale commercialization that will significantly reduce GHG emissions in future.

Chapter 3

The development of techno-economic assessment models for hydrogen production via photoelectrochemical water splitting

3.1 Introduction

Climate change resulting from the rise in levels of atmospheric greenhouse gas (GHG) emissions caused by human activities is one of the most pressing global concerns [113]. Fossil fuel combustion is the primary source, accounting for 80% of global GHG emissions in 2018 [47, 49, 114]. To address the negative impacts of anthropogenic GHG emissions, the Paris Agreement, which set a target of limiting the global average temperature rise to below 2 ^{o}C above pre-industrial levels, was established in 2015 [115]. Large-scale reform of the global energy system is required to meet this goal. Renewable energy technologies, carbon capture and storage, energy efficiency improvements, and switching to zero-emission energy carriers like electricity and hydrogen (H2) are some of the options for the energy transition. [51, 52]. H_2 can play a key role in achieving global climate change mitigation targets because of its properties such as clean combustion and high energy density [6, 52]. Global demand for H_2 is projected to increase 10 times by 2050 from 2015 levels [52, 53]. More than 90% of the present H_2 demand is met by fossil fuel-based processes such as steam methane reforming (SMR) and coal gasification [53, 54]. Renewable-based H_2 accounts for less than 5% of the current demand [55]. The high dependence on fossil fuels has led to the development of renewable and low-carbon H_2 production methods like wind and solar electrolysis, SMR, and coal gasification with carbon capture and storage [57]. Given the abundance of solar energy, solar-based H_2 technologies are expected to become technologically feasible in future [58].

The phenomenon of water molecules decomposing on the surface of a photocatalytic material under sun irradiation to produce oxygen and hydrogen is known as photoelectrochemical water splitting. Currently, the technology is in its early stages of development, with much research being conducted to analyze and create photocatalytic materials. However, Fujishima and Honda exploited titanium dioxide (TiO2) as a photocatalyst for hydrogen production at a laboratory scale for the first time in 1972. [18]. Following this, several other photocatalysts were developed [19]. Currently, most emphasis is given to the design and evaluation of active, stable, and earth-abundant photocatalytic materials with a low fabrication cost [20]. These properties will establish the base for the commercialization of the photoelectrochemical water splitting pathway for the mass-scale production of hydrogen [20]. TiO_2 is the most studied photocatalyst because of its applicability to this pathway. Properties such as hydrogen production rate (activity), low-cost fabrication, and stability under a wide range of conditions make it a fundamental photocatalyst [23]. However, it responds only to ultraviolet radiation, which constitutes the minority fraction of solar light [22]. Also, it has high charge recombination, which inhibits maximum use [22]. Another photocatalyst is graphitic carbon nitride (g-C_3N_4), which responds to visible light and has high thermal and chemical stability, and low fabrication cost [26, 27]. Because of its smaller surface area, g-C_3N_4 has small and less active sites for the decomposition of water molecules, and this leads to the moderate oxidation reaction of water to produce protons (H^+) and low charge mobility that disrupts the delocalization of electrons [26]. A combination of both photocatalysts can produce variants that can have enhanced hydrogen production capabilities under visible irradiation [28]. Yet present studies are still aimed at optimizing the composition that will produce an ideal photocatalyst that can function under a range of physical conditions. These developments will need

to be evaluated in terms of technological and economic feasibility to be accepted as mainstream pathways for hydrogen production.

Economic feasibility is the most critical aspect of the acceptance of technology. However, there are only a few published techno-economic assessment (TEA) studies of photocatalytic H_2 production [42-45, 116]. Pinaud et al. carried out a technical and economic feasibility analysis of four hypothetical large-scale production plants based on four reactor types, a fixed panel array, a tracking concentrator array, a single bed particle suspension system, and a dual bed particle suspension system [45]. All capital expenditures and operating costs, such as compressor and reactor assembly, were considered; the final cost ranges from \$1.6-\$10.4 per kg H_2. The study considered one type of photocatalyst material for a fixed panel array type, thus the high H_2 production cost [45]. With the arrival of new photocathodes, the effect of photocatalyst material on H_2 production (and hence cost) can be properly analyzed and will lead to more reliable and accurate results. Also, Pinaud et al.'s study fails to consider factors such as inflation and its effect on capital investment. Including these factors will give more realistic H_2 production costs. Goto et al. designed a prototype for hydrogen production by photoelectrochemical water splitting [43]. Most of the study's focus was on panel fabrication and cost optimization by reducing the cost of panel production; the study does not emphasize the importance of photocatalyst material and photocatalyst production. Moreover, photoelectrochemical water splitting technology requires assistance from other technologies such as photovoltaic (PV) or photoelectrochemical (PEC) water splitting, which brings uncertainties in cost [43]. Also, the design of the panel is such that hydrogen and oxygen are produced on the same side of the compartment and hence the panel requires a separator to safely segregate the produced gases. Grube et al. examined several renewable H_2 production pathways for the year 2025 considering various locations and climate conditions [44].

The levelized cost of hydrogen (LCOH) production in all cases was significantly higher than the US Department of Energy's (DOE) target for 2020 [44]. The study lacked a framework to quantify the costs from each life cycle stage of H_2 production, making it difficult to locate cost-intensive processes or stages. Moreover, although PV coupling was found to produce more H_2, it came with high investment costs. James et al. carried out a techno-economic analysis of several photoelectrochemical systems for large-scale hydrogen production [116]. Their detailed study considered photocell design and auxiliary equipment. A constant-performing system was assumed [116]. However, with time, the performance of a photocell reduces because of irregularities and degradation in the photocatalyst. Also, different materials can have a range of H_2 production rates. Hence, it is important to consider the change of photocatalyst materials as the material can significantly affect the cost of hydrogen production. This study aims at addressing these gaps.

There are many gaps in the TEAs of photoelectrochemical water splitting H_2 technology and thus many avenues for improvement of the technology. To the best of the authors' knowledge, no study considered the effect of using a range of photocatalytic materials on the cost of H_2 production. To improve the performance of photocatalytic materials, changes are needed in the fabrication steps. These changes affect the overall cost of H_2 production for scaled quantities. Existing studies do not consider the photocatalytic material fabrication steps. Nor do they demonstrate a proper method to scale up H_2 production from laboratory/pilot- to mass-scale and hence the cost variation trend. There is also a need for the inclusion of economic factors such as inflation to improve the results by making them more accurate. Also, the criteria for the selection of photocatalysts need attention, as, for future adaptation of the technology, photocatalysts should be stable, active, and available in abundance. Hence, this study aims at addressing these research gaps by developing a

TEA framework to evaluate the economic feasibility of large-scale photocatalytic H_2 production using alternative materials. The specific objectives are to:

- Assess the scale-up of photocatalytic cell fabrication from laboratory data to a large scale in a real-life scenario.
- Conduct TEAs of photocatalytic H_2 production for four photocatalysts, TiO_2 nanorods, CNF: TNR/TiO_2, g-C_3N_4, and g-C_3N_4/BiOI.
- Develop scale factors to establish the relationship between production capacity and overall module costs.
- Calculate the cost performance indicator of the technology in terms of LCOH ($/kg of H_2).
- Identify the economic trade-offs among alternative photocatalyst materials.
- Perform sensitivity and uncertainty analyses to identify the critical parameters and provide a range of values.

3.2 Method

Figure 3.1 shows the methodological framework used in this study. The key stages are the goal and scope definition, system design, H_2 production facility setup, and cost estimation/LCOH calculations. The goal and scope stage defines the problem, specifies the key systems considered in the assessment, and establishes the system boundary. The photocatalytic cell system design includes identifying all the unit processes, developing scale factors for sizing the equipment based on the cell design, and inputting output requirements in each process. With these scale factors, appropriate equipment is selected for each process in the H_2 production facility setup. Operational parameters are determined based on the overall capacity assumed from the facility. Finally, from the manufacturing cost, operating cost, and other factors, we calculated the LCOH for all four photocatalyst pathways. The aim was to focus on earth-abundant, stable, and active photocatalysts

so that with further commercialization of the pathway, material scarcity or implied costs in their excavations and refining processes can be mitigated. The four photocatalysts considered are titanium nanorods (TNRs), TNRs embedded with fluorine-doped carbon nitride quantum dots (CNF: TNR), and carbon nitride sheets (g-C3N4-S), and pristine bismuth iodide-doped carbon nitride sheets (BiOI/g-C3N4-S).

i. Titanium nanorods (TNR): Due to their abundance, stability, and high activity under normal conditions, titanium and its derivatives are among the most commonly used photocatalyst materials [73]. It is, however, particularly sensitive to ultraviolet radiation and so requires additional development. Titanium nanorods were created to increase the surface area of photocatalysts, which improves photocatalytic activity even further. [76].

ii. TNR embedded with fluorine-doped carbon nitride quantum dots (CNF: TNR): Carbon nitride quantum dots are implanted on TNRs in CNF: TNRs, which is a modified version of TNR.[81]. By minimizing charge recombination, the photocatalyst's activity improves. The inclusion of carbon nitride quantum dots also permits the photocatalyst to have a visible range response. [81].

iii. Carbon nitride sheets (g-C3N4-S): Carbon nitride sheets are non-metallic photocatalysts that have been produced to respond in the visible range. They have a lot of photocatalytic activity and make carbon nitride sheets out of carbon. They do, however, have a tiny surface area and a high charge recombination rate, which restricts their activity [83]. To overcome these restrictions, they are frequently doped with other chemicals [84].

iv. Pristine bismuth iodide-doped carbon nitride sheets (BiOI/g-C3N4-S): These are carbon nitride sheets that have been changed. Because BiOIs have a large surface area, they have a faster redox reaction rate on their surfaces [77]. Recombination is also reduced as a result of the increased surface area [77]. However, BiOI is uncommon due to the presence of bismuth in the molecule, which requires a lot of work and money to extract.

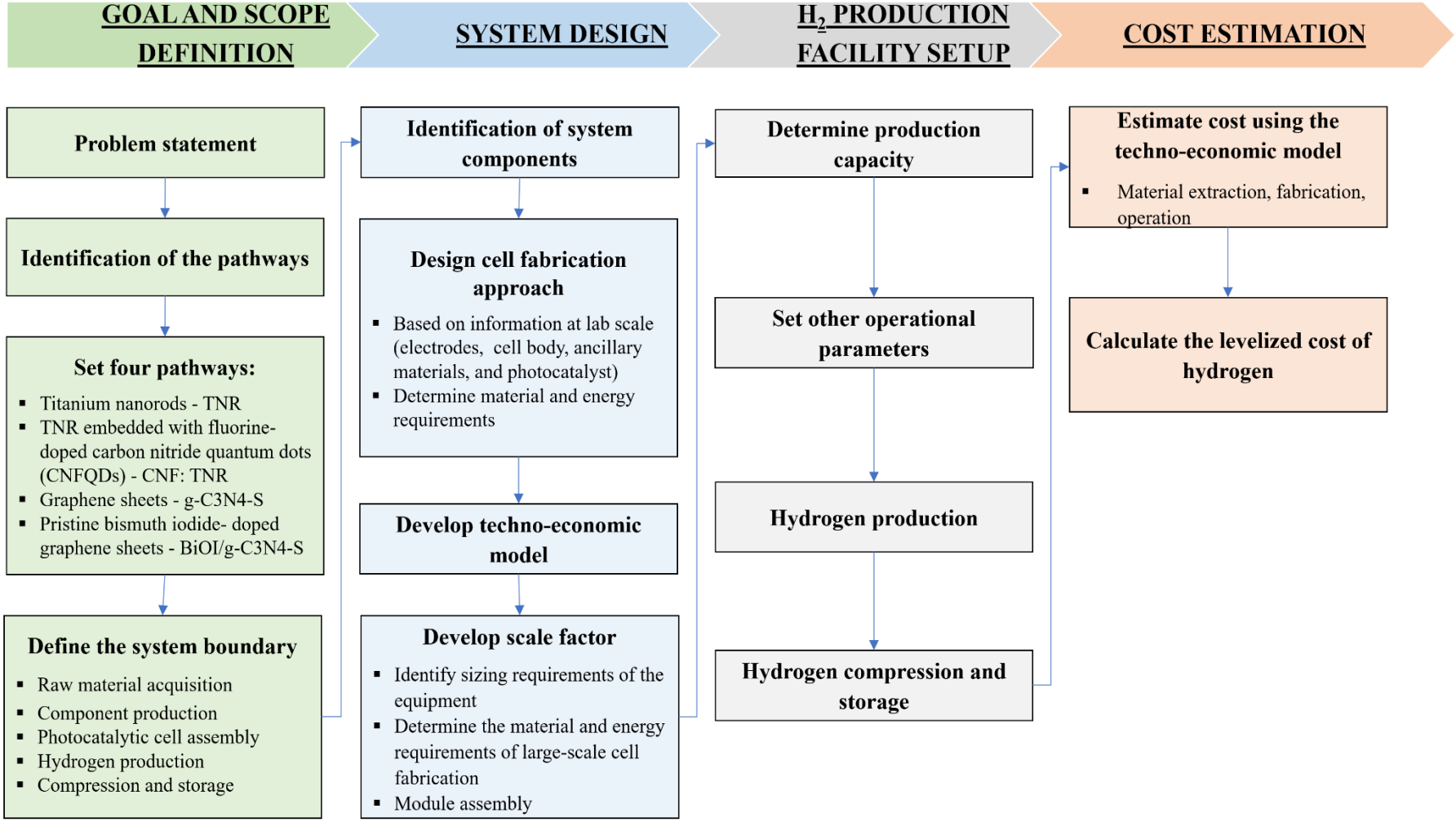

Figure 3.1: Framework of the study

3.1.1 Goal and scope definition

The primary goal of this study is to develop a bottom-up TEA model of the photoelectrochemical water splitting pathway to determine the economic feasibility, which will help to understand its economic viability and limitations. We investigated the cost implications of using advanced photocatalysts. We chose photocatalysts because of their abundance, stability in operations, life span, and activity, as discussed above. Given these parameters, it would be possible in the future to scale up the technology in an H_2 production facility without technological or economic constraints.

The main stages are material extraction and the production of precursors, component fabrication, hydrogen production, and storage. Hydrogen transportation to the distribution and end-use site is not considered in the system boundary.

3.1.2 System design

The process of photocatalytic hydrogen production involves the production, fabrication, and assembly of the key system components. These components can be broadly classified as material for electrodes, photocatalytic cells, ancillary processes, and photocatalysts. The precursors are extracted and fabricated to produce the components and then assembled to form a photocatalytic cell. Platinum is used as a photocathode today due to its stability, activity, and long life span under a range of physical conditions [69, 70]. Silver is assumed to be used as a counter electrode [69, 70]. Table 3.1 shows the list of materials considered in this study and their sources.

Table 3.1: Components of photocatalytic cell

Key systems	Component	Material used	Reference and comments
Electrodes	Photocathode	Platinum	Fan et al. and Peter et al. [69, 70]
	Counter electrode	Silver	Fan et al. and Peter et al. [69, 70]
	Photoanode	Photocatalysts (I-IV)	Kumar et al. and Alam et al. [69, 70]
Cell body	Outer casing	Polyvinyl chloride (PVC)	Zhai et al. [35] -Lightweight and high transmittance
	Separating Membrane	Teflon polytetrafluoroethylene [PTFE]	Zhai et al.[35] -Separates the compartments of the cell
Ancillary materials	Electrolyte	Potassium hydroxide (KOH), sodium sulphate (Na_2SO_4)	Chae et al. [73] Different electrolytes are used depending on the photocatalyst pathway: KOH for TNR & CNF: TNR) and Na_2SO_4 for g-C_3N_4-S & BiOI/g-C_3N_4

Laboratory data for the photocatalysts fabrication was based on work by Kumar et al. [64] and Alam et al. [65]. For TNR and CNF: TNR, Kumar et al. performed numerous tests and suggested the most optimized way to synthesize the photocatalysts [64]. Similarly, for g-C_3N_4-S and g-C_3N_4-S/BiOI, Alam et al. suggested the best configuration [65]. As photocatalysts were the focus of the Alam et al. study, it was interesting to see how H_2 costs change with changes in the type of photocatalyst. In our case, we considered the 1 x 1 x 0.02 m^3 cell designed by Sathre et al. [37]. The size of the cell was determined based on the weight-holding capacity of the structure, surface area of the cell, and water flows through each cell. The optimization of these factors leads to increase water splitting and long-lasting facility operations [37]. To fabricate this cell, we first designed the facility layout. Each photocatalyst has a fabrication pathway, as outlined in section B1 of appendix. When the photocatalyst is synthesized on the glass substrate, it is attached to previously acquired electrodes and other ancillary materials to form a photocatalytic cell. We adapted the design and layout of the photocatalytic cell from Zhai et al. [35] and Sathree et al. [37]. Except for photocatalyst fabrication, all the processes (i.e., the subassembly of the electrode or ancillary materials) are labour intensive as photocatalyst fabrication involves mostly automated machine interactions as compared to other processes. After the assembly of a photocatalytic cell, 14 such cells are arranged to form a panel. The size was assumed based on the frame strength required to handle water volume, transportability of the panels, and advancement of the technologies, among other aspects [37]. The material and processes required to fabricate these panels from cells is shown in section B2 of appendix. Figure 3.2 shows the schematic

representation of the facility layout for panel fabrication.

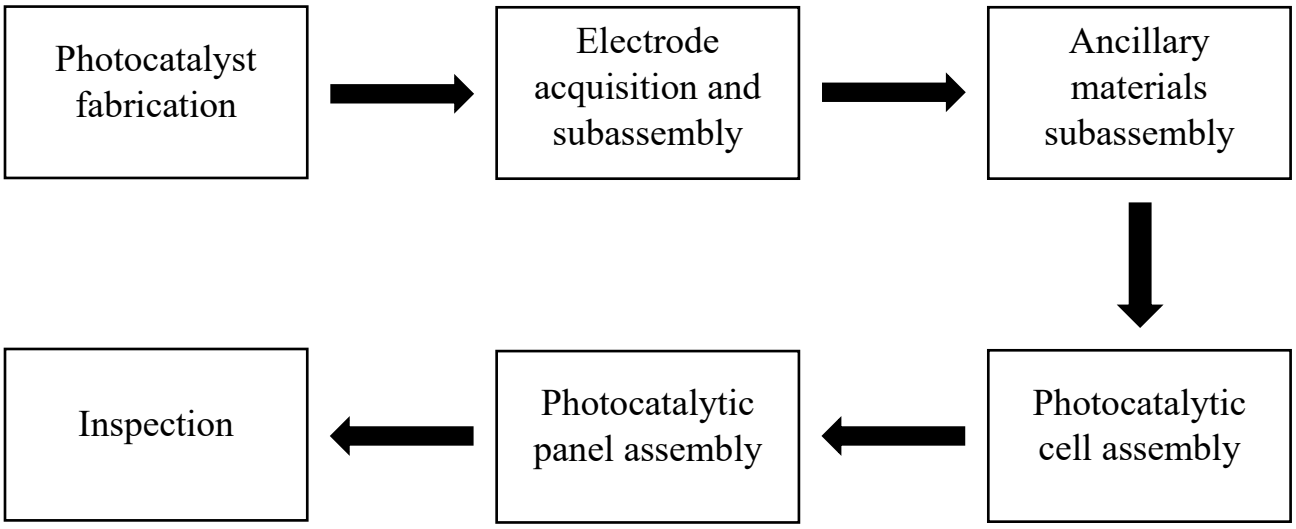

Figure 3.2: Schematic facility layout for panel fabrication

3.2.3 Hydrogen production facility setup

The manufactured panels from the production line are erected and installed facing the sun. Each panel consists of 14 photocatalytic cells combined to form a unit as per the work done by Sathre et al. [37]. . These are in turn connected with other panels via water pumps, vacuum pumps, and compressors, forming a grid [37]. Water pumps maintain the supply of water in the panels, as water decomposes into hydrogen and oxygen with time. The produced gases are captured in separate compartments and hence are collected and compressed using vacuum pumps and compressors, respectively. The collected hydrogen is stored in storage tanks before being dispatched for upstream applications. The water for panels is deionized in a water deionization plant in the solar field before being fed to the panels. We assume that overall hydrogen production capacity will depreciate by 5% every year due to the ageing of the facility [37]. To observe the performance of all four different photocatalyst-based pathways, we set up the facility and installed and operated

the equipment and panels to observe performance over the lifetime of the field. Hydrogen production was then weighed against the overall cost to determine the most economical pathway. Table 3.2 shows the overview of the costs associated with the field setup for hydrogen production and storage considering 2021 as the base year for calculations.

The production pathway components were developed and then evaluated in terms of cost. There are two cost types in the system. The first, the fixed or one-time setup cost, is the cost of the water pump, vacuum pump, compressors and PVC piping, land acquisition, panel installation, water filter system capital charges, storage tanks, and land preparation. The second type is an ongoing cost. These are the utility costs required to operate the machinery and include the electricity for the water filter system and water fed to the system, as well as employee salaries. All of these costs were evaluated for each pathway to determine the operational costs of hydrogen production over the life span of the facility. The detailed calculations and assumptions are shown in section B8 of the appendix

Table 3.2: Operating field cost calculations

No.	Component	Cost	Unit	Comment or references
1.	Panel installation	0.4	Multiplied by the cost of panel production	Includes erection, labour, and installation cost. We assume that solar panel installation is like that of photocatalytic panels; from HomeGuide [117].
2.	Pump	10000	$/No.	10 pumps are needed to drive water to panels [118].

No.	Component	Cost	Unit	Comment or references
3.	Vacuum pump	6254	$/No.	10 vacuum pumps are needed to extract hydrogen from panels [119].
4.	Compressor	50000	$/No.	5 compressors are required to compress the collected hydrogen [120]. Maintenance 10% / year.
5	Connecting pipe	15	$/metre	Used to connect all the panels to supply water and transfer hydrogen [121]. Maintenance 10% / year.
6.	Land acquisition	376.6	$/$m^2$	Needed to install and operate the panels; from USA Today [122].
7.	Land levelling	45	$/acre	Levelling and preparation of land for the proper erection of panels; from Alberta.ca [123].
8.	Labour to operate field	1,927,100*	$/year	Needed to operate machinery, deionize water plant, and maintain cleanliness.
9.	Water to feed	1.66	$/$m^3$	Needed as a supply for the functioning of photocatalytic panels; from EPCOR [124].
10.	Water filter system	26,500	$/No.	(Qty: 1), needed to purify the collected water from an Alberta municipality before feeding it to panels; 7.5 Tonnes of water per day, from Alibaba.com [125].

No.	Component	Cost	Unit	Comment or references
11.	Storage tank (Water)	3,513.3	$/No.	(Qty: 2), needed to collect and store water from an Alberta municipality;15 tonnes, from Alibaba.com [126].
12.	Storage tank unit (Hydrogen)	150,000	$/No.	(Qty: 1), needed to store compressed hydrogen at a regulated temperature and pressure; 10 tonnes, from Alibaba.com [127].

* Calculation details are shown in section B6 of the appendix.

3.2.4 H_2 production facility setup

The facility setup can be inflated or deflated based on hydrogen demand. Every photocatalyst has its H_2 generation potential per unit area, hence, the number of panels required to produce a certain amount is different for each type of photocatalyst. The total production capacity per day was assumed to be 5 metric tonnes, because of the area needed for the facility setup and the general capacity of the equipment currently available in the market. Table 3 shows the number of panels required for each type of photocatalyst that produces 5 tonnes of hydrogen/day. An adjustment factor of 10% is assumed to cover the minor losses in the facility. The mass of hydrogen per day is derived from the current density generated under normal insolation by the photocatalyst. The detailed table for photocatalyst activity is in section B7 of the appendix.

Table 3.3: Input data and assumptions for the design of the panels

Photocatalyst type	H_2 production potential ($g/day/m^2$)	Total number of panels (5 tonnes/day)	Total field area required (Km^2)
		1 panel = 14 cells	
TNR	0.11	3306878	60.2
CNF: TNR	0.18	1984127	36.1
g-C3N4-S	0.08	4409171	80.2
BiOI/g-C3N4-S	0.54	661376	12.0

Because many cells and panels need to be produced, it is important to properly size the equipment and scale up from laboratory to utility-scale. This was done by pricing each piece of equipment with a specific capacity for each unit operation. Then a curve was plotted to observe the capacity vs price relationship. The cost of equipment was then determined based on the capacity to be produced. The same process was repeated for the other unit operations. Scaling up is important because the cost does not change linearly when laboratory equipment is scaled up to produce quantities in a field. Because of economies of scale, the cost drops as capacity increases.

It was observed that the calcination process was the longest (time-consuming) in the cell fabrication process for all the photocatalysts. Hence, a range of furnaces was considered and a relationship was derived between the capacity of the system to produce a range of H_2 and the number of panels that can be produced by furnaces. This helped in selecting the right furnace for the hydrogen demand requirement. Other processes were scaled with a range of hydrogen

production capacities. The model in the study can be used for this H_2 production capacity range; however, with the sizing and output capacity from currently available commercial furnaces, it can be ascertained that 5 tonnes of hydrogen/day output are most feasible in present times. This study is set in the Canadian province of Alberta however the models developed in this study can be adapted for other jurisdictions with appropriate modification of data. The geopolitical costs, capacities, and physical parameters are affected by geographical factors, and the production of hydrogen is based on solar insolation available in Alberta. For 5 tonnes/day of hydrogen production, equipment details are shown in section B3 of the appendix along with various assumptions.

3.2.5 Large-scale hydrogen production cost estimation

The manufacturing cost of photocatalytic H_2 production is comprised of annual utility cost, labour cost, material cost, depreciation of the machines and the facility building, and operation and maintenance cost. Figure 3 shows an overview of the manufacturing cost and its components, which were used to calculate the minimum sustainable price of photocatalytic panels.

Most of the capital cost is for the equipment for the facility. The sizing of the equipment for every process depends on the facility's production capacity. The equipment cost is taken from commercial vendor websites and published sources. The equipment's capital cost is expected to depreciate linearly over 15 years [128] and will need to be replaced then. It was also assumed that the life span of the facility is 15 years [37].

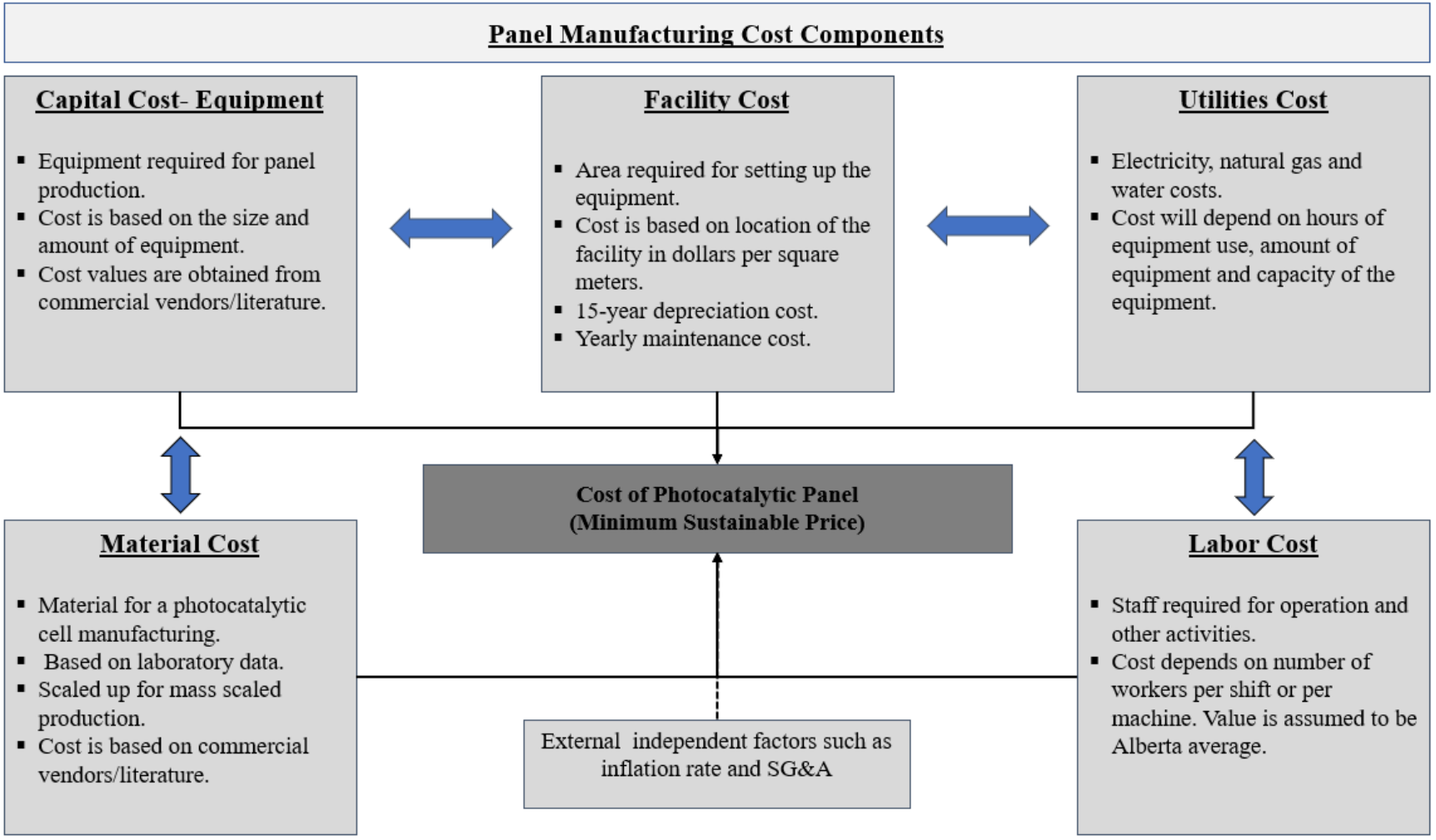

Figure 3.3: Methodology for estimation of the manufacturing cost (MSP)

The material cost is predominantly for the chemicals required in the production of the photocatalytic cell. These were adapted from Kumar et al. and Alam et al. for the four photocatalysts considered here [64, 65] and then scaled up from laboratory- to mass-scale hydrogen production. Most of the materials for photocatalyst synthesis are chemicals. The framework developed by Piccinno et al. for scaling up the materials was used [129]. Most of the materials and chemicals had linear scaling except for some solvents, and in these cases, a reduction factor of 20% was assumed [129]. The cost of these materials was obtained from commercial websites and published sources. The bulk price of the materials was assumed such that it would lead to a more realistic final cost. The equipment and material requirements are such that the output from the facility is 5000 cells per day or 114107 panels per year in each case. The material details for 5 tonnes/day of hydrogen production for all four pathways are shown in Table 4. The detailed and bifurcated material cost by pathway is shown in section B4 of the appendix.

Table 3.4: Input data and assumptions for material cost calculations

Process	Material	Amount (gram/lab Cell)	For 5 tonnes of H_2 (tonnes)	Total cost (USD)	Comments
Material for electrodes	Pt	0.13	15.31	7,655,182	Used commercially available electrodes; from CH Instruments and Alibaba.com [130, 131]

Process	Material	Amount (gram/lab Cell)	For 5 tonnes of H_2 (tonnes)	Total cost (USD)	Comments
	Ag	0.08	9.36	3,893,472	Used commercially available electrodes; from Ch Instruments and Monex [130, 132]
Material for cell body	PVC	0.52	58.80	79,378	Cell size: (L*B*T): 10cm*10cm*0.2cm; from Zhai et al. and Alibaba.com [35, 133]
	Glass (PVC Coat)	0.05	5.88	7,938	Used for coating electrodes, assumed 10% of PVC for the body; from Zhai et al. and Alibaba.com [35, 133]
Ancillary materials	PTFE	5	568.0	18,070,920	Assumed based on cell size; from Alibaba.com [134]
	Water	100	1136.0	371,756	Assumed based on cell size; from Walmart.com [135]

Process	Material	Amount (gram/lab Cell)	For 5 tonnes of H_2 (tonnes)	Total cost (USD)	Comments
	KOH	60.5	687.3	23,368	Adapted from Kumar et al. and Alibaba.com [64, 136]
	Na_2SO_4	50	5680.0	5,725,440	Adapted from Kumar et al. and Alibaba.com [64, 137]
Photocatalyst material	$Ti(C_4H_9O)_4$	0.9	96.8	1,935,744	Adapted from Kumar et al. and Alibaba.com [64, 138]
	CH_3COOH	2.6	297.9	148,958	Adapted from Kumar et al. and Alibaba.com [64, 139]
	FTO	10.0	1136.0	22,720	Adapted from Kumar et al., Alam et al., and Alibaba.com [35, 64, 65]
	CH_4N_2O	3.6	408.96	91,607	Adapted from Kumar et al. and Alibaba.com [64, 140]

Process	Material	Amount (gram/lab Cell)	For 5 tonnes of H_2 (tonnes)	Total cost (USD)	Comments
	NH_4F	0.3	34.08	1,238,126	Adapted from Kumar et al. and Avantor [64, 141]
	$C_6H_8O_7$	1.94	220.38	583,445	Adapted from Kumar et al. and Aromatics [64, 142]
	$C_2H_4N_4$	2	227.20	4,771,200	Adapted from Alam et al. and TCI [65, 143]
	NH_4Cl	10	1136.00	496,205	Adapted from Alam et al. and Intratec.us [65, 144]
	$Bi(NO_3)_3$	10.0	1136.00	22,720	Adapted from Alam et al. [65]
	$C_2H_6O_2$	22.3	2528.74	2,301,150	Adapted from Alam et al. and Intratec.us [65, 145]
	KI	10.0	1136.00	22,720	Adapted from Alam et al. and Ingrdientdepot.com [65, 146]

The utility cost includes the electricity and natural gas needed to operate the machines in the facility. The utility use was based on the power rating of the equipment, usage hours, use factor, and the number of machines in the facility. The use factor helps make calculations more accurate and realistic, especially when a machine is not running at its maximum rated output. The use factor is adapted from the detailed study by Valverde et al. [147]. Canadian commercial business electricity and natural gas costs were used to calculate usage costs. This is in line with Alberta's average, and electricity and natural gas prices are $0.09/kWh and $0.016/MJ, respectively [148]. Utility costs mainly depend on the energy demand of the equipment at the facility. A detailed distribution of utility costs is available in section A5 of the appendix.

The facility needs to provide a basic framework for the setup of the production line for the panels. The area required is the sum of the individual equipment's floor space requirements along with offices and miscellaneous use (i.e., washrooms). It was assumed that a depreciation period of 15 years along with an annual maintenance expense of 10% of the building depreciation cost [128]. Labour cost constitutes the salary of the staff operating machines, staff working on the floor as supervisors, and technical staff including research and development engineers. Alberta's average wage is used for all of these positions. Section B6 of the appendix provides detailed calculations on the building and labour costs used in this study.

3.2.6 Levelized cost of hydrogen

A discounted cash flow was developed with a 15-year analysis period to calculate the levelized cost of hydrogen (LCOH). Also, an annual maintenance cost of 3% was added to the total project

cost. This was based on the framework given by Brown et al. and by Akbari et al. describing the increase in the cost of labour, services, and goods with time [149, 150]. For cost estimation, it was assumed that manufacturing and operating the photocatalytic panels are close to the manufacturing of solar photovoltaic panels because of the similarities in facility setup and production line function [151, 152]. The costs are aggregated over 15 years to find the total life cycle cost of the photocatalytic system. The H_2 cost is then determined by using the total life cycle cost by the total hydrogen produced over the life of the facility. The LCOH was estimated using the techno-economic model. Finally, the LCOH value was calculated for each pathway and compared with similar technologies to study the feasibility of the technology.

3.2.7 Sensitivity and uncertainty analyses

The output of the system depends on multiple inputs but is sensitive to a few specific inputs. Hence, a sensitivity analysis is used to identify key inputs on which the output is most dependent. For this, Morris's statistical method was used, a non-linear model that identifies the main inputs [104]. The details of the model are given in an earlier study [106]. The system that was considered in this study has a high number of inputs and hence Morris's statistical method was used for sensitivity analysis [104]. A uniform distribution was considered for the inputs.

Once the key input parameters are identified in sensitivity analysis, uncertainty analysis is done on these inputs. This is because marginal errors can accumulate while collecting data, some assumed values might change with time, or some assumptions are amended in system scaling. These small errors can result in a wide range of uncertainties in the final results. Hence, to understand and observe the range of these uncertainties and their effects, a Monte Carlo uncertainty analysis is conducted. The Regression, Uncertainty, and Sensitivity Tool (RUST) developed by Di

Lullo et al. [106] for uncertainty analysis was used. A uniform distribution for all inputs was used, and random samples were selected for the distribution of the inputs and iterated 10,000 times to obtain the final uncertainty results.

Apart from the factors directly involved in the process, independent factors can significantly impact the results. Hence, along with the key parameters from sensitivity analysis, some parameters were added to investigate the results further. The technology relies on solar insolation, which varies depending on the facility location. Hence, solar insolation was considered which is a key parameter for the analysis. The solar insolation region is in Alberta. The range of 3400-5000 MJ/m^2/year was adapted from the Agricultural Land Resource Atlas of Alberta [92]. Another major parameter is the panel cost. Hence, the panel manufacturing cost was considered as the second parameter. Panel costs range from $75-$150/per panel. Labour rates change from region to region and can bring variability to the analysis. So, the labour rate was selected as the last parameter for uncertainty analysis; it can range from $16-$24/hr [153]. Other inputs were varied by ± 25% to observe their impact. The key parameters and their ranges are specified in Table 3.5.

Table 3.5: Uncertainty range for input parameters

Parameter	**Unit**	**Range**	**Comments**
Insolation	MJ/m^2/year	3400-5000	Highest and lowest insolation in Alberta, Canada [92]
Panel cost	$/panel	75-150	The MSP range was obtained from this

Parameter	Unit	Range	Comments
			study's uncertainty analysis and used as an input to calculate the LCOH.
Labour hourly rate	$/hour	16-24	[153]

3.3 Results and Discussion

The study addresses four aspects of photocatalytic hydrogen production: first, the panel manufacturing cost for 5 tonnes of hydrogen per day for a plant in Alberta, Canada; second, the effect of economies of scale (due to increased production capacity) on the manufacturing cost of the photocatalytic panels; third, the calculation of the LCOH in the four pathways and the feasibility for mass-scale production of hydrogen; and fourth, the key components affecting cost for future improvements, identified through sensitivity and uncertainty analyses. Each of these is discussed in the following sections.

3.3.1 Panel manufacturing cost

For 5000 cells per day and their respective capacity potential, the manufacturing cost of panels for each pathway was evaluated.

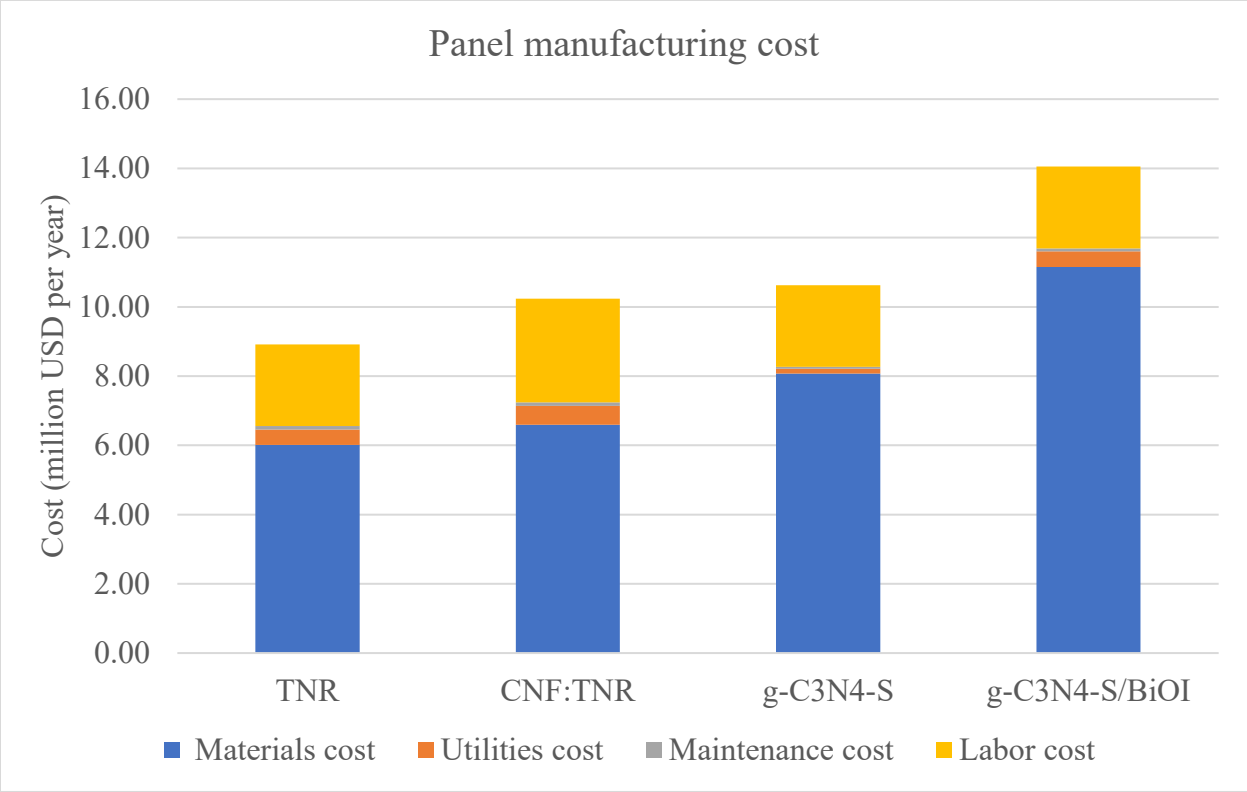

Figure 3.4: Manufacturing cost contributions for photocatalytic panels manufacturing

Figure 3.4 shows the contributions of the major cost components to the manufacturing cost of the panels. The results show that material cost is the sole majority contributor to the overall manufacturing cost. The amount ranged from 8.9 to 14 million dollars annually (64 to 80%). The huge cost is due to the large number of materials required for the synthesis of photocatalysts. Materials such as potassium iodide (KI), silver, and platinum either need considerable refining or are precious metals [154]. In either case, the cost is high. Also, the material needed to manufacture the cell body and ancillary materials is novel. This leads to high costs. A further breakdown of these material costs is given in the next section. Labour cost is the second-highest contributor, at

2.3 to 3 million dollars annually (16 to 30%). The range is due to the size of the machinery required to produce a particular number of photocatalytic cells per day. Some machinery requires more labour for each unit operation and some needs little or none. Different machinery is used for each photocatalytic pathway, and hence the labour requirement differs. This varying labour demand leads to a range of labour costs. The utility contribution is relatively low, in the range of 0.1 to 0.5 million dollars annually (1 to 5%). This is because of the cheap utility rates in Alberta. The maintenance cost is insignificant, as shown. The range was from 0.06 to 0.11 million dollars annually (0.005 to 0.01% of the total cost). It is low because of the availability of highly automated machinery, which helps staff to adopt corrective and preventive actions, saving any breakdowns and maintenance failures [155]. A further breakdown of the majority contributor, material cost, is needed to understand the cost-incurring sources in depth. Figure 3.5 shows the detailed breakdown of material costs for panel manufacturing.

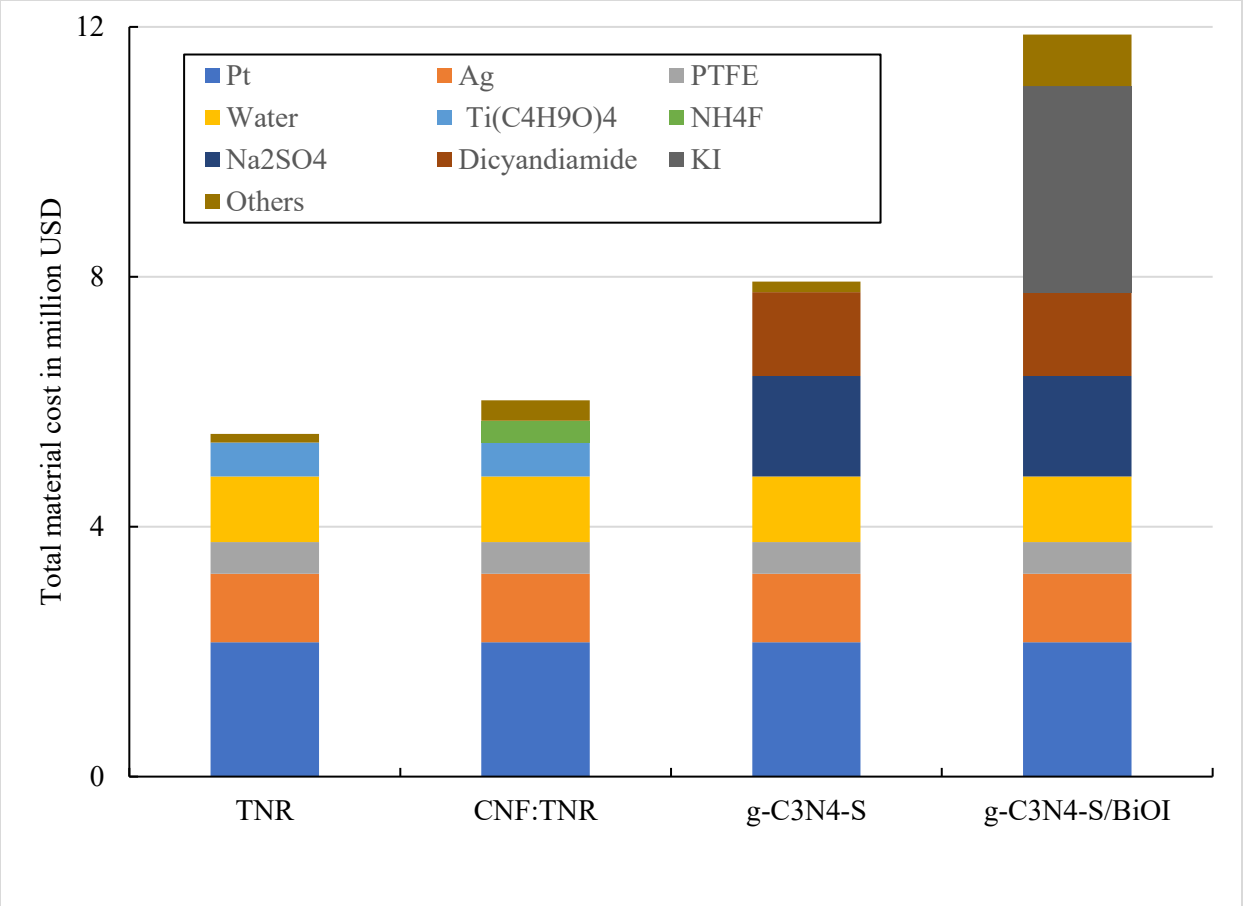

Figure 3.5: Breakdown of material cost

Materials for electrodes (silver and platinum) contribute the most to the material cost. Platinum, a noble metal, has a very high cost per gram. The cost contribution from platinum ranges from 19% in g-C3N4-S/BiOI to 46% in TNR. Silver ranges from 10% in g-C3N4-S/BiOI to 24% in TNR. These metals are costly because they are less abundant and because more processes are needed to refine or purify them from the raw form. For silver, key processes include blasting, ore extraction, and ore processing. Machinery such as semi-autogenous grinding (SAG) mills are responsible for 52% of the total energy required per tonne of processing and ball mills for 84%; these values were obtained from Noussan et al. [154]. These processes require considerable energy and heavy machinery and hence the production cost is high. Another important costly input is water. A huge

amount of water is needed and even if it is inexpensive, the high demand adds significantly to the total cost. Water as feed contributes 4% to the cost in g-C_3N_4-S/BiOI and 8% in CNF: TNR. The water needs to be deionized before being used for operations and fed into panels; this adds to the filtration and delivery costs of water. Other chemicals include potassium iodide (KI), sodium sulphate (Na_2SO_4), titanium butoxide ($Ti(C_4H_9O)_4$), and dicyandiamide, which partially contribute to one or two pathways but do not affect all four pathways significantly. The advancement of technology and the development of electrodes from abundant materials with similar functions will help lower the production cost of photocatalytic panels significantly in the future.

3.3.2 Economies of scale in panel manufacturing

The production cost per panel decreases with an increase in the capacity of the facility because of economies of scale. For photocatalytic panel production, the facility capacity range was varied in steps depending on the size of the commercially available machinery, such as furnaces. The capacities were set to 500, 1000, 5000, 10000, 15000, and 20000 photocatalytic cell production per day. Figure 6 shows the cost of panel production for these capacities. It was observed that in every case, the cost dropped drastically in the initial changes in capacity. This is because the same machinery can produce more cells while running at partial or full load. No upgrade is needed for most processes to increase from 500 to 1000 cells per day production. However, with further increments, new machinery with a higher production capacity and power rating is required with every step to meet production demand. This machinery generally has a high power rating and hence the price does not come down as prominently as in the previous steps. This series continues for further capacities. The cost of panel production decreased from $229-$288 per panel for 500 cells per day to $81-$129 per panel for 5000 cells per day. This is more than a 50% reduction in

production cost. For the next increment of 5000, that is, for 10000 cells/day, the cost range was $70-$117 per panel. This is about a 9% reduction in cost. Hence, it is not economical to further increase the capacity as the reduction in cost is negligible. This also justifies the 5000 cells/day consideration of production cost as an analysis point for all four pathways considered.

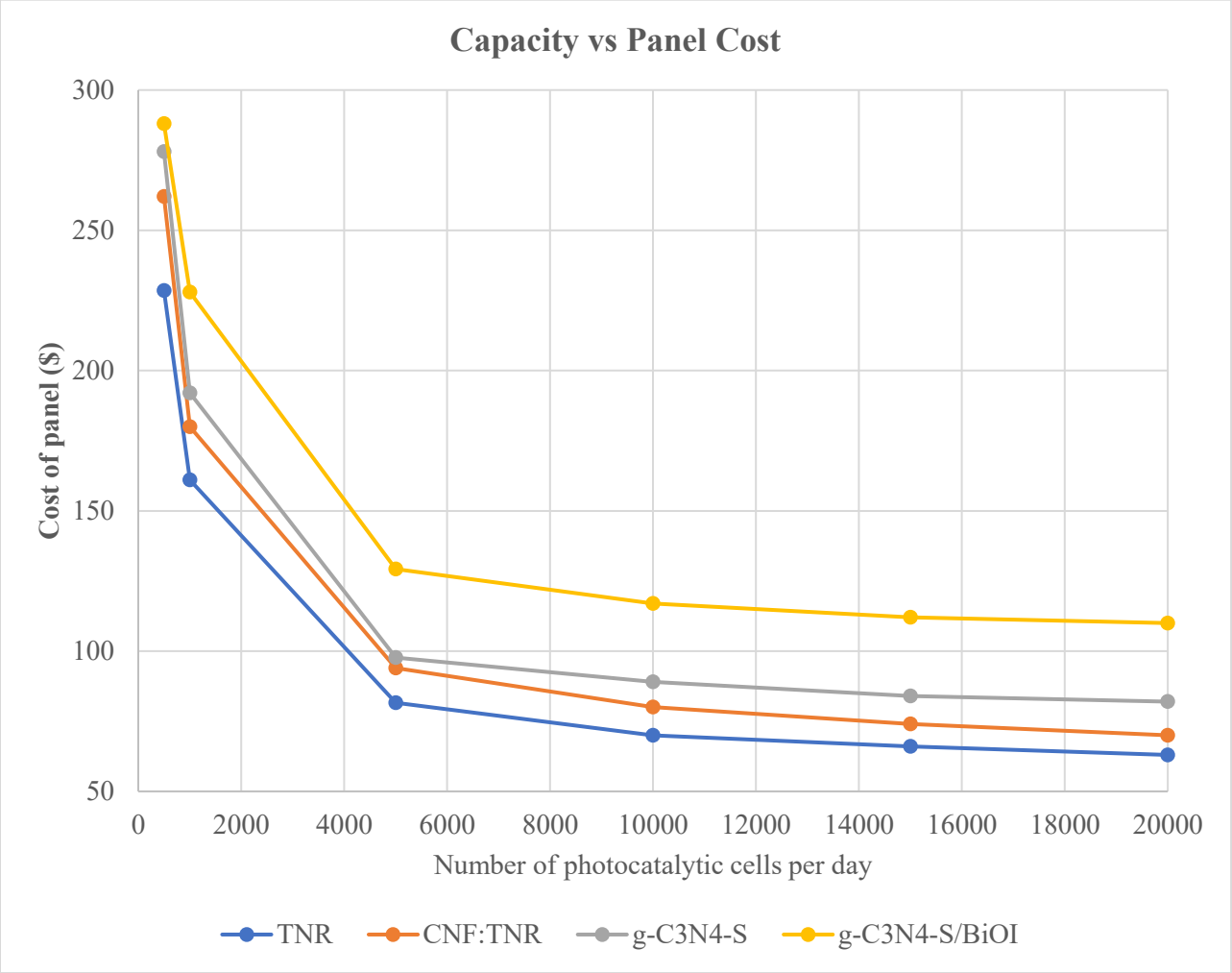

Figure 3.6: Cost versus capacity of panel manufacturing

The capacity of the panel was converted to a megawatt (MW) equivalent potential for electricity. So, for each photocatalyst with 5000 cells per day of production, the H_2 produced (5 tonnes) is converted to equivalent energy demand. Table 3.6 shows the capacity of each pathway in MW.

Table 3.64: Equivalent capacity (in MW) for each photocatalytic production pathway

Photocatalyst	**Cells per day**	**H_2 production per day (gram of H_2)**	**Capacity per year (MW equivalent)**
TNR	5000	405	56.7
CNF: TNR	5000	675	94.5
g-C_3N_4-S	5000	304	42.5
g-C_3N_4-S/BiOI	5000	2025	283.5

The conversion of hydrogen to electricity is based on electrolyzer performance, assuming an overall efficiency of 60% [156]. Also, only 350 days of operation were assumed due to miscellaneous breaks. As g-C_3N_4-S/BiOI had the highest hydrogen production per day, overall capacity was the largest at 283.5 MW equivalent per year and 10% more than the second-largest contribution from CNF: TNR of 94.5 MW. Because of the low activity of TNR and g-C_3N_4-S, they are on the lower lines of the comparison chart.

3.3.3 Levelized cost of hydrogen production (LCOH)

For 5 tonnes of hydrogen production per day, the LCOH ranges from 4.9-7.8 $/kg of H_2. TNR had the lowest hydrogen cost and g-C3N4-S/BiOI the highest. The difference in cost is due to differences in the activities of the photocatalyst materials. g-C3N4-S/BiOI had the highest activity of 2025 grams of H_2 per day for 5000 cells. However, given the greater amount of chemicals and material requirements for the synthesis, its overall LCOH is higher than CNF: TNRs. CNF: TNR

had active materials with high abundance and hence less cost in the synthesis of the precursors. The costs of hydrogen obtained in this study are in line with the values found in the literature. Noussan et al. assessed green hydrogen production costs using water electrolysis and found green hydrogen costs to be 3-6 \$/kg of H_2 [157]. The results in this study have a broader range of 4.9-7.8 \$/kg of H_2. The results in this study are more robust because Noussan et al. considered an average of several technologies (such as power generation from renewables) and water electrolysis costs from several countries. Also, the photocatalysts in this study are relatively new, and hence more research is needed to improve their activity. The cost is higher than the currently established technologies like SMR and coal gasification [158]. The cost of hydrogen production from these conventional technologies ranges from 0.85-2 \$/kg of H_2, which is significantly lower than the photocatalytic hydrogen production cost. Olufemi et al. conducted a detailed estimation of grey, blue, and green H_2 production costs [159]. The supply cost of blue H_2 was found to be in the range of \$1.6-3.2/kg of H_2 for SMR and autothermal reforming (ATR) along with a carbon capture and storage (CCS) system. This pathway has a marginally higher cost than the grey hydrogen pathways [159]. Hence, it provides an opportunity for established conventional grey H_2-based technologies to transition towards the green mode via blue H_2 pathways. However, photoelectrochemical water splitting technology is in the initial stage of development and shows the potential to be adapted for mass-scale hydrogen production in the mid-to long-term. Figure 7 shows the cost of hydrogen production broken into its cost components.

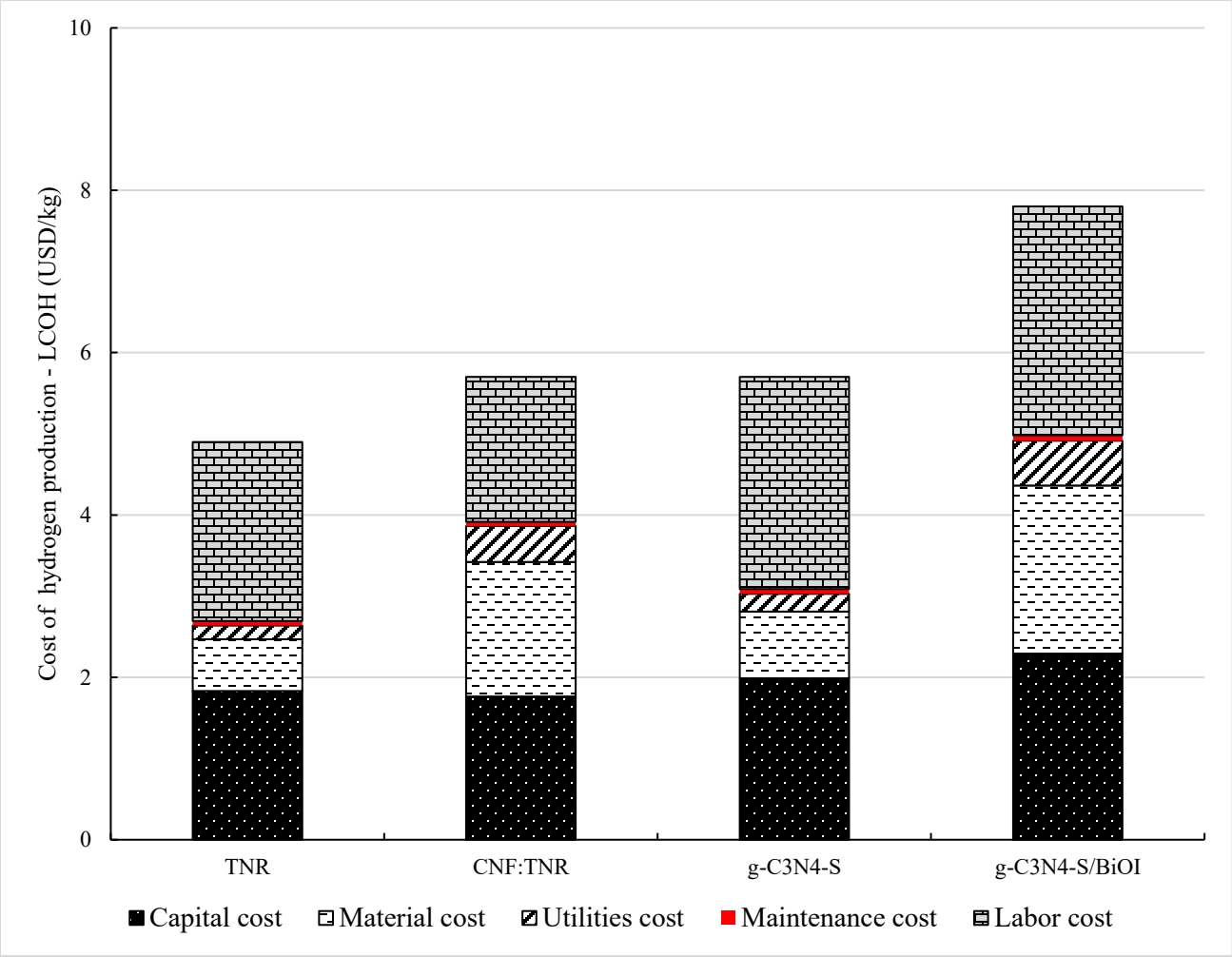

Figure 3.7: Levelized cost of hydrogen production from photocatalytic pathways

The cost of hydrogen is comprised of five major cost components: capital cost, material cost, utility cost, maintenance cost, and labour cost. Of these, capital and labour are the most significant, contributing 30-37% and 32-46% of the total cost, respectively. Material cost is the third largest cost at 13-29% of the total. Labour is required for field maintenance and to continuously monitor the panels during operations. Labour is also needed to operate machinery related to pumps, compressors, deionized water plants, hydrogen storage, and field maintenance. Labour costs contribute significantly to the overall cost. Panel costs from the manufacturing facility, pumps, compressors, and storage equipment contribute to capital costs. Panel acquisition is the most

costly, adding 40% to the capital cost. Material cost is mainly from materials like silver and platinum. So, with further improvements in panel production and fabrication methods, along with the use of low-cost materials that can perform with the same effectiveness as cost-intensive materials, hydrogen cost could be further reduced to make it competitive with conventional technologies.

3.3.4 Sensitivity and uncertainty analysis

Figure 8 shows the combined sensitivity analysis results for the CNF: TNR pathway. The graph shows the inputs that have a significant impact on the output. The x-axis is the Morris mean and shows the range of outputs based on the variations in inputs from lowest to highest values. The y-axis is Morris's standard deviation; it shows the magnitude of deviation in the output for every change in the input parameter. So, the inputs located near the top right corner of the graph are the most critical and cost is most sensitive to these and should be given more weight than the others. The inputs are the same for all four photocatalysts and hence a common plot is shown for the LCOH as the output. The graph shows that the LCOH is most sensitive to panel manufacturing cost, Alberta's insolation, and the life span of the facility. Current density (photocatalytic activity), land rate, electricity rate, and panel manufacturing capacity are the other inputs that affect the LCOH. The sensitivity results for the other three pathways were similar and produced close results, so only the results from one pathway, that is, CNF: TNR, are presented and discussed here.

The amount of hydrogen produced is directly proportional to the solar insolation incidence on the heterojunction of photocatalytic cells. This is because, as solar insolation increases, more photons are available to cause photocatalytic decomposition of water molecules on the photocatalyst's

surface. This increased decomposition will release more hydrogen. Hence, solar insolation has a significant impact on the overall LCOH of the system.

A panel manufacturing facility was designed for this study. The cost of panels manufactured from this facility depends on factors such as the combined equipment acquisition cost, the capacity of the facility, and labour. These factors contribute to the cost of panel manufacturing and are liable to variations depending on technological progress. These variations can be significant and are shown in the graph plot. The study considers 15 years as the life span for the hydrogen production facility. The considered life span is in line with the assumed value in recent literature [37]. However, the variation in the life span of the hydrogen production facility impacts the operations stage. Hence, if the facility has a higher life span (due to factors such as less maintenance), more hydrogen will be produced in the overall life span of the facility. This will reduce the LCOH. The rates of land and electricity are significant as land is needed to set up the facility for panel manufacturing and hydrogen production, and electricity is needed to operate it. The panel manufacturing capacity in the facility, considered in this study, is 5000 cells per day; this was assumed based on the current capacity of equipment available in the market for panel fabrication. However, this capacity can be varied depending on upcoming higher capacities of equipment or technologically advanced machines that can fabricate panels at faster rates.

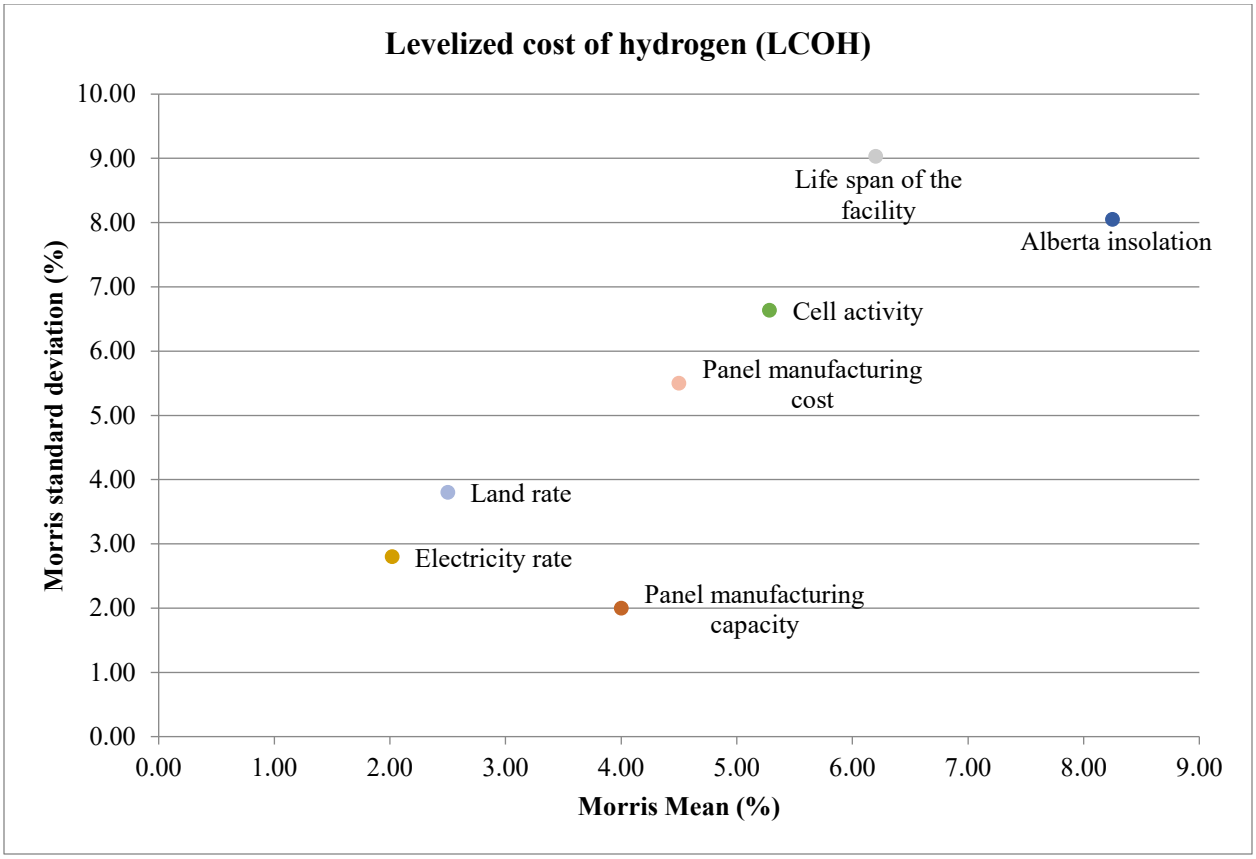

Figure 3.8: Sensitivity analysis for CNF: TNR pathway of hydrogen production

Because insolation, panel manufacturing cost, and facility life span are the most critical inputs as the cost is more sensitive to these, an error in the values of these parameters can amplify the error in the overall LCOH values. So, an uncertainty analysis was conducted to understand the range of these errors and corresponding limits in the results using the RUST model [106] and a Monte Carlo simulation. With a uniform distribution of the inputs, minimum and maximum values were specified and then a randomly selected input from this range was selected and iterated 300 times to obtain the final distribution.

The results of the uncertainty analysis are shown in Figure 9. The LCOH values are $4.9^{+0.75}_{-0.70}$, $5.7^{+0.45}_{-0.65}$, $5.8^{+0.55}_{-1.15}$, and $7.8^{+0.45}_{-0.95}$ $ per kg of H_2 produced for TNR, CNF: TNR, g-C_3N_4-S, and

BiOI/g-C_3N_4-S, respectively. Most uncertainties were caused by panel manufacturing costs and the life span of the facility. A higher life span of the facility resulted in a lower LCOH and vice versa. For panel manufacturing costs, higher costs led to a higher LCOH and vice versa. The uncertainty in the values of g-C_3N_4-S is higher than in other photocatalysts because of the lower activity. Hence, g-C_3N_4-S/BiOI has higher panel manufacturing costs (due to added material requirements to meet the demand). Existing research is focused on developing more reliable material production methods and improving the life span of the hydrogen production facility. Certainty in parameters in future will considerably improve the quality of the results. With a location change, the insolation also changes, and the output from the model will change accordingly. These results show that the model can be adapted to many geographical locations and produce consistent results.

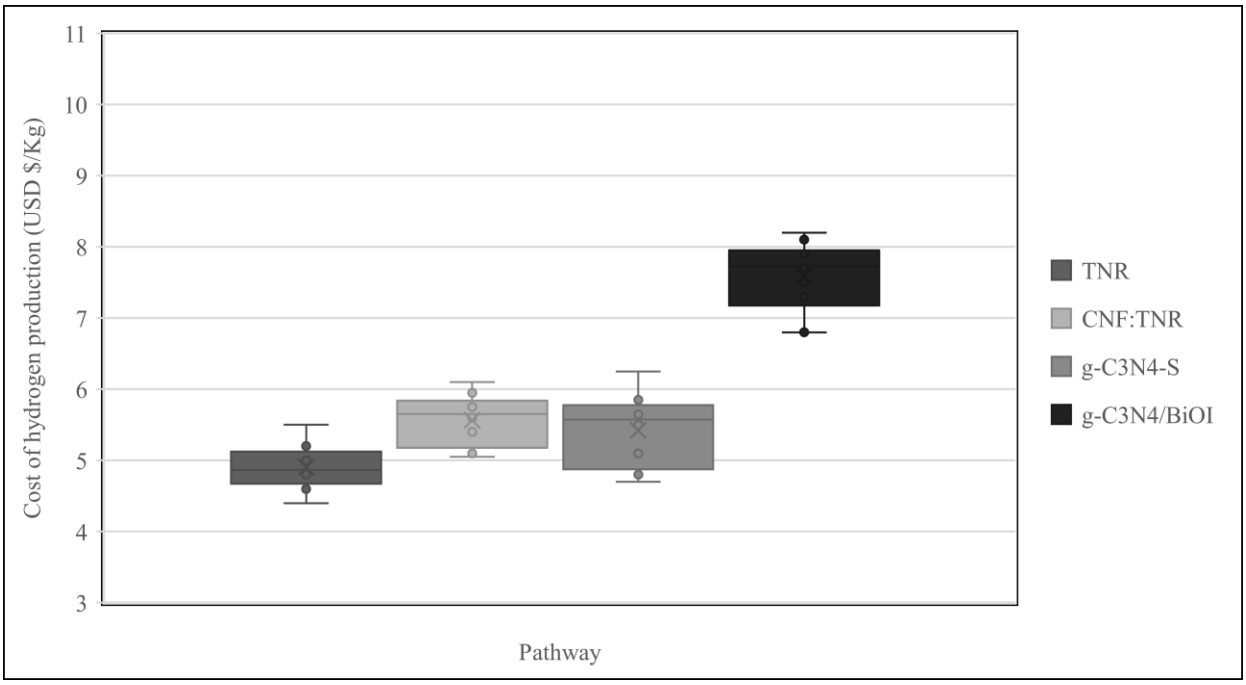

Figure 3.9: Results of uncertainty analysis

3.4 Conclusion

Photocatalytic hydrogen production is among the promising future energy systems as it provides green hydrogen with less mechanical processing. As the technology is new, studies focus on its feasibility. The primary aim of this study was to develop a bottom-up techno-economic model to examine the economic feasibility of four photocatalyst-based (TNR, CNF: TNR, g-C_3N_4-S, and BiOI/g-C_3N_4-S) water splitting pathways to generate hydrogen. The scale-up of the production plant capacity was done from laboratory to mass scale of 5 tonnes/day of hydrogen production for panel fabrication, manufacturing, and operation in the field. Unlike other studies, this study examined all the capacities of the facility and selected the most feasible based on the current state of the technology. Finally, the LCOH of all four pathways was calculated to understand the performance of photocatalyst materials on the hydrogen production cost.

The panel manufacturing cost was calculated for all four pathways. The material cost made up the highest portion, 64-80%. This is due to the large number of chemicals needed to synthesize the photocatalysts. Another important cost component is labour cost, in the range of 14-30%. Labour is mainly needed in the facility for operating machinery and floor maintenance. Other factors that contribute to manufacturing costs are utility and maintenance costs. The bulk of the material cost is from the electrodes, mainly platinum and silver. Both are noble metals and thus cost-intensive. Together they make up 29-66% of the material cost. In the current stage of the technology, they are needed because they fit the most within the set of physical parameters and inputs to the system and are important for the effective functioning of the cell. Thus, there is an economic trade-off between noble metal use and the LCOH. Costs can be lowered by using or developing alternative materials that serve a similar purpose. Further development of new electrodes made from earth-abundant materials may bring down panel manufacturing costs and ultimately the LCOH.

Economies of the scale benefits were observed by increasing the capacity of the panel manufacturing facility from 500 to 20000 cells per day. The cost of the panel reduced from 229-288 $/panel to 63-110 $/panel with the increasing capacity. The rate of decreasing cost decreases with increased capacities of cell or panel production. For higher capacities, the technology becomes competitive with other green hydrogen production technologies such as wind electrolysis [160]. Hence, with further advancements, large-scale adaptation is feasible with the technology.

The LCOH was calculated for 5000 cells per day and ranged from 4.9-7.8 $/kg of H_2. CNF: TNR had the lowest hydrogen production cost because of the high activity of the photocatalyst material along with fewer materials required for the synthesis of the photocatalyst. g-C_3N_4-S/BiOI had the highest LCOH of 7.8 $/kg of H_2. This is because of the higher material costs which compensate for the higher activity as compared to g-C_3N_4-S This shows that more studies are needed to develop active photocatalysts, and this can further lower the LCOH.

Sensitivity and uncertainty analyses were performed through the RUST model to understand the impact of input parameters on the output of the system. The ranges of LCOH values are $4.9^{+0.75}_{-0.70}$, $5.7^{+0.45}_{-0.65}$, $5.8^{+0.55}_{-1.15}$, and $7.8^{+0.45}_{-0.95}$ $ per kg of H_2 produced for TNR, CNF: TNR, g-C_3N_4-S, and BiOI/g-C_3N_4-S, respectively. It was found that the LCOH varies because of differences in the manufacturing costs of photocatalyst panels. It also found that solar insolation had a great impact on overall costs. With sensitivity and uncertainty analyses, the reliability of the results increases, and the results can be used to develop new policies for photoelectrochemical water splitting technology.

To summarise, currently, photoelectrochemical water splitting has a higher H_2 production cost than conventional technologies, and further research is needed to bring down the cost components. We observed that high panel production capacity can significantly lower manufacturing costs. This

also shows that, with further developments, the technology can easily become a mainstream technology for hydrogen production. Replacing high-cost materials such as silver and platinum and improvements in panel production processes can further reduce the hydrogen production cost.

The developed information can be used for investment decision-making and policy formulation.

Chapter 4: Conclusion and Recommendations

4.1 Conclusion

Past and current energy systems for hydrogen production have left us with a slew of issues that must be solved to make the transition to a low-carbon economy as smooth as possible. To mitigate the effects of climate change, we must reduce our reliance on fossil fuel-based energy sources. This transition can occur if the worldwide focus on energy systems moves to renewable energy sources, such as solar energy, which is abundant, clean, and easy to obtain. Solar energy can be harnessed and converted into useful forms through a variety of technologies. Because the source of solar energy is dispersed and intermittent, and technology is not yet mature, solar energy is costly and requires the use of energy storage systems.

Photocatalytic hydrogen production through solar water splitting is a technology under development that has the potential to be commercialized in the foreseeable future. The hydrogen produced, moreover, has immense potential to mitigate GHG emissions and become cost-competitive with conventional technologies. This thesis developed information for policymakers on the environmental and techno-economic performances of four key photocatalysts: TNR, CNF: TNR, g-C3N4, and g-C_3N_4/BiOI. To accomplish this, LCA and TEA were used.

The LCA provides details on the environmental performance of photocatalysts with GHG emissions and energy consumption as a comparison matrix. A bottom-up LCA model was developed for this analysis considering the life cycle inventory data associated with raw material extraction, photocatalytic cell fabrication, panel production and assembly, operations, and end-of-life phases of the photoelectrochemical water splitting.

- The results showed that in every pathway, energy use in material extraction processes has the largest GHG contribution, between 8% and 89%.

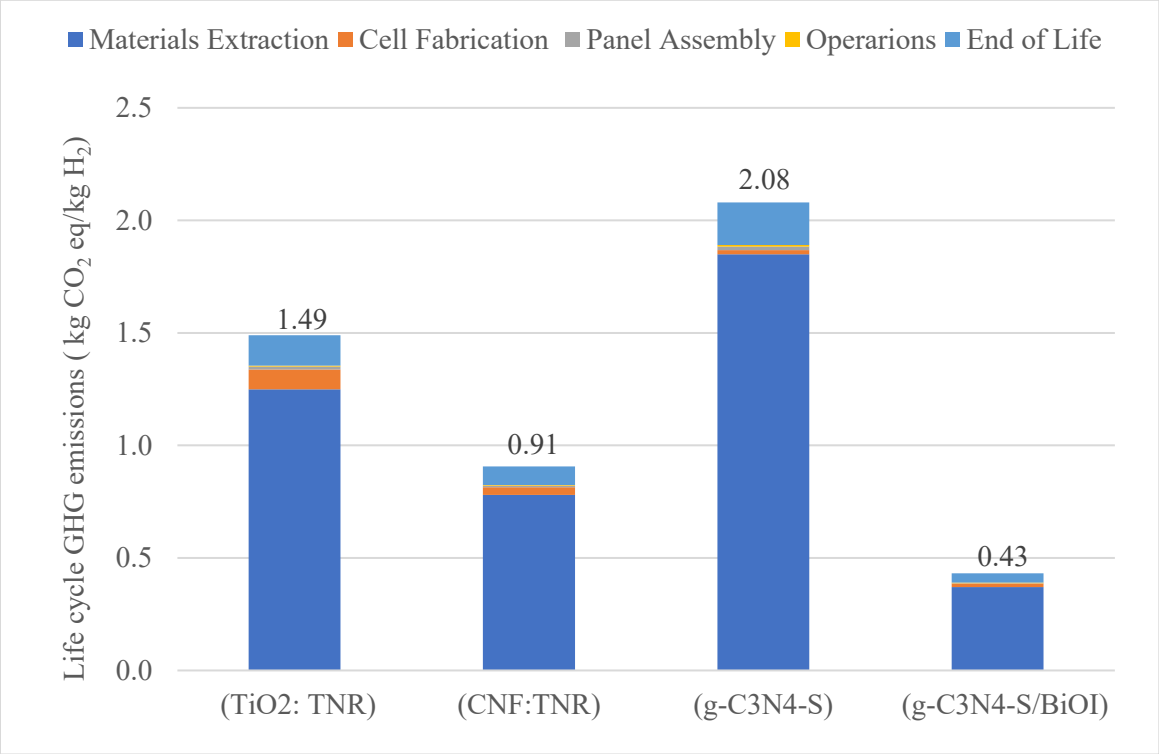

Figure 4.1: Life cycle GHG emissions

- The EPBT was calculated to show how fast the system can pay back the energy consumed during the life cycle. The EPBT ranges from 0.4 to 1.35 years.
- Of the four pathways, the hydrogen production per photocatalytic cell is highest for the g-C_3N_4-S/BiOI; that is, more hydrogen is produced per unit time, which helps recover energy sooner.
- These results also provide leverage to select alternative materials with relatively little higher energy demand, with a trade-off of improved productivity.

- The results from the sensitivity analysis suggest that photocatalytic cell lifetime is the parameter that most influences life cycle GHG emissions.
- It was also found that extracting KOH generates considerable GHG emissions. The results of uncertainty analysis show GHG emissions values of $1.4^{+0.4}_{-0.55}, 0.89^{+0.16}_{-0.24}, 1.96^{+0.24}_{-0.26}$, and $0.49^{+0.21}_{-0.11}$ kg of CO_2 eq per kg of H_2 produced for TNR, CNF: TNR, g-C_3N_4-S, and BiOI/g-C_3N_4-S, respectively. The most uncertainty is in the life span of the cell. The GHG emissions range is higher for TNRs because more photocatalytic cells are required to produce the same amount of hydrogen than for CNF: TNRs.

A bottom-up techno-economic model was developed to evaluate the cost performance of the four hydrogen production pathways. The photocatalytic fabrication is scaled from laboratory to mass production at a base case factory capacity of 5000 cells per day. 5 tonnes of hydrogen per day capacity was considered. Figure 4.2 shows the LCOH breakdown for all the pathways.

- The TEA results show that the LCOH in $/kg of hydrogen ranges from 4.9 (for CNF: TNR) to 7.8 (for g-C3N4-S).
- The two major cost components are capital and labour costs, which contribute 30-37% and 36-46% of the total cost, respectively.
- Material cost is the third major cost, at 14-29% of the total cost. Economies of the scale are found when the panel manufacturing facility capacity increases from 500 to 20000 cells per day. The cost of the panel was reduced from 229-288 $/panel to 70-110 $/panel.

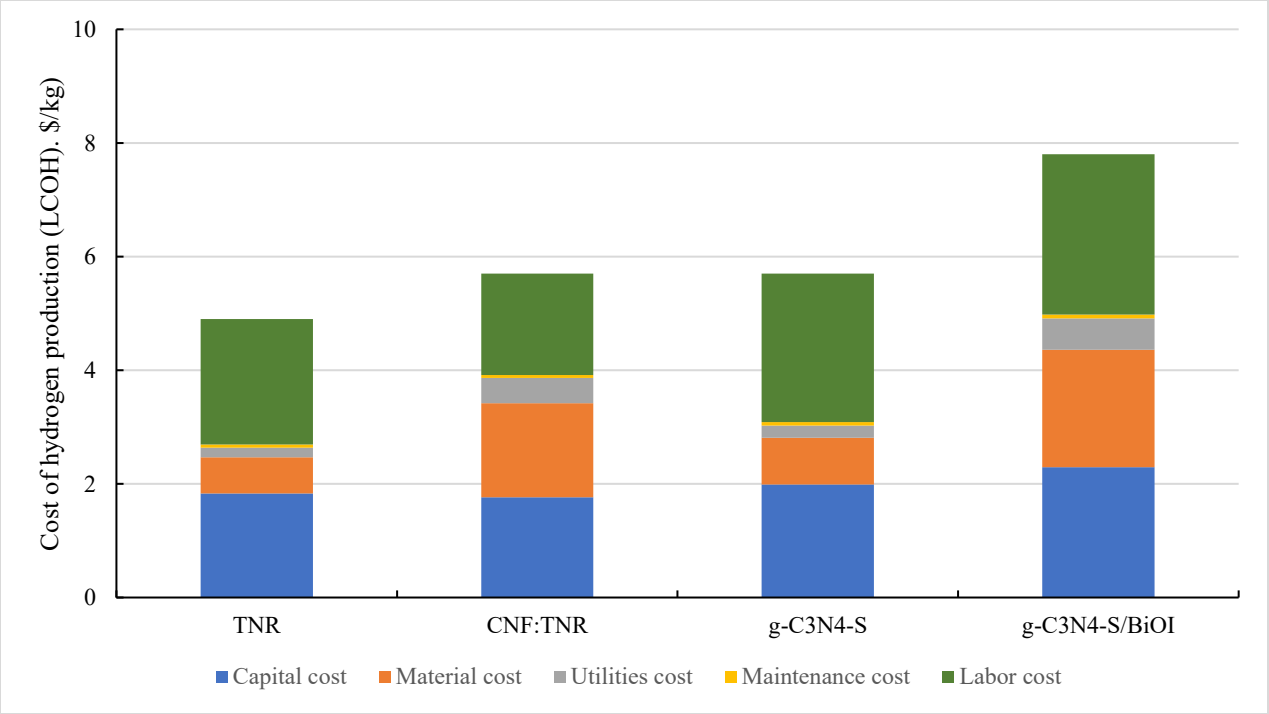

Figure 4.2: LCOH breakdown for all pathways.

- The sensitivity analysis results show that LCOH is sensitive to Alberta's insolation, panel manufacturing cost, and the life span of the facility.
- The uncertainty analysis results show the LCOH range for all the pathways. The LCOH values are $4.9^{+0.75}_{-0.70}$, $5.7^{+0.45}_{-0.65}$, $5.8^{+0.55}_{-1.15}$, and $7.8^{+0.45}_{-0.95}$ $ USD $ per kg of H_2 produced for TNR, CNF: TNR, g-C_3N_4-S, and BiOI/g-C_3N_4-S, respectively.
- The uncertainties are due to panel manufacturing costs and the life span of the facility. A longer facility life span leads to a lower LCOH and vice versa. For panel manufacturing costs, higher costs lead to a higher LCOH and vice versa. The uncertainty in g-C_3N_4-S values is higher than in other photocatalysts because of lower activity.

4.2 Recommendations for future work

The study explored a photocatalytic hydrogen generation pathway from an environmental and economic perspective. To obtain uniform and organized estimates, several assumptions were made about physical parameters and quantities. Following further research is recommended.

- The photocatalytic hydrogen generation pathway assessed here considered four major photocatalysts based on titanium and carbon nitride. With further development and research, new photocatalysts will be developed. There are alternative materials for photocatalyst synthesis. With these new synthesis materials and upcoming photocatalysts, LCA and TEA can be carried out to determine their potential and performance. This approach will provide better insights and points of improvement, which will ultimately assist in improving the technology's environmental and economic performance.
- As hydrogen yield is highly dependent on solar insolation, which ultimately depends on geographical location, location needs to be considered. In this study, Alberta is the geographical location considered. However, the study can be extended by considering other locations, and related hydrogen yields can be compared to observe the correlation between yield, solar insolation, and location.
- The study considers all the parameters such as the cost of equipment or material, supply and demand, solar insolation, and equipment capacity as per present rates or values. The LEAP model can be used to project the cost, GHG reduction potential, and potential to give better insights into planning approaches for future strategies.
- In this study, the photocatalytic panel cost was estimated based on a plant capacity of 5000 cells per day. The results were extended to other plant capacities with a focus on every cost

component up to 20000 cells per day, and cost curves were developed for even higher capacities. Scale factors were developed for several components based on the capacities available in global markets. With the advancement of technology in the manufacturing and design of equipment, higher system capacities are expected to be available soon. More research efforts can be dedicated to extending the work done in this study to include higher capacities and diseconomies of scale to assess the LCOH according to the technological feasibilities.

- GHG emissions were the key and most prominent metric used in this study to compare the environmental performance of photocatalysts. Other environmental indicators such as water footprint can be included to expand the model results. The water footprint is especially relevant because photocatalytic hydrogen generation consumes a huge amount of water and hence is a critical component of studying from an environmental performance point of view.
- The thesis focuses on a high-level comparison of hydrogen production pathways. A detailed study can be carried out for other technologies for a detailed comparative assessment with other conventional modes of hydrogen production.

References

1. British Petroleum, Statistical review of world energy in 2012. [cited January 12, 2022]; Available from: https://www.laohamutuk.org/DVD/docs/BPWER2012report.pdf.
2. Wu, X. and G. Chen, *Global primary energy use associated with production, consumption and international trade.* Energy Policy, 2017. **111**: p. 85-94.
3. Sartbaeva, A., et al., *Hydrogen nexus in a sustainable energy future.* Energy & Environmental Science, 2008. **1**(1): p. 79-85.
4. Collins, M., et al., *Long-term climate change: projections, commitments and irreversibility*, in *Climate Change 2013: The Physical Science Basis: Contribution of Working Group I to the Fifth Assessment Report of the Intergovernmental Panel on Climate Change*, T.F. Stocker, et al., Editors. 2013, Cambridge University Press: Cambridge, United Kingdom and New York, NY, USA. p. 1029-1136.
5. Jones, G.A. and K.J. Warner, *The 21st century population-energy-climate nexus.* Energy Policy, 2016. **93**: p. 206-212.
6. Staffell, I., et al., *The role of hydrogen and fuel cells in the global energy system.* Energy & Environmental Science, 2019. **12**(2): p. 463-491.
7. Statistics Canada. Table 25-10-0029-01 Supply and demand of primary and secondary energy in terajoules, annual. Statistics Canada. Table 2022 [cited 2021 July 1]; Available from: https://www150.statcan.gc.ca/t1/tbl1/en/tv.action?pid=2510002901.
8. Hydrogen Council, Hydrogen scaling up: A sustainable pathway for the global energy transition. 2017, Hydrogen Council: Brussels, Belgium. [cited June 13, 2021]; Available from: https://hydrogencouncil.com/wp-content/uploads/2017/11/Hydrogen-scaling-up-Hydrogen-Council.pdf.
9. IRENA, Hydrogen from renewable power: Technology outlook for the energy transition,. 2018, International Renewable Energy Agency: Abu Dhabi. [cited October 10, 2020];

Available from: https://www.irena.org/-/media/Files/IRENA/Agency/Publication/2018/Sep/IRENA_Hydrogen_from_renewable_power_2018.pdf.

10. Spath, P.L. and M.K. Mann, *Life cycle assessment of hydrogen production via natural gas steam reforming*. 2000, National Renewable Energy Lab., Golden, CO (US).
11. Verma, A. and A. Kumar, *Life cycle assessment of hydrogen production from underground coal gasification.* Applied Energy, 2015. **147**: p. 556-568.
12. Bauer, C., et al., *On the climate impacts of blue hydrogen production.* Sustainable Energy & Fuels, 2022. **6**(1): p. 66-75.
13. Navas-Anguita, Z., et al., *Revisiting the role of steam methane reforming with CO2 capture and storage for long-term hydrogen production.* Science of the total Environment, 2021. **771**: p. 145432.
14. Granovskii, M., I. Dincer, and M.A. Rosen, *Exergetic life cycle assessment of hydrogen production from renewables.* Journal of Power Sources, 2007. **167**(2): p. 461-471.
15. Hoogwijk, M.M., *On the global and regional potential of renewable energy sources*. 2004.
16. Wu, H., Tan, H. L., Toe, C. Y., Scott, J., Wang, L., Amal, R., & Ng, Y. H. (2020). *Photocatalytic and photoelectrochemical systems: similarities and differences.* Advanced Materials, 32(18), 1904717.
17. Bahnemann, D.W., *Current challenges in photocatalysis: Improved photocatalysts and appropriate photoreactor engineering.* Research on Chemical Intermediates, 2000. **26**(2): p. 207-220.
18. Fujishima, A. and K. Honda, *Electrochemical photolysis of water at a semiconductor electrode.* Nature, 1972. **238**(5358): p. 37-38.

19. Yuan, L., et al., *Photocatalytic water splitting for solar hydrogen generation: fundamentals and recent advancements.* International Reviews in Physical Chemistry, 2016. **35**(1): p. 1-36.

20. Kahng, S., H. Yoo, and J.H. Kim, *Recent advances in earth-abundant photocatalyst materials for solar H2 production.* Advanced Powder Technology, 2020. **31**(1): p. 11-28.

21. Corredor, J., et al., *Comprehensive review and future perspectives on the photocatalytic hydrogen production.* Journal of Chemical Technology & Biotechnology, 2019. **94**(10): p. 3049-3063.

22. Zhu, J. and M. Zäch, *Nanostructured materials for photocatalytic hydrogen production.* Current Opinion in Colloid & Interface Science, 2009. **4**(14): p. 260-269.

23. Pulido Melián, E., et al., *Efficient and affordable hydrogen production by water photo-splitting using TiO_2-based photocatalysts.* International Journal of Hydrogen Energy, 2013. **38**(5): p. 2144-2155.

24. Lin, Y., et al., *The optical absorption and hydrogen production by water splitting of (Si,Fe)-codoped anatase TiO2 photocatalyst.* International Journal of Hydrogen Energy, 2013. **38**(13): p. 5209-5214.

25. Ali, A. and P.K. Shen, *Recent progress in carbon nitride-based nanostructured electrocatalysts for overall water splitting.* Electrochemical Energy Reviews, 2020. **3**: p. 370-394.

26. Xie, G., et al., *Graphene-based materials for hydrogen generation from light-driven water splitting.* Advanced Materials, 2013. **25**(28): p. 3820-3839.

27. Lu, Y.-C., et al., *Facile synthesis of oxygen and sulfur co-doped graphitic carbon nitride fluorescent quantum dots and their application for mercury (II) detection and bioimaging.* Journal of Materials Chemistry C, 2015. **3**(1): p. 73-78.

28. Kumar, P., Kar, P., Manuel, A. P., Zeng, S., Thakur, U. K., Alam, K. M., ... & Shankar, K. (2020). *Noble metal free, visible light driven photocatalysis using TiO2 nanotube arrays sensitized by P-doped C3N4 quantum dots.* Advanced Optical Materials, 8(4), 1901275.

29. Maeda, K. and K. Domen, *Photocatalytic water splitting: recent progress and future challenges.* The Journal of Physical Chemistry Letters, 2010. **1**(18): p. 2655-2661.

30. Standardization, I.O.f., *Environmental management: life cycle assessment; Principles and Framework*. 2006, ISO.

31. Standardization, I.O.f., *Environmental management: life cycle assessment; requirements and guidelines*. 2006, ISO Geneva, Switzerland.

32. Twidell, J., *Renewable energy resources*. 2021: Routledge.

33. Finnveden, G., et al., *Recent developments in life cycle assessment.* Journal of environmental management, 2009. **91**(1): p. 1-21.

34. Buchner, G.A., N. Wulfes, and R. Schomäcker, *Techno-economic assessment of CO2-containing polyurethane rubbers.* Journal of CO2 Utilization, 2020. **36**: p. 153-168.

35. Zhai, P., et al., *Net primary energy balance of a solar-driven photoelectrochemical water-splitting device.* Energy & Environmental Science, 2013. **6**(8): p. 2380-2389.

36. Trudewind, C.A., A. Schreiber, and D. Haumann, *Photocatalytic methanol and methane production using captured CO2 from coal power plants. Part II–well-to-wheel analysis on fuels for passenger transportation services.* Journal of Cleaner Production, 2014. **70**: p. 38-49.

37. Sathre, R., et al., *Life-cycle net energy assessment of large-scale hydrogen production via photoelectrochemical water splitting.* Energy & Environmental Science, 2014. **7**(10): p. 3264-3278.

38. U.S. Geological Survey. Mineral Commodity Summaries 2019. 2019, U.S. Geological Survey [cited November 30, 2021]; Available from: https://prd-wret.s3-us-west-2.amazonaws.com/assets/palladium/production/atoms/files/mcs2019_all.pdf.

39. Vinothkumar, N. and M. De, *Enhanced photocatalytic hydrogen production from water–methanol mixture using cerium and nonmetals (B/C/N/S) co-doped titanium dioxide.* Materials for Renewable and Sustainable Energy, 2014. **3**(2): p. 1-10.

40. Xie, F., et al., *A critical review on solvent extraction of rare earths from aqueous solutions.* Minerals Engineering, 2014. **56**: p. 10-28.

41. Chaudhari, S., D. Gupta, and B. Gopalakrishnan, *Investigation of Relationship between System Efficiency Curve & Measurement and Verification (M&V) of Energy Savings.* SAE International Journal of Materials and Manufacturing, 2011. **4**(1): p. 486-494.

42. Grimm, A., W.A. de Jong, and G.J. Kramer, *Renewable hydrogen production: A techno-economic comparison of photoelectrochemical cells and photovoltaic-electrolysis.* International Journal of Hydrogen Energy, 2020. **45**(43): p. 22545-22555.

43. Goto, Y., et al., *A particulate photocatalyst water-splitting panel for large-scale solar hydrogen generation.* Joule, 2018. **2**(3): p. 509-520.

44. Grube, T., et al., *A techno-economic perspective on solar-to-hydrogen concepts through 2025.* Sustainable Energy & Fuels, 2020. **4**(11): p. 5818-5834.

45. Pinaud, B.A., et al., *Technical and economic feasibility of centralized facilities for solar hydrogen production via photocatalysis and photoelectrochemistry.* Energy & Environmental Science, 2013. **6**(7): p. 1983-2002.

46. James, B.D., G.N. Baum, J. Perez, and K.N. Baum. Technoeconomic Analysis of Photoelectrochemical (PEC) Hydrogen Production. 2009: Arlington, Virginia [cited August 28, 2021]; Available from: https://www1.eere.energy.gov/hydrogenandfuelcells/pdfs/pec_technoeconomic_analysis.pdf.

47. U.S. Energy Information Administration. *World Energy Balances: Overview*. 2019 [cited 2020 August 3]; Available from: https://www.iea.org/reports/world-energy-balances-overview

48. Herzog, H. and J. David. *The Cost of Carbon Capture*. in *Fifth International Conference on Greenhouse Gas Control Technologies. Cairns, Australia*. 2000.

49. Huang, C.-H. and C.-S. Tan, *A review: CO2 utilization.* Aerosol and Air Quality Research, 2014. **14**(2): p. 480-499.

50. van Vuuren, D.P., M. van Sluisveld, and A.F. Hof, *Implications of long-term scenarios for medium-term targets (2050).* PBL Netherlands Environmental Assessment Agency, 2015.

51. Can, S., *Supply and demand of primary and secondary energy in terajoules, annual, Nova Scotia.* Statistics Canada. Table, 2007: p. 128-0009.

52. Hydrogen Council, *Hydrogen scaling up, A sustainable pathway for the global energy transition.* Hydrogen Council: Brussels, Belgium, 2017.

53. Gielen, D., *Hydrogen from renewable power technology outlook for the energy transition.* Institution of Gas Engineers & Managers, 2018.

54. Stiegel, G.J. and M. Ramezan, *Hydrogen from coal gasification: An economical pathway to a sustainable energy future.* International Journal of Coal Geology, 2006. **65**(3-4): p. 173-190.

55. Taibi, E., et al., *Hydrogen from renewable power: Technology outlook for the energy transition.* 2018.

56. Sun, P., et al., *Criteria Air Pollutants and Greenhouse Gas Emissions from Hydrogen Production in US Steam Methane Reforming Facilities.* Environmental Science & Technology, 2019. **53**(12): p. 7103-7113.

57. Olateju, B. and Kumar A., *Hydrogen production from wind energy in Western Canada for upgrading bitumen from oil sands.* Energy, 2011. **36**(11): p. 6326-6339.

58. Kabir, E., et al., *Solar energy: Potential and future prospects.* Renewable and Sustainable Energy Reviews, 2018. **82**: p. 894-900.

59. Utgikar, V. and T. Thiesen, *Life cycle assessment of high temperature electrolysis for hydrogen production via nuclear energy.* International Journal of Hydrogen Energy, 2006. **31**(7): p. 939-944.

60. Patyk, A., T.M. Bachmann, and A. Brisse, *Life cycle assessment of H2 generation with high temperature electrolysis.* International Journal of Hydrogen Energy, 2013. **38**(10): p. 3865-3880.

61. Ghandehariun, S. and A. Kumar, *Life cycle assessment of wind-based hydrogen production in Western Canada.* International Journal of Hydrogen Energy, 2016. **41**(22): p. 9696-9704.

62. Ozbilen, A., I. Dincer, and M.A. Rosen, *Comparative environmental impact and efficiency assessment of selected hydrogen production methods.* Environmental Impact Assessment Review, 2013. **42**: p. 1-9.

63. Tolcin, A., *Mineral Commodity Summaries 2019.* US Geological Survey: Virginia, VA, USA, 2011: p. 74-75.

64. Kumar, P., et al., *Arrays of TiO2 nanorods embedded with fluorine doped carbon nitride quantum dots (CNFQDs) for visible light driven water splitting.* Carbon, 2018. **137**: p. 174-187.

65. Alam, K.M., et al., *Enhanced charge separation in gC 3 N 4–BiOI heterostructures for visible light driven photoelectrochemical water splitting.* Nanoscale Advances, 2019. **1**(4): p. 1460-1471.

66. Ameta, R. and S.C. Ameta, *Photocatalysis: principles and applications*. 2016: Crc Press.

67. Qu, Y. and X. Duan, *Progress, challenge and perspective of heterogeneous photocatalysts.* Chemical Society Reviews, 2013. **42**(7): p. 2568-2580.

68. Braham, R.J. and A.T. Harris, *Review of major design and scale-up considerations for solar photocatalytic reactors.* Industrial & Engineering Chemistry Research, 2009. **48**(19): p. 8890-8905.

69. Fan, K., et al., *Pt-free tandem molecular photoelectrochemical cells for water splitting driven by visible light.* Physical Chemistry Chemical Physics, 2014. **16**(46): p. 25234-25240.

70. Peter, L.M. and K. Upul Wijayantha, *Photoelectrochemical water splitting at semiconductor electrodes: fundamental problems and new perspectives.* ChemPhysChem, 2014. **15**(10): p. 1983-1995.

71. Li, X., et al., *Light illuminated α− Fe 2 O 3/Pt nanoparticles as water activation agent for photoelectrochemical water splitting.* Scientific Reports, 2015. **5**(1): p. 1-7.

72. Papageorgiou, N., *Counter-electrode function in nanocrystalline photoelectrochemical cell configurations.* Coordination Chemistry Reviews, 2004. **248**(13-14): p. 1421-1446.

73. Chae, S.Y., et al., *Improved photoelectrochemical water oxidation kinetics using a TiO 2 nanorod array photoanode decorated with graphene oxide in a neutral pH solution.* Physical Chemistry Chemical Physics, 2015. **17**(12): p. 7714-7719.

74. Kistler, T.A., et al., *Integrated Membrane-Electrode-Assembly Photoelectrochemical Cell under Various Feed Conditions for Solar Water Splitting.* Journal of The Electrochemical Society, 2018. **166**(5): p. H3020.

75. Maeda, K., *Photocatalytic water splitting using semiconductor particles: history and recent developments.* Journal of Photochemistry and Photobiology C: Photochemistry Reviews, 2011. **12**(4): p. 237-268.

76. Wang, X., et al., *One-dimensional titanium dioxide nanomaterials: nanowires, nanorods, and nanobelts.* Chemical reviews, 2014. **114**(19): p. 9346-9384.

77. Wang, Z., et al., *Multiply structural optimized strategies for bismuth oxyhalide photocatalysis and their environmental application.* Chemical Engineering Journal, 2019. **374**: p. 1025-1045.

78. Yang, B., et al., *Perovskite solar cells with near 100% internal quantum efficiency based on large single crystalline grains and vertical bulk heterojunctions.* Journal of the American Chemical Society, 2015. **137**(29): p. 9210-9213.

79. Ball, J.M., et al., *Low-temperature processed meso-superstructured to thin-film perovskite solar cells.* Energy & Environmental Science, 2013. **6**(6): p. 1739-1743.

80. Thakur, U.K., et al., *Halide perovskite solar cells using monocrystalline TiO2 nanorod arrays as electron transport layers: impact of nanorod morphology.* Nanotechnology, 2017. **28**(27): p. 274001.

81. Liang, Z., et al., *Hydrogenated TiO2 nanorod arrays decorated with carbon quantum dots toward efficient photoelectrochemical water splitting.* ACS Applied Materials & Interfaces, 2019. **11**(21): p. 19167-19175.

82. Wang, W., et al., *gC 3 N 4 quantum dots: direct synthesis, upconversion properties and photocatalytic application.* Chemical Communications, 2014. **50**(70): p. 10148-10150.

83. Mishra, A., et al., *Photocatalysis of graphene and carbon nitride-based functional carbon quantum dots*, in *Nanoscale Materials in Water Purification*. 2019, Elsevier. p. 759-781.

84. Zhou, L., et al., *Recent advances in non-metal modification of graphitic carbon nitride for photocatalysis: a historic review.* Catalysis Science & Technology, 2016. **6**(19): p. 7002-7023.

85. Wang, J., *Barriers of scaling-up fuel cells: cost, durability and reliability.* Energy, 2015. **80**: p. 509-521.

86. James, R., *Life cycle analysis: power studies compilation report.* National Energy Technology Laboratory, US Department of Energy, Pittsburgh, PA, 2011.

87. Wernet, G., et al., *The ecoinvent database version 3 (part I): overview and methodology.* The International Journal of Life Cycle Assessment, 2016. **21**(9): p. 1218-1230.

88. Wang, M.Q., *GREET 1.5: Transportation Fuel-Cycle Model. Vol. 1: Methodology, Development, Use, and Results*. 1999, Argonne National Laboratory.

89. CH Instrumentation. *Electrochemical Instrumentation*. 2020 18/5/2020 (dd/mm/yyyy)]; Available from: qrins.com/ckseo/chi/ctlg/CHI.pdf.

90. Dai, Q., et al., *Update of bill-of-materials and cathode materials production for lithium-ion batteries in the GREET model.* Argonne National Laboratory, 2018.

91. Wang, M., et al., *Summary of Expansions and Updates in GREET® 2020*. 2020, Argonne National Lab.(ANL), Argonne, IL (United States).

92. Agricultural Land Resource Atlas of Alberta. *Annual solar radiation of Alberta, 1971 to 2000*. 2020 [cited 2021 February 2]; Available from: https://www1.agric.gov.ab.ca/$Department/deptdocs.nsf/all/agdex10305/$FILE/pg_10_annual_solar.pdf.

93. Koroneos, C., et al., *Life cycle assessment of hydrogen fuel production processes.* International Journal of Hydrogen Energy, 2004. **29**(14): p. 1443-1450.

94. Maljusch, A. and M. Wullenkord, *Technoeconomic Analysis of PEC Water Splitting at Various Scales*, in *Advances in Photoelectrochemical Water Splitting*. 2018, Royal Society of Chemistry. p. 266-284.

95. Stewart, M., *Surface production operations: pumps and compressors*. Vol. IV. 2018: Gulf Professional Publishing.

96. Acklands Grainger. *Air compressor 3/60/460V*. 2020 [cited 2020 March 3]; Available from: https://www.grainger.ca/en/product/AIR-COMPRESSOR-15HP-3-60-460V/p/IRGUP6-15T15-46-3?analytics=RecommendationZones&cm_sp=IDP-_-RV-_-RR-_-PR-_-NT-NA-_-EN.

97. Alibaba. *PLant water desalination equipment*. 2020 [cited 2020 March 3]; Available from: https://www.alibaba.com/product-detail/Plant-Water-Desalination-Equipment-Portable-Water_1600192721306.html?spm=a2700.galleryofferlist.normal_offer.d_title.6e881c66Eh854i&s=p.

98. Purchasing.com. *Introduction to the Air Compressor Buying Process*. 2021 [cited 2020 March 3]; Available from: https://www.purchasing.com/construction-equipment/air-

compressors/purchasing-guide/index.html#:~:text=For%20example%2C%20it's%20estimated%20that,of%2010%20to%2015%20years.

99. Nieuwlaar, E. and E. Alsema, *Energy pay-back time (EPBT) and CO2 mitigation potential.* Environmental Aspects of PV Power Systems, IEA PVPS Task, 1997. **1**: p. 25-27.

100. Government of Canada. *Platinum facts*. 2020 [cited 2021 March 3]; Available from: https://www.nrcan.gc.ca/our-natural-resources/minerals-mining/minerals-metals-facts/platinum-facts/20520.

101. Davis, M., M. Ahiduzzaman, and A. Kumar, *How will Canada's greenhouse gas emissions change by 2050? A disaggregated analysis of past and future greenhouse gas emissions using bottom-up energy modelling and Sankey diagrams.* Applied Energy, 2018. **220**: p. 754-786.

102. United States Environmental Protection Agency. *Emission factors for greenhouse gas inventories*. 2020 [cited 2020 November 11]; Available from: https://www.epa.gov/sites/production/files/2020-04/documents/ghg-emission-factors-hub.pdf.

103. Environment and Climate Change Canada. *Emission factors*. 2020 [cited 2021 January 2]; Available from: http://data.ec.gc.ca/data/substances/monitor/canada-s-official-greenhouse-gas-inventory/Emission_Factors.pdf.

104. Campolongo, F., J. Cariboni, and A. Saltelli, *An effective screening design for sensitivity analysis of large models.* Environmental Modelling & Software, 2007. **22**(10): p. 1509-1518.

105. Muller, S., et al., *The application of the pedigree approach to the distributions foreseen in ecoinvent v3.* The International Journal of Life Cycle Assessment, 2016. **21**(9): p. 1327-1337.

106. Di Lullo, G., et al., *Extending sensitivity analysis using regression to effectively disseminate life cycle assessment results.* The International Journal of Life Cycle Assessment, 2020. **25**(2): p. 222-239.

107. BCS Incorporated. *Mining industry of the future: energy and environmental profile of the U.S. mining industry*. 2002 [cited 2021 March 3]; Available from: https://www.energy.gov/sites/prod/files/2013/11/f4/gold-silver.pdf.

108. A.O. Oni, K.A., T. Giwa, G. Di Lullo, A. Kumar,, *Comparative assessment of blue hydrogen from steam methane reforming, autothermal reforming, and natural gas decomposition technologies for natural gas-producing regions.* Energy Conversion and Management, 2022.

109. Bhandari, R., C.A. Trudewind, and P. Zapp, *Life cycle assessment of hydrogen production via electrolysis–a review.* Journal of Cleaner Production, 2014. **85**: p. 151-163.

110. Ministry of Foreign Affairs of Denmark. *Wind energy FAQs: carbon and GHG payback period*. 2020 [cited 2021 April 1]; Available from: https://www.offshorewindadvisory.com/faqs-ghg-payback/.

111. Gómez-Camacho, C.E. and B. Ruggeri, *Energy sustainability analysis (ESA) of energy-producing processes: A case study on distributed H2 production.* Sustainability, 2019. **11**(18): p. 4911.

112. Celik, I., et al., *Life cycle assessment (LCA) of perovskite PV cells projected from lab to fab.* Solar Energy Materials and Solar Cells; Life cycle, Environmental, Ecology and Impact Analysis of Solar Technology, 2016. **156**: p. 157-169.

113. Bloomfield, P., *Trends in global temperature.* Climatic change, 1992. **21**(1): p. 1-16.

114. David, J. and H. Herzog. *The Cost of Carbon Capture*. in *Fifth International Conference on Greenhouse Gas ControlTtechnologies*. 2012. Cairns, Australia.

115. United Nations Climate Change. What is the Paris Agreement? 2015 [cited 2020; Available from: https://unfccc.int/process-and-meetings/the-paris-agreement/what-is-the-paris-agreement.

116. James, B.D., et al., Technoeconomic analysis of photoelectrochemical (PEC) hydrogen production. DOE report, 2009. Available from: https://pubs.rsc.org/en/content/articlepdf/2020/se/d0se00896f

117. HomeGuide. How much do solar panels cost? 2020; [cited 2021 March 15]; Available from: https://homeguide.com/costs/solar-panel-cost#factors.

118. Systems, P. Pump cost. 2020; [cited 2021 March 15]; Available from: https://www.pumpsandsystems.com/how-much-do-electric-motors-really-cost-0.

119. Cole-Palmer. Pumps. 2020; [cited 2021 March 15]; Available from: https://www.coleparmer.ca/i/masterflex-i-p-brushless-process-drive-with-high-performance-pump-head-for-high-performance-precision-tubing-33-to-650-rpm-90-to-260-vac/7796320?PubID=UZ&persist=true&ip=no&gclid=Cj0KCQiAjKqABhDLARIsABbJrGknhFEqUq0viN19LCTH_epxWXGR3bTA_l5eaaSLF8648AlQ3SYjZZwaAqq-EALw_wcB.

120. Grainger. Compressor Air Rotary. 2020 [date accessed 24-11-2020]; Available from: https://www.grainger.ca/en/product/COMPRESSOR-AIR-ROTARY-75HP-575V-3PH/p/CPCCPE75-575?analytics=RecommendationZones&cm_sp=IDP-_-CAV-_-TR-_-PR-_-PLA-NA-_-EN&cm_mmc=PPC:+Google+PLA.

121. Corp., U.S.P. PVC Pipe. 2020 [date accessed 24-11-2021]; Available from: https://www.usplastic.com/catalog/item.aspx?itemid=23979.

122. Today, U. *Land Cost. 2020* [date accessed 24-11-2021]; Available from: https://www.usatoday.com/story/money/2019/05/08/the-most-and-least-valuable-states/39442329/.

123. Alberta. Custom rates 2017-Land clearing and breaking. 2020 [date accessed 24-11-2021]; Available from: https://www.alberta.ca/custom-rates-2017-land-clearing-and-breaking.aspx.

124. EPCOR. Water Rates. 2020 [date accessed 24-11-2021]; Available from: https://www.epcor.com/products-services/water/rates-terms-conditions/Pages/residential-water-wastewater-rates.aspx.

125. Alibaba. Water Filter System. 2020 [date accessed 24-11-2021]; Available from: https://www.alibaba.com/product-detail/1500LPH-Purified-Water-Deionized-EDI-Water_62237239845.html?spm=a2700.wholesale.deiletai6.4.25e45459woTn5U.

126. Alibaba. Water Storage Tank. 2020 [date accessed 24-11-2021]; Available from: https://www.alibaba.com/product-detail/50000-Liter-Water-Storage-Tank-Underground_60523189322.html?spm=a2700.galleryofferlist.normal_offer.d_title.2d8b77ecAR6WXd&s=p.

127. Alibaba. Regulated Storage Tank. 2020 [date accessed 24-11-2021]; Available from: https://www.alibaba.com/product-detail/Skid-mounted-LNG-Tank-Automobile-Filling_62380186225.html?spm=a2700.details.deiletai6.52.4086305dWDgbyA.

128. Chang, N.L., et al., *A manufacturing cost estimation method with uncertainty analysis and its application to perovskite on glass photovoltaic modules.* Progress in Photovoltaics: Research and Applications, 2017. **25**(5): p. 390-405.

129. Piccinno, F., et al., *From laboratory to industrial scale: A scale-up framework for chemical processes in life cycle assessment studies.* Journal of Cleaner Production, 2016. **135**: p. 1085-1097.

130. CH Instruments. Electrochemical Instrumentation. 2020 18/5/2020 (dd/mm/yyyy)]; Available from: qrins.com/ckseo/chi/ctlg/CHI.pdf.

131. Alibaba.com. Platinum Electrodes. 2020 [date accessed 24-11-2021]; Available from: https://tjaida.en.alibaba.com/product/1600159860619-822561765/Best_Price_Superior_Quality_Platinum_Electrodes_Cell.html?spm=a2700.shop_pl.41413.24.19e07fe2904VnZ.

132. Metals, M.P. Monex Live Silver Spot Price. 2020 [date accessed 24-11-2021]; Available from: monex.com/silver-prices/.

133. Alibaba. 2020 24-11-2020]; [date accessed 24-11-2021]; Available from: https://www.alibaba.com/product-detail/Pvc-Pvc-Recycled-Plastic-Sheet-Pvc_1600142626900.html?spm=a2700.galleryofferlist.normal_offer.d_title.357543d59U12ab&s=p.

134. Alibaba. Membranes. 2020 [date accessed 24-11-2021]; Available from: https://www.alibaba.com/product-detail/Ptfe-Membrane-Ptfe-Membrane-UNM-

Best_1600164492115.html?spm=a2700.galleryofferlist.topad_classic.d_title.4e39d82dstPxie.

135. Walmart. Great Value 4L Distilled Water. 2021 [date accessed 24-11-2021]; Available from: https://www.walmart.ca/en/ip/great-value-4l-distilled-water/6000143710020.

136. Alibaba. Potassium Hydroxide Powder. 2020 [date accessed 24-11-2021]; Available from: https://www.alibaba.com/product-detail/Caustic-potash-industrial-flakes-potassium-hydroxide_1600101372883.html?spm=a2700.galleryofferlist.topad_classic.d_title.76655ed4wmZLh5&fullFirstScreen=true.

137. Canada, B. Sodium Sulphate. 2020 [date accessed 24-11-2021]; Available from: https://www.bioshopcanada.com/secure/detail.asp?Pin=SOS513&PriceShow=CDN.

138. Alibaba. Tetrabutyle Titanate. 2020 [date accessed 24-11-2021]; Available from: https://www.alibaba.com/product-detail/cas-5593-70-4-Tetrabutyl-titanate_1600062037670.html?spm=a2700.galleryofferlist.normal_offer.d_title.7f57798537nEiL.

139. Alibaba. Acetic Acid Liquid. 2020 [date accessed 24-11-2021]; Available from: https://www.alibaba.com/product-detail/Acetic-Acid-TOP-1-Manufacturer-Glacial_2010801458.html?spm=a2700.galleryofferlist.topad_classic.d_title.7ff456badFi6R1.

140. Alibaba. Granular Urea. 2020 [date accessed 24-11-2021]; Available from: https://www.alibaba.com/product-detail/Urea-Granular-Ammonium-Sulfate-Fertilizer-Urea_1600280386310.html?spm=a2700.galleryofferlist.normal_offer.d_title.298146eeD7XxpB&s=p.

141. avantor. Ammonium Floride 40% in aqueous solution. 2020 [date accessed 24-11-2021]; Available from: https://ca.vwr.com/store/product/en/9354924/ammonium-fluoride-40-in-aqueous-solution-finyte-j-t-baker.

142. Aeromatics, N.D. Citric Acid (Anhydrous). 2020 24-11-2020]; Available from: https://www.newdirectionsaromatics.ca/products/raw-materials/citric-acid-anhydrous-uspfcc.html.

143. TCI. 2020 24-11-2020]; Available from: https://www.tcichemicals.com/CA/en/p/C0454.

144. Intratec. Ammonium Chloride Prices. 2020 [date accessed 24-11-2021]; Available from: https://www.intratec.us/chemical-markets/ammonium-chloride-price.

145. Intratec. Ethylene Glycol Prices. 2020 [date accessed 24-11-2021]; Available from: https://www.intratec.us/chemical-markets/ethylene-glycol-price.

146. Depot, I. Potassium Iodide +99%. 2020 [date accessed 24-11-2021]; Available from: https://www.ingredientdepot.com/products/potassium-iodide-1-kg?variant=13020212592712&currency=CAD&utm_medium=product_sync&utm_source=google&utm_content=sag_organic&utm_campaign=sag_organic&utm_campaign=gs-2020-05-30&utm_source=google&utm_medium=smart_campaign.

147. García-Valverde, R., J.A. Cherni, and A. Urbina, *Life cycle analysis of organic photovoltaic technologies.* Progress in Photovoltaics: Research and Applications, 2010. **18**(7): p. 535-558.

148. Abuazza, O.A., A. Labib, and B.M. Savage, *Development of an auditing framework by integrating ISO 9001 principles within auditing.* International Journal of Quality & Reliability Management, 2019.

149. Akbari, M., A.O. Oyedun, and A. Kumar, *Comparative energy and techno-economic analyses of two different configurations for hydrothermal carbonization of yard waste.* Bioresource Technology Reports, 2019. **7**: p. 100210.

150. Brown, T., *Engineering economics and economic design for process engineers*. 2016: CRC Press.

151. Li, J. and N. Wu, *Semiconductor-based photocatalysts and photoelectrochemical cells for solar fuel generation: a review.* Catalysis Science & Technology, 2015. **5**(3): p. 1360-1384.

152. Tutorials, A.E. Photovoltaics Turn Photons into Electrons. 2021 [date accessed 12-09-2021]; Available from: https://www.alternative-energy-tutorials.com/photovoltaics/photovoltaics-turn-photons-into-electrons.html.

153. Payscale. Production Worker. 2021 [date accessed 12-09-2021]; Available from: https://www.payscale.com/.

154. BCS Incorporated, Mining industry of the future: energy and environmental profile of the U.S. mining industry. 2002.

155. Poór, P., M. Šimon, and M. Karková, *CMMS as an effective solution for company maintenance costs reduction.* Production Management and Engineering Sciences, 2015: p. 241-246.

156. Magazine, P. Hydrogen, Don't give up! 2020 [date accessed 12-09-2021]; Available from: https://www.pv-magazine.com/2018/04/09/hydrogen-dont-give-up/.

157. Noussan, M., et al., *The Role of Green and Blue Hydrogen in the Energy Transition: A Technological and Geopolitical Perspective. Sustainability 2021, 13, 298*. 2020, s Note: MDPI stays neu-tral with regard to jurisdictional clai-ms in ….

158. Lemus, R.G. and J.M.M. Duart, *Updated hydrogen production costs and parities for conventional and renewable technologies.* International Journal of Hydrogen Energy, 2010. **35**(9): p. 3929-3936.

159. Ayodeji Okunlola, M.D., Temitayo Giwa, Giovanni Di Lullo, Eskinder Gemechu, Karina Anaya, Abayomi Olufemi Oni, Minza Haider, Amit Kumar, Tanveer Hassan Mehedi, *Identification and assessment of opportunities for hydrogen in Alberta's economy*. 2021.

160. Olateju, B., A. Kumar, and M. Secanell, *A techno-economic assessment of large scale wind-hydrogen production with energy storage in Western Canada.* International Journal of Hydrogen Energy, 2016. **41**(21): p. 8755-8776.

161. Alibaba. Ultrasonic Spray. 2021 [date accessed 12-09-2021]; Available from: https://www.alibaba.com/product-detail/Ultrasonic-spray-pyrolysis-coating-machine-for_62464262527.html?spm=a2700.galleryofferlist.normal_offer.d_title.11d73b43NeV0RU&bypass=true.

162. Alibaba. Nano Spray Coating. 2021 [date accessed 12-09-2021]; Available from: https://www.alibaba.com/product-detail/Ultrasonic-Spray-Coater-Nano-Thin-Film_60759453258.html?spm=a2700.details.deiletai6.8.19394a21eteIib.

163. Alibaba. Ultrasonic Spray coater. 2021 [date accessed 12-09-2021]; Available from: https://www.alibaba.com/product-detail/Ultrasonic-Spray-Coater-Nano-Thin-Film_60759453258.html?spm=a2700.details.deiletai6.8.19394a21eteIib.

164. Alibaba. Industrial Conveying Ultrasonic Machine. 2021 02-02-2021]; Available from: https://www.alibaba.com/product-detail/UAM8000-Industrial-Conveying-Ultrasonic-Spraying-

Machine_62381664164.html?spm=a2700.galleryofferlist.normal_offer.d_title.2b055deaTZW3h1.

165. Alibaba. Industrial Spray Machine. 2021 [date accessed 12-09-2021]; Available from: https://www.alibaba.com/product-detail/UAM8000-Industrial-Conveying-Ultrasonic-Spraying-Machine_62381664164.html?spm=a2700.galleryofferlist.normal_offer.d_title.2b055deaTZW3h1.

166. Alibaba. Industrial Furnace. 2021 [date accessed 12-09-2021]; Available from: https://www.alibaba.com/product-detail/Furnace-Industrial-Furnace-Manufacturers-IR-Drying_60815572522.html?spm=a2700.galleryofferlist.normal_offer.d_title.5d4f2616ltDcB3&s=p&bypass=true.

167. Alibaba. High Temperature Furnace. 2021 [date accessed 12-09-2021]; Available from: https://www.alibaba.com/product-detail/High-temperature-heat-treatment-annealing-furnace_60640324143.html?spm=0.details.0.0.40b75b5anQ8l2i.

168. Alibaba. Industrial Furnace Large Capacity. 2021 [date accessed 12-09-2021]; Available from: https://www.alibaba.com/product-detail/Furnace-Industrial-Industrial-Furnace-Car-bottom_1918774410.html?spm=a2700.galleryofferlist.normal_offer.d_title.5d4f2616ltDcB3&s=p.

169. Alibaba. Calcinating Furnace. 2021 [date accessed 12-09-2021]; Available from: https://www.alibaba.com/product-detail/Furnace-Industrial-Industrial-Furnace-Car-bottom_1918774410.html?spm=a2700.galleryofferlist.normal_offer.d_title.5d4f2616ltDcB3&s=p.

170. Alibaba. Oven GMH Series 100. 2021 [date accessed 12-09-2021]; Available from: https://www.alibaba.com/product-detail/Oven-DMH-Series100-Class-Purification-Dry_1600177199068.html?spm=a2700.galleryofferlist.normal_offer.d_title.3c744e89RdTPaP&s=p.

171. Alibaba. Industrial Oven. 2021 [date accessed 12-09-2021]; Available from: https://www.alibaba.com/product-detail/Industrial-Powder-Coating-Batch-Oven_62239589044.html?spm=a2700.wholesale.deiletai6.10.975923d8KU1FUk.

172. Alibaba. Large Curing Oven. 2021 [date accessed 12-09-2021]; Available from: https://www.alibaba.com/product-detail/Large-Powder-Coating-Curing-Oven_62247149143.html?spm=a2700.wholesale.deiletai6.6.28ad1fcfV6gHFJ.

173. Alibaba. Ultrasonic Equipment Processor. 2021 [date accessed 12-09-2021]; Available from: https://www.alibaba.com/product-detail/Ultrasonic-Dispersion-Ultrasonic-Ultrasonic-Equipment-Processor_60797910600.html?spm=a2700.galleryofferlist.normal_offer.d_title.3a8121bd0Fm623&s=p&bypass=true.

174. Agricultural Land Resource Atlas of Alberta. Annual Solar Radiation of Alberta, 1971 to 2000. 2020 [date accessed 12-09-2021]; Available from: https://www1.agric.gov.ab.ca/$Department/deptdocs.nsf/all/agdex10305/$FILE/pg_10_annual_solar.pdf.

175. Government of Canada. Regulations. 2021 [date accessed 12-09-2021]; Available from: https://laws.justice.gc.ca/eng/regulations/sor-86-304/page-19.htm.

176. Solar choice. How much do Solar Panels cost? 2021 [date accessed 12-09-2021]; Available from: https://www.solarchoice.net.au/blog/solar-power-system-prices.

177. ElectronicDesign. The True Cost of Solar Energy. [date accessed 12-09-2021]; Available from: https://www.powerelectronics.com/technologies/alternative-energy/article/21864098/the-true-cost-of-solar-energy.

Appendix A

A1: Flowchart of synthesis of TNR and CNF: TNR Photocatalyst

The flowchart is prepared by adapting the methodology explained by Kumar et al. [64, 65]. The synthesis of photocatalyst is used to design the system for the fabrication of photocatalytic cells for mass-scale production.

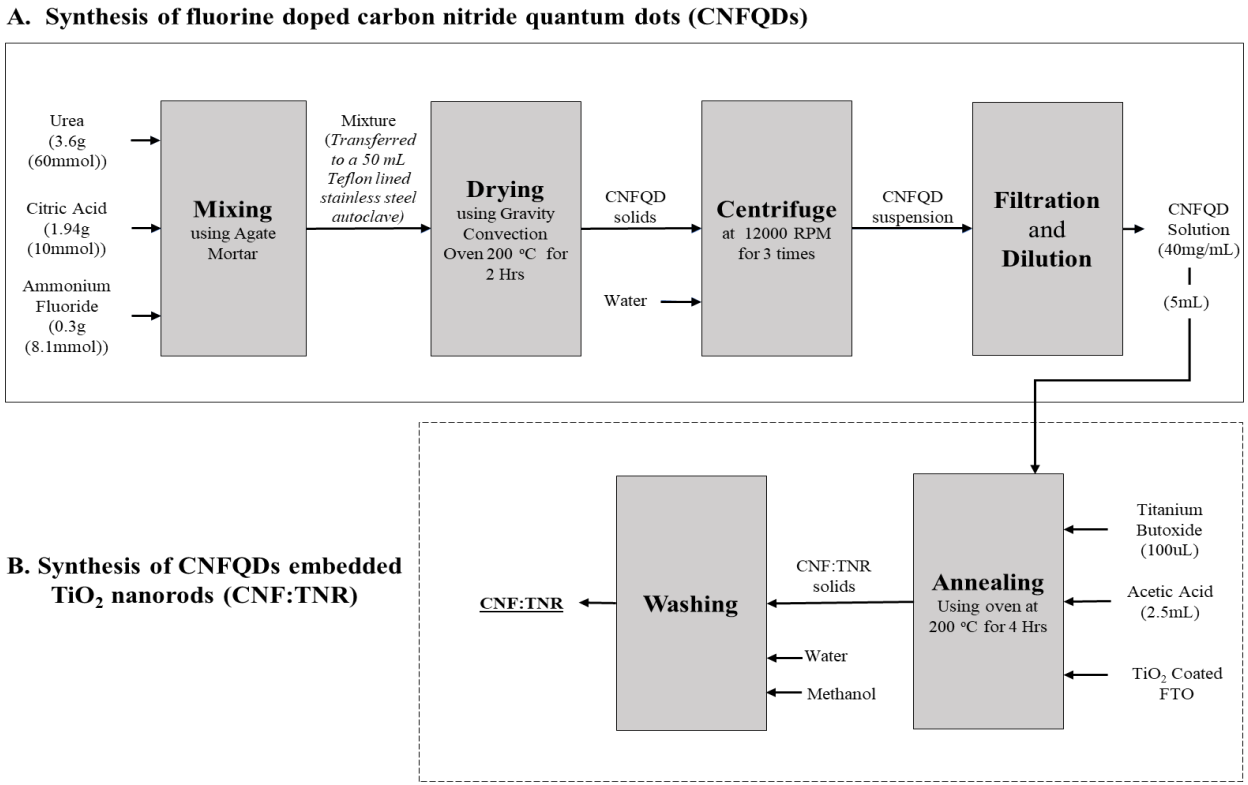

Figure A9: Flowchart of synthesis of TNR and CNF: TNR

A2: Flowchart of synthesis of g-C_3N_4-S and g-C_3N_4/BiOI Photocatalyst

The flowchart is prepared by adapting the methodology explained by Kumar et al. [64, 65]. The synthesis of photocatalyst is used to design the system for the fabrication of photocatalytic cells for mass-scale production.

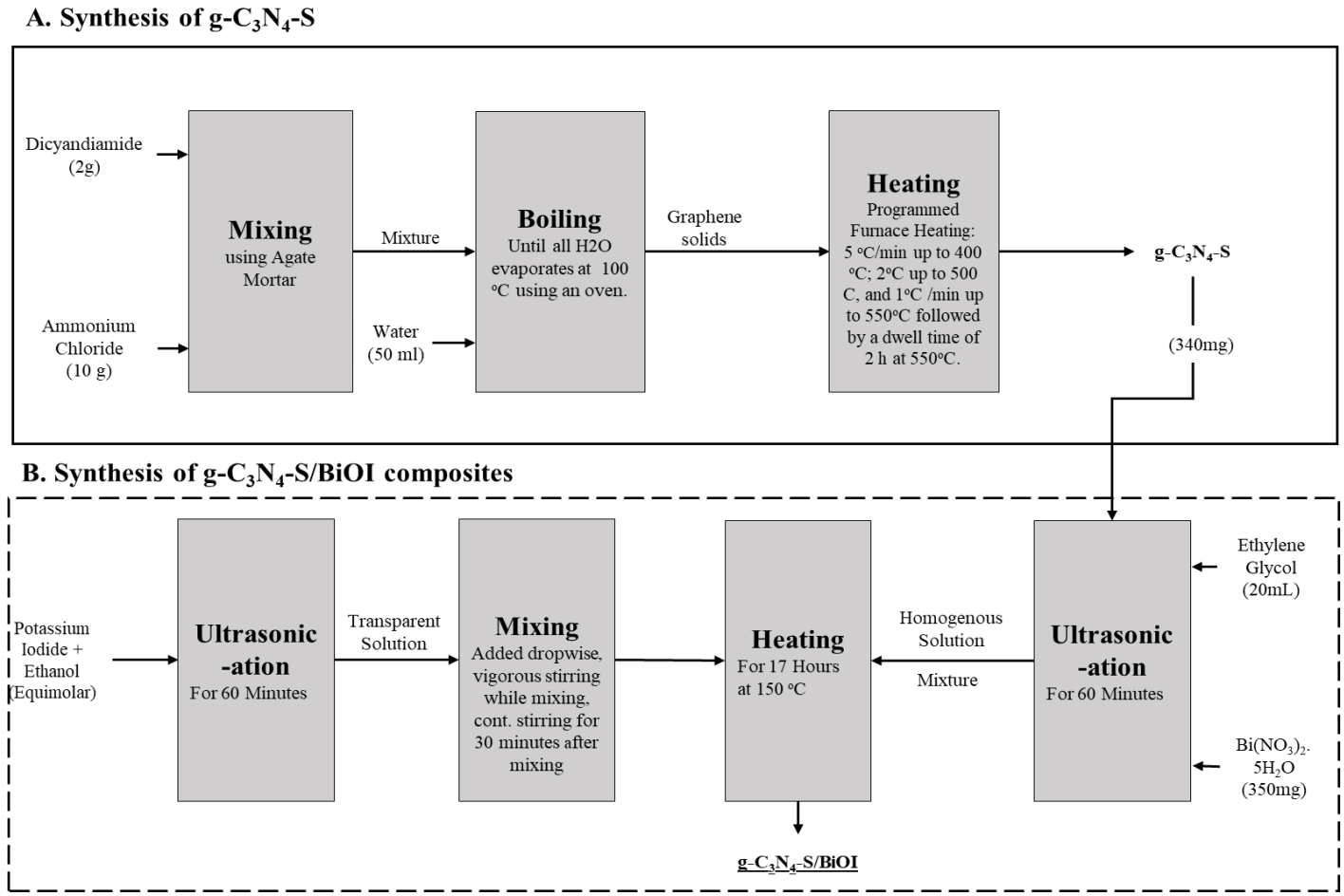

Figure A10: Flowchart of synthesis of g-C_3N_4-S and g-C_3N_4/BiOI

A3: Fabrication and Process design

A3 cites all the processes required for the fabrication of photocatalysts for mass production. Processes such as stirring, and cleaning systems are not critical for the overall system and hence are supportive (shown as white boxes) in nature. Processes such as ultrasonic coating, calcination and annealing govern the overall production capacity of the facility in terms of cells per day, and hence are important to the system. These are part of the critical path of the process. For every process, the critical path is highlighted and the time duration for each activity is cited to find the key process in the critical path.

i. Fabrication of TNR:

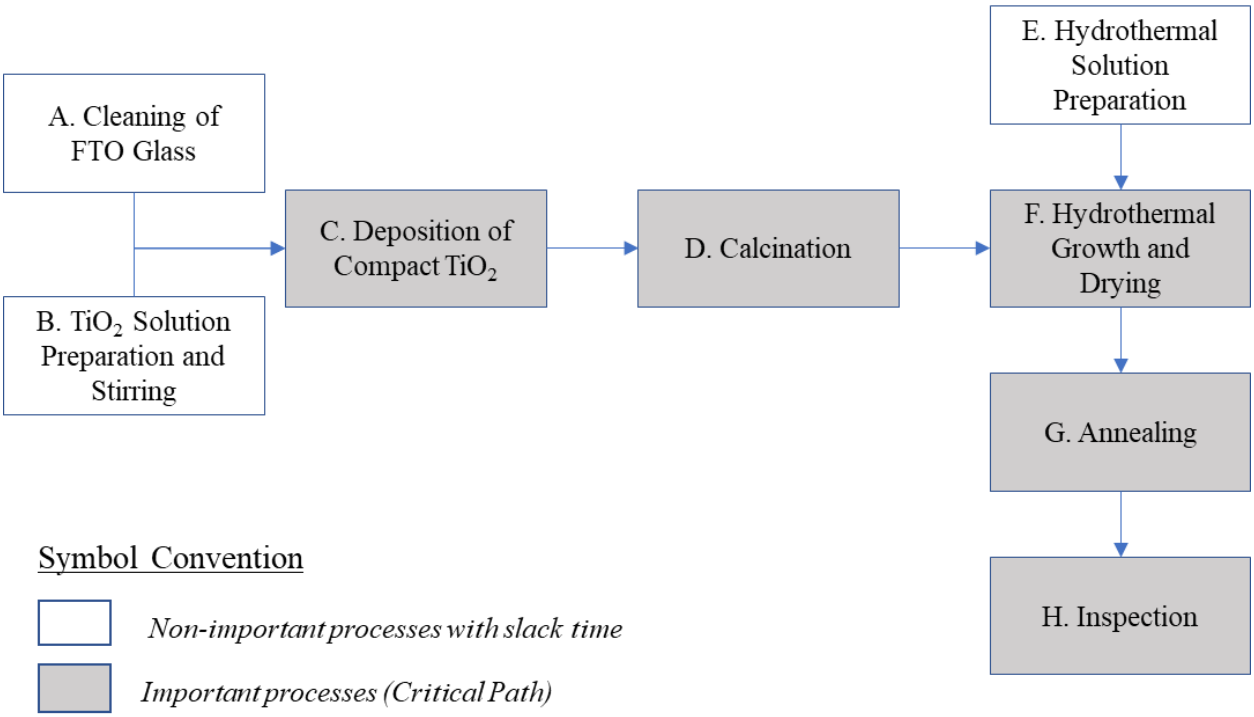

Figure A11: Layout for Process Design and Fabrication for TNR

Table A5: Process parameter description for TNR

Component series	Component Name	Process Name	Process Duration
A	Ultrasonic Cleaning System	Cleaning of FTO Glass	30 Minutes
B	Stirrer	TiO_2 Solution Preparation and Stirring	8 Hours
C	Ultrasonic Coating System	Deposition of Compact TiO_2	30 Seconds
D	Large Walk-in Furnace-I	Calcination	30 Minutes
E	Preparation of Hydrothermal Solution	Hydrothermal Solution Preparation	2 Hours
F	Large Walk-in Furnace-II	Hydrothermal Growth and Drying	1 Hour
G	Large Walk-in Furnace-III	Annealing	4 hours
H	Testing Table	Inspection	15 Minutes

ii. Fabrication of CNF:TNR:

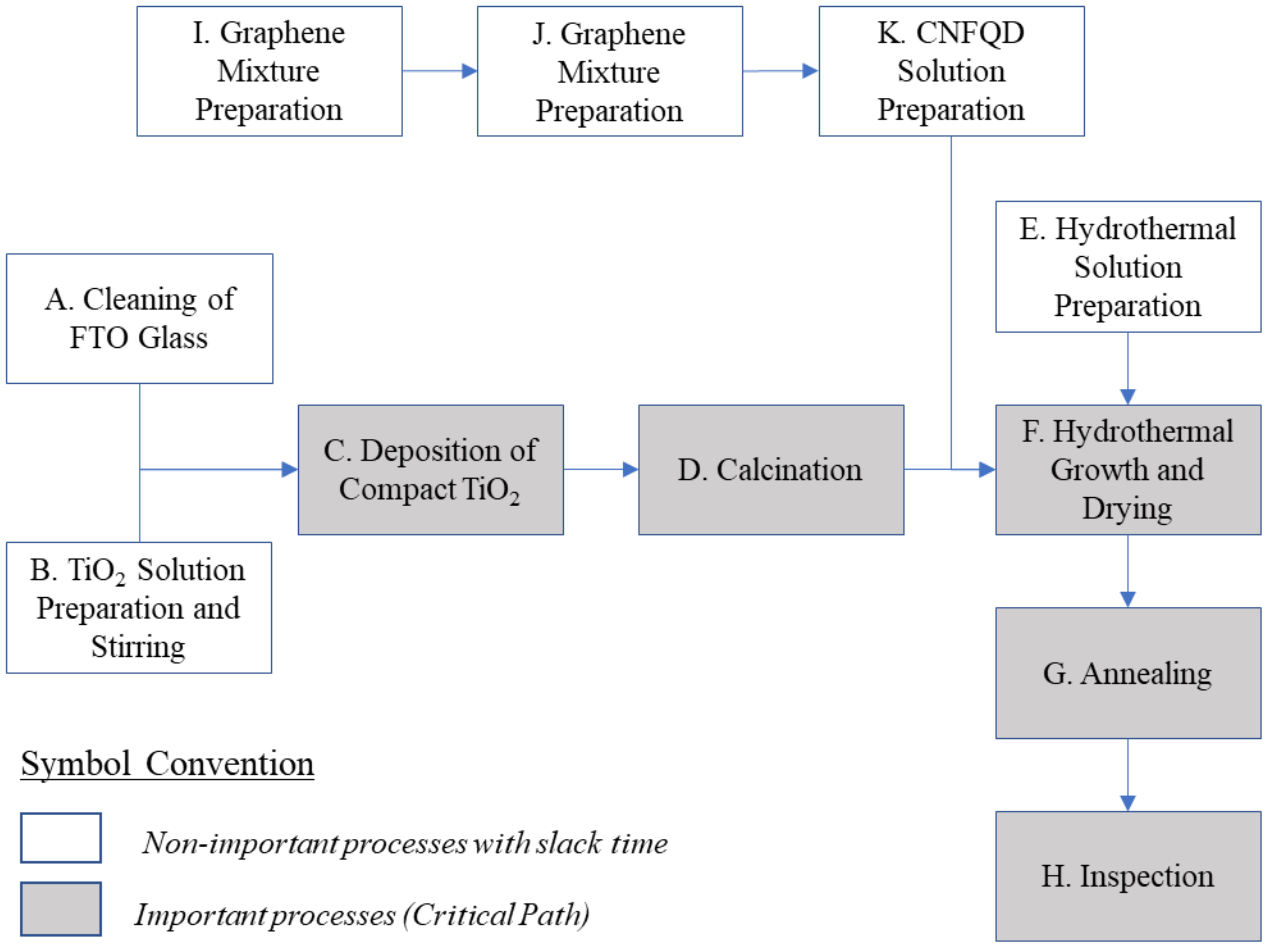

Figure A12- Layout for Process Design and Fabrication for CNF: TNR

Table A6- Process parameter description for CNF: TNR

Component series	Component Name	Process Name	Process Duration
A	Ultrasonic Cleaning System	Cleaning of FTO Glass	30 Minutes
B	Stirrer	TiO_2 Solution Preparation and Stirring	8 Hours
C	Ultrasonic Coating System	Deposition of Compact TiO_2	30 Seconds
D	Large Walk-in Furnace-I	Calcination	30 Minutes
E	Preparation of Hydrothermal Solution	Hydrothermal Solution Preparation	2 Hours
F	Large Walk-in Furnace-II	Hydrothermal Growth and Drying	1 Hour
G	Large Walk-in Furnace-III	Annealing	4 hours
H	Testing Table	Inspection	15 Minutes
I	Gravity Convection Oven	Carbon nitride Mixture Preparation	2 Hours
J	Centrifuge	CNFQD Suspension Preparation	15 Minutes
K	Filtration and Dilution	CNFQD Solution Preparation	2 Hours

iii. Fabrication of g-C_3N_4-S:

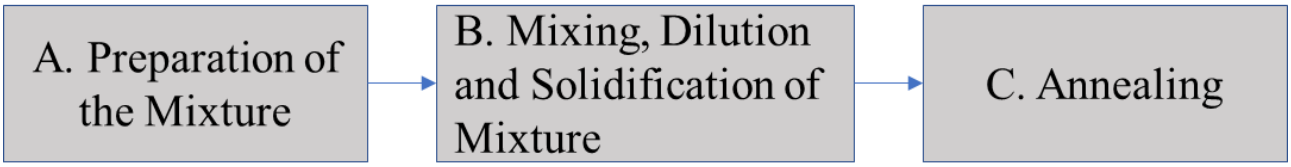

Figure A13- Layout for Process Design and Fabrication for g-C3N4-S

Table A7- Process parameter description for g-C3N4-S

Component series	Component Name	Process Name	Process Duration
A	Agate Mortar	Preparation of the Mixture	5 Minutes
B	Solidification	Mixing, Dilution and Solidification of Mixture	15 Minutes
C	Large Walk-in Furnace	Annealing	5 Hours

iv. Fabrication of g-C_3N_4/BiOI:

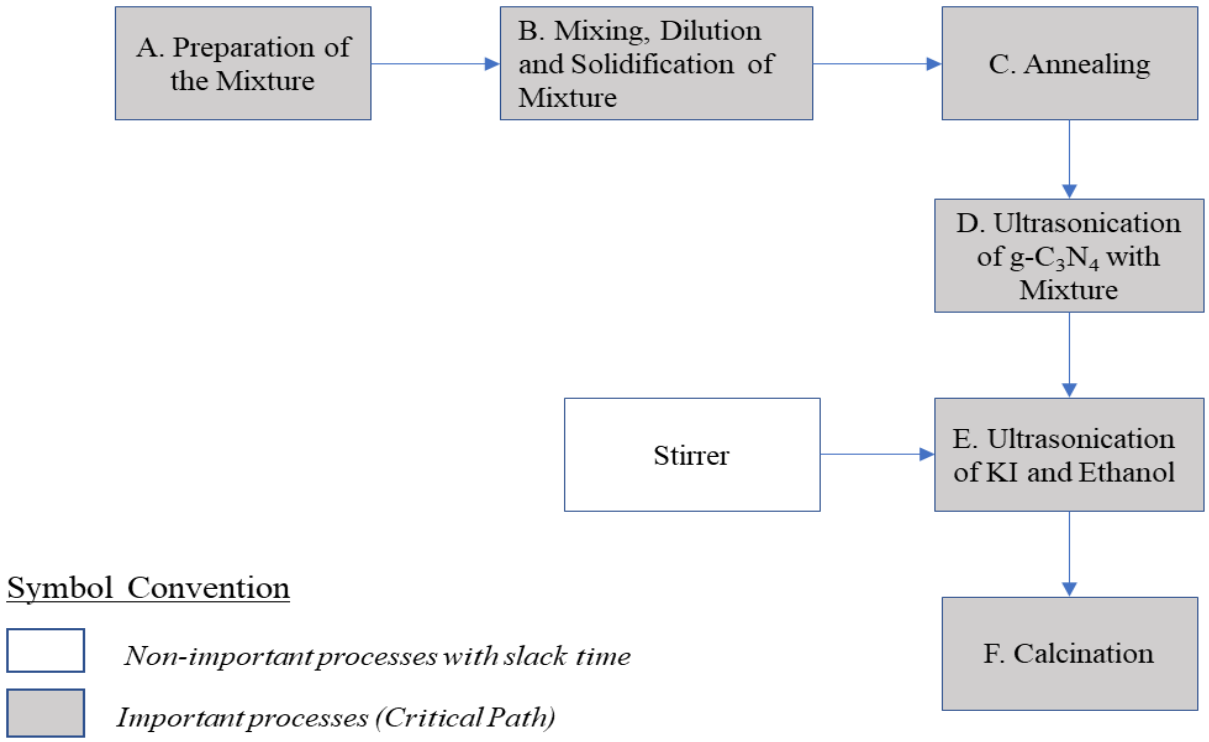

Figure A14- Layout for Process Design and Fabrication for g-C3N4/BiOI

Table A8- Process parameter description for g-C3N4/BiOI

Component series	Component Name	Process Name	Process Duration
A	Agate Mortar	Preparation of the Mixture	5 Minutes
B	Solidification	Mixing, Dilution and Solidification of Mixture	15 Minutes
C	Large Walk-in Furnace-I	Annealing	5 Hours
D	Ultrasonication-I	Ultrasonication of g-C_3N_4 with Mixture	1 Hour
E	Ultrasonication-II	Ultrasonication of KI and Ethanol	30 Minutes
F	*Stirrer*	Mixing the Solution	1 Hour
G	Large Walk-in Furnace-II	Calcination	14 Hours

A4: Inventory analysis of fabrication steps

Refers to the quantification of materials and energy for photocatalyst fabrication for one cell at a lab scale. The methodology of fabrication is adapted from Kumar et al. [64, 65]**.** Depending on the quantity of material or amount of primary energy consumed, cumulative energy demand (CED) and greenhouse gas emissions (GHG) were calculated.

Table A9- Inventory analysis of fabrication steps for TNR

Process	Material/Energy/Output	Material	Amount	Unit	CED (MJ/Unit)	GHG (Gram Eq CO_2/Unit)
Cleaning the FTO Glass (P1)	**Material**	FTO coated glass slides	11.14	g	0.28	21.17
		Acetone	10.00	ml	0.39	20.21
		Methanol	10.00	ml	0.38	19.80
		Deionized water	10.00	ml	0.0001	8.56
	Energy	Electrical (Sonication)	Machine Input		0.003	0.003
	Output	**Sonicated FTO Glass**			0.77	40.47
Deposition of compact TiO_2 (P2)	**Material**	Sonicated FTO Glass				
		Titanium (IV) iso propoxide	0.43	g	0.03	2.34
		1 M HCl	0.07	ml	0.002	0.16
		iso propanol	2.53	ml	0.12	7.92
	Energy	Energy (Stirring)	Machine Input		0.02	0.02
		Energy (Spin cast)	Machine Input		0.005	0.01
		Electricity (Calcination)	Machine Input		0.002	0.002
	Output	**TiO_2 deposited FTO glass slides**			0.16	12.05

Table A10- Inventory analysis of fabrication steps for CNF: TNR

Process	Material/Energy/Output	Material	Amount	Unit	CED (MJ/Unit)	GHG (Gram Eq CO_2/Unit)
Cleaning the FTO Glass (P1)	Material	FTO coated glass slides	11.14	g	0.28	21.17
		Acetone	10.00	ml	0.39	20.21
		Methanol	10.00	ml	0.38	19.80
		Deionized water	10.00	ml	0.0001	8.56
	Energy	Electrical (Sonication) (1)	Machine Input		0.003	0.46
	Output					
		Sonicated FTO Glass			0.77	40.47
Deposition of compact TiO_2 (P2)	Material	Sonicated FTO Glass				
		Titanium (IV) iso propoxide	0.43	g	0.03	2.34
		1 M HCl	0.07	ml	0.002	0.16
		iso propanol	2.53	ml	0.12	7.92
	Energy	Energy (Stirring)	Machine Input		0.02	2.80
		Energy (Spin cast)	Machine Input		0.01	0.83
		Electricity (Calcination)	Machine Input		0.002	0.34
	Output	**TiO2 deposited FTO glass slides**			0.16	12.05
Synthesis of fluorine-doped carbon nitride quantum dots (CNFQDs) (P3)	Material	PTFE Membrane	5.00	g	0.56	36.33
		Citric Acid	1.94	g	0.07	6.04
		Urea	3.60	g	0.10	1.29
		Ammonium Fluoride	0.30	g	0.01	0.67
	Energy	Energy (Agate Morter)	Manual Input		0.0000	0.00
		Energy (Gravity Convection Oven)	Machine Input		0.02	2.86
		Electricity (Centrifuge)	Machine Input		0.04	5.61
	Output	**Fluorine doped carbon nitride quantum dots (CNFQDs)**			0.056	8.47
Synthesis of CNFQDs embedded TiO_2 nanorods	Material	CNFQD	From the previous Step			
		Titanium Butoxide	0.43	g	0.03	2.34
		Acetic Acid	2.62	g	0.08	2.52
		HCl	2.50	ml	0.09	5.89

(CNF: TNR) (P4)	**Energy**	Energy (Gravity Convection Oven)	Machine Input	0.01	1.43
	Output	**CNFQDs embedded TiO_2 nanorods (CNF: TNR)**		0.11	7.32

Table A11- Inventory analysis of fabrication steps for g-C3N4-S

Process	Material/Energy/Output	Material	Amount	Unit	CED (MJ/Unit)	GHG (Gram Eq CO_2/Unit)
Synthesis of g-C_3N_4-S (CNS) (P5)	**Material**	Dicyandiamide	2.00	g	0.12	9.38
		NH_4Cl	10.00	g	0.40	26.49
		Water	50.00	mL	0.001	4.28
	Energy	Energy (Agate Morter)	Manual Input		0.0000	0.0000
		Energy (Programmed Heating)	Machine Input		0.032	0.03
	Output	**g-C_3N_4-S (CNS)**			0.032	4.91

Table A12- Inventory analysis of fabrication steps for g-C3N4/BiOI

Process	Material/Energy/Output	Material	Amount	Unit	CED (MJ/Unit)	GHG (Gram Eq CO_2/Unit)
Synthesis of g-C_3N_4-S (CNS) (P5)	Material	Dicyandiamide	2.00	g	0.12	9.38
		NH_4Cl	10.00	g	0.40	26.49
		Water	50.00	mL	0.001	4.28
	Energy	Energy (Agate Morter)	Manual Input		0.0000	0.00
		Energy (Programmed Heating)	Machine Input		0.03	4.91
	Output	**g-C_3N_4-S (CNS)**			0.03	4.91
Synthesis of g-C_3N_4-S (CNS) (P6)	Material	g-C3N4-S (CNS)	From the previous Step			
		Bismuth Nitrate	0.35	g	0.03	3.10
		Ethylene Glycol	22.26	g	0.86	56.82
		KI	10.00	g	0.83	72.85
		Ethanol	10.00	g	0.47	24.51
	Energy	Energy (Ultrasonication)	Machine Input		0.03	5.30
		Energy (Ultrasonication-KI)	Machine Input		0.01	1.79
		Energy (Stirring)	Machine Input		0.04	6.44
		Energy (Oven Heating)	Machine Input		0.06	9.12
	Output	**Fluorine-doped carbon nitride quantum dots (CNFQDs)**			0.62	47.15

A5: Equipment Sizing

This is the list of equipment available commercially for unit operations of the system. The power vs capacity relationship clarifies that power and capacity are not linearly dependent. Depending on the number of cells to be produced, appropriate equipment is selected to optimize the power consumption. This directly impacts the GHG emissions per kg of H_2 production. In this study, 5000 cells per day capacity of the facility is assumed. Cycle time for each piece of equipment in overall photocatalyst fabrication is noted. The closest equipment to the capacity of 5000 cells (or more) is selected.

Table A13- Equipment for process design

Applicable to TNR, CNF: TNR				Process: Spray Coating
Power (W)	**Spray area(cm^2)**	**Time per cell (MIN)**	**Capacity**	**Source**
3500	400	0.5	102	Alibaba. com[161]
5000	1750	0.5	448	Alibaba.com [162]
8000	2500	0.5	640	Alibaba.com [163]
11000	3240	0.5	829	Alibaba.com [164]
110000	120000	0.5	30720	Alibaba.com [165]
Applicable to TNR, CNF: TNR				Process: Calcination (Furnace)
Power (W)	**Volume(cm^3)**	**Time per cell (MIN)**	**Capacity**	**Source**
15000	468300	30	681	Alibaba.com [166]
40000	2456400	30	3573	Alibaba.com [167]
950000	30000000	30	43636	Alibaba.com [168]
210000	57600000	30	83782	Alibaba.com [169]
Applicable to TNR, CNF: TNR				Process: Drying + HT growth (Furnace)
Power (W)	**Volume(cm^3)**	**Time per cell (MIN)**	**Capacity**	**Source**
15000	468300	60	341	Alibaba.com [166]
39000	2456400	60	1786	Alibaba.com [167]
950000	24000000	60	17455	Alibaba.com [168]
210000	134750000	60	98000	Alibaba.com [169]

Applicable to TNR, CNF:TNR			Process: Annealing (Furnace)	
Power (W)	**Volume(cm^3)**	**Time per cell (MIN)**	**Capacity**	**Source**
15000	468300	240	85	Alibaba.com [166]
39000	2456400	240	447	Alibaba.com [167]
950000	30000000	240	5455	Alibaba.com [168]
210000	134750000	240	24500	Alibaba.com [169]

Applicable to CNF:TNR			Process: Oven Heating (Gravity Convection Oven*)	
Power (W)	**Volume(cm^3)**	**Time per cell (MIN)**	**Capacity**	**Source**
15000	3328000	240	4538	Alibaba.com [170]
18000	4032000	240	5498	Alibaba.com [171]
20000	18050000	240	24614	Alibaba.com [172]

**The convection oven can work overnight, and hence have a lead of 8 hrs.*

Applicable to g-C_3N_4-S			Process: Solidification (Furnace)	
Power (W)	**Volume(cm^3)**	**Time per cell (MIN)**	**Capacity**	**Source**
15000	468300	15	1362	Alibaba.com [166]
39000	2456400	15	7146	Alibaba.com [167]
950000	30000000	15	87273	Alibaba.com [168]
210000	57600000	15	167564	Alibaba.com [169]

Applicable to g-C_3N_4-S			Process: Annealing (Furnace)	
Power (W)	**Volume(cm^3)**	**Time per cell (MIN)**	**Capacity**	**Source**
15000	468300	300	68	Alibaba.com [166]
39000	2456400	300	357	Alibaba.com [167]
950000	30000000	300	4364	Alibaba.com [168]
210000	134750000	300	20533	Alibaba.com [169]

Applicable to g-C_3N_4/BiOI			Process: Ultrasonication of Carbon nitride	
Power (W)	**Volume (L)**	**Time per cell (MIN)**	**Capacity**	**Source**
1500	25	60	1800	Alibaba.com [173]
2250	50	60	3600	Alibaba.com [173]
3000	300	60	21600	Alibaba.com [173]

Applicable to g-C_3N_4/BiOI				Process: Ultrasonication of KI+Ethanol
Power (W)	**Volume (L)**	**Time per cell (MIN)**	**Capacity**	**Source**
1500	25	30	2400	Alibaba.com [173]
2250	50	30	4800	Alibaba.com [173]
3000	300	30	28800	Alibaba.com [173]

Applicable to g-C_3N_4/BiOI				Process: Calcination (Furnace)
Power (W)	**Volume(cm^3)**	**Time per cell (MIN)**	**Capacity**	**Source**
15000	2341500	1020	100	Alibaba.com [166]
39000	12282000	1020	525	Alibaba.com [167]
950000	150000000	1020	6417	Alibaba.com [168]
210000	480000000	1020	20535	Alibaba.com [169]

A6: Inventory of Material for Cell Production

For mass-scale production of hydrogen laboratory fabrication of cells is scaled up to produce 5 tonnes of hydrogen per day. For this, the cell manufacturing facility is assumed to have an output capacity of 5000 cells per day based on equipment adapted for the process. Depending on the hydrogen production capacity, each photocatalyst type will need a different number of cells to produce the same amount of hydrogen (5 tonnes per day). For example, TNR has lower productivity than CNF: TNR. So, to produce the same amount of hydrogen in a specific given time, the number of cells needed for TNR will be more than CNF: TNR. So, the material needed to produce those cells will vary as well. This inventory of material according to the hydrogen demand is shown in tables from Table 10 to Table 13.

Output: 5 tonnes per day, capacity: 5000 cells per day

Table A14- Material Extraction Inventory for TNR

Process	Material	Amount (Gram/Unit)	Total amount (Tons)	CED (MJ/gram)	Total CED (GJ)
Material for Electrodes	Pt	0.13	1.17	1.03	1201.16
	Ag	0.08	0.71	10.69	7623.79
Material for Cell Body	PVC	0.52	4.48	0.06	273.20
	Glass (PVC Coat)	0.05	0.45	0.06	27.32
					0.00
Ancillary Materials	PTFE	5	43.3	0.11	4845.58
	Water	100	86.5	0.000014	1.25
	KOH	60.5	52.3	0.03	1413.44
Photocatalyst Material	$Ti(C_4H_9O)_4$	0.9	7.4	0.08	552.91
	Acetic Acid	2.6	22.7	0.03	748.84

	FTO	10.0	86.5	0.03	2163.20

Table A15- Material extraction inventory for CNF: TNR

Process	Material	Amount (Gram/Unit)	Total amount (Tons)	CED (MJ/gram)	Total CED (GJ)
Material for Electrodes	Pt	0.13	57.41	1.03	59136.28
	Ag	0.08	35.10	10.69	375338.55
Material for Cell Body	PVC	0.52	220.49	0.061	13450.18
	Glass (PVC Coat)	0.05	22.05	0.061	1345.02
Ancillary Materials	PTFE	5	2130.0	0.11	238560.00
	Water	100	4260.0	0.00001	61.34
	KOH	60.5	2577.3	0.04	69587.10
Photocatalyst Material	$Ti(C_4H_9O)_4$	0.9	363.0	10.69	27221.40
	Acetic Acid	2.6	1117.2	0.03	36867.11
	FTO	10.0	4260.0	0.03	106500.00
	Urea	3.6	1533.60	0.03	42940.80
	NH4F	0.3	127.80	0.03	3450.60
	Citric Acid	1.94	826.44	0.04	31404.72

Table A16- Material extraction inventory for g-C3N4-S

Process	Material	Amount (Gram/Unit)	Total amount (Tons)	CED (MJ/gram)	Total CED (GJ)
Material for Electrodes	Pt	0.13	57.41	1.03	59136.28
	Ag	0.08	35.10	10.69	375338.55
	PVC	0.52	220.49	0.061	13450.18

Material for Cell Body	Glass (PVC Coat)	0.05	22.05	0.061	1345.02
Ancillary Materials	PTFE	5	2130.00	0.11	238560.00
	Water	100	42600.00	0.00001	61.34
	Na_2SO_4	50	21300.00	0.04	849582.45
Photocatalyst Material	Dicyandiamide	2	852.00	0.12	104623.65
	NH4Cl	10	4260.00	0.40	1713123.22
	FTO	10.0	4260.0	0.03	130677.20

Table A17- Material extraction inventory for g-C3N4/BiOI

Process	Material	Amount (Gram/Unit)	Total amount (Tons)	CED (MJ/gram)	Total CED (GJ)
Material for Electrodes	Pt	0.13	57.41	1.03	59136.28
	Ag	0.08	35.10	10.69	375338.55
Material for Cell Body	PVC	0.52	220.49	0.061	13450.18
	Glass (PVC Coat)	0.05	22.05	0.061	1345.02
Ancillary Materials	PTFE	5	2130.00	0.11	238560.00
	Water	100	42600.00	0.00001	61.34
	Na_2SO_4	50	21300.00	0.04	849582.45
Photocatalyst material	Dicyandiamide	2	852.00	0.12	104623.65
	NH_4Cl	10	4260.00	0.40	1713123.22
	Bismuth Nitrate	10.0	4260.00	0.03	130677.20
	Ethylene Glycol	2.2	948.28	0.87	823236.33

	FTO	10.0	4260.00	0.03	130677.20
	KI	5	2130.00	0.83	1781712.44

A7: Fabrication Process Inventory

The fabrication process of the photocatalytic cell is based on system design as shown in S3. Using cycle time for each process, every equipment's energy consumption is calculated for producing 5000 cells per day. The use factor is the percentage of the total power rating that is used by every piece of equipment. This gives the amount of energy consumed. The power consumption is based on the equipment selected from S5 for the 5000 cells per day capacity of the facility.

Table A18- Fabrication process inventory for TNR

Activity	Machine	Power (W)	Number of equipment used	Hours of use	Operating time per day (s)	Electricity use (kWh)
Sonication of FTO glass	Ultrasonic cleaner	7200	1	2	7200	3.8
TiO2 solution preparation and stirring	Stirrer	590	1	8	28800	4.72
Deposition of compact TiO2	Ultrasonic coating system	110000	1	1	1875	57.29166667
Calcination	Heating Oven I	40000	1	4	32400	141.69
Preparation of the hydrothermal (HT) soln	Tank I	-	-		-	-
HT growth	Furnace II	39000	1	3	11755	74.25
Annealing	Furnace III	950000	1	16	16200	3973.05
Testing	Testing table	1200	2	8	64800	43.2

Table A19- Fabrication process inventory for CNF: TNR

Activity	Machine	Power (W)	Number of equipment used	Hours of use	Operating time per day (s)	Electricity use (kWh)
Sonication of FTO glass	Ultrasonic cleaner	7200	1	0.5	1800	0.9

TiO_2 solution preparation and stirring	Stirrer	590	1	1	28800	4.72
Deposition of compact TiO_2	Ultrasonic coating system	120000	1	10	37500	1250
Calcination	Furnace I	950000	1	7	32400	3365.16
Preparation of the hydrothermal (HT) soln	Tank I	-	-		-	-
HT growth & Drying the nanorods	Furnace II	210000	1	3	11755.10204	399.83
Annealing	Furnace III	210000	1	16	16200	878.25
Preparation of CNFQD solids	Gravity Convection Oven	20000	5	24	86400	2068.97
Preparation of CNFQD solution	Centrifuge	6600	5	8	28800	132.00
Testing	Testing table	11000	1		64800	198

Table A20- Fabrication process inventory for g-C3N4-S

Activity	Machine	Power (W)	Number of equipment used	Hours of use	Operating time per day (s)	Electricity use (kWh)
Mixture preparation	Centrifuge	950000	1	12	42281	5578.69
Mixture annealing	Gravity Convection Oven	210000	1	16	57600	2896.55
Testing	Testing table	500	1		64800	9

Table A21- Fabrication process inventory for g-C3N4/BiOI

Activity	Machine	Power (W)	Number of equipment used	Hours of use	Operating time per day (s)	Electricity use (kWh)
Mixture preparation	Centrifuge	950000	1	6	21140.	2789.3
Mixture annealing	Furnace III	210000	1	16	16200	878.2
Ultrasonication of C_3N_4 Mixture	Ultrasonic coating system	3000	3	4	16000	40
Ultrasonication of KI mixture	Ultrasonic coating system	3000	2	3	12000	20
Stirring and mixing	Stirrer	590	1	4	28800	4.72

Annealing of the mixture	Furnace II	210000	1	8	28800	979.5
Testing	Testing table	500	1		64800	9

A8: Panel Assembly (For all cases)

Steel is needed as a structure for panels to rest. Glass cover is needed on the top to protect the panel from some impacts or accidents during operations. The amount requirement was adapted from Sathre et al.[37].

Table A22- Inventory for panel assembly

Material	Amount	Unit	Mass/Panel	Unit	CED(MJ/Kg)	Total CED (MJ)	GHG (g/kg H_2)
Steel Structure	340	kg	340.00	Kg/Panel	37.00	12580.0	1142.4
Glass Cover	207	kg	207.00	Kg/Panel	0.06	12.6	529.92
CED For 1-panel assembly 12592.6 MJ/Panel					**Total**	**12592.627**	**1672.32**

A9: Hydrogen produced per photocatalytic cell considering laboratory and real conditions

Current densities were used from the results of Kumar et al. [25, 26] under no bias condition (no external electricity supply). The current is produced by the area of heterojunction. Multiplying the two gives the current produced in each case. This current is then used to quantify the amount of hydrogen produced under an artificial Solar simulator (AM 1.5G).

When the setup is scaled to a larger photocatalytic cell, the area of heterojunction increases. This results in higher hydrogen production. Now, solar to hydrogen efficiency is assumed to be 10%. When scaled to real Alberta insolation of 4500 MJ/m^2 or 150 W/m^2 [174], we assumed that only

30% of this radiation is utilized by the cell to produce hydrogen. This gives a multiplication factor of 63.5 for scaling up in each case.

Table A23- Hydrogen Production from laboratory conditions

Case	Current Density	Area of Heterojunction	Current =CD* Area	Time	Charge =Q=I*t	Number of moles	Mass of H_2 Produced
Unit	mA/cm^2	cm^2	Ampere	Seconds	Coulomb	n= Q/Zf	g/day
TNR	0.1	14.06	0.0014	3600	5.06	2.62346E-05	0.0013
CNF: TNR-4h	0.36	14.06	0.005	3600	18.22	9.44447E-05	0.0045
g-C3N4-S	0.13	14.06	0.002	3600	6.58	3.4105E-05	0.0016
BiOI/g-C3N4-S	0.39	14.06	0.005	3600	19.74	0.000102315	0.0049

Table A24- Hydrogen production in real conditions by one photocatalytic cell

Photocatalyst	Assumed Efficiency	Input	Output	Output	Output H_2	Number of cells needed for 5 tonnes per day
	%	W/m^2	W/m^2	$J/Day/m^2$	G/Day/Cell	
TNR	0.24	150	0.36	12960	0.11	46296296.30
CNF:TNR-4h	0.4	150	0.6	21600	0.18	27777777.78
g-C3N4-S	0.18	150	0.27	9720	0.08	61728395.06
BiOI/g-C3N4-S	1.2	150	1.8	64800	0.54	9259259.26

Number of electrons, Z= 2, Faraday's constant, F= 96485, Calorific value of H_2= 138 MJ/Kg

Appendix B

B1:A. Flowchart of the synthesis of TNR and CNF: TNR photocatalysts

The flowchart is prepared by adapting the method explained by Kumar et al. [64, 65]. The synthesis of the photocatalysts is used to design the system for the fabrication of photocatalytic cells for mass-scale production.

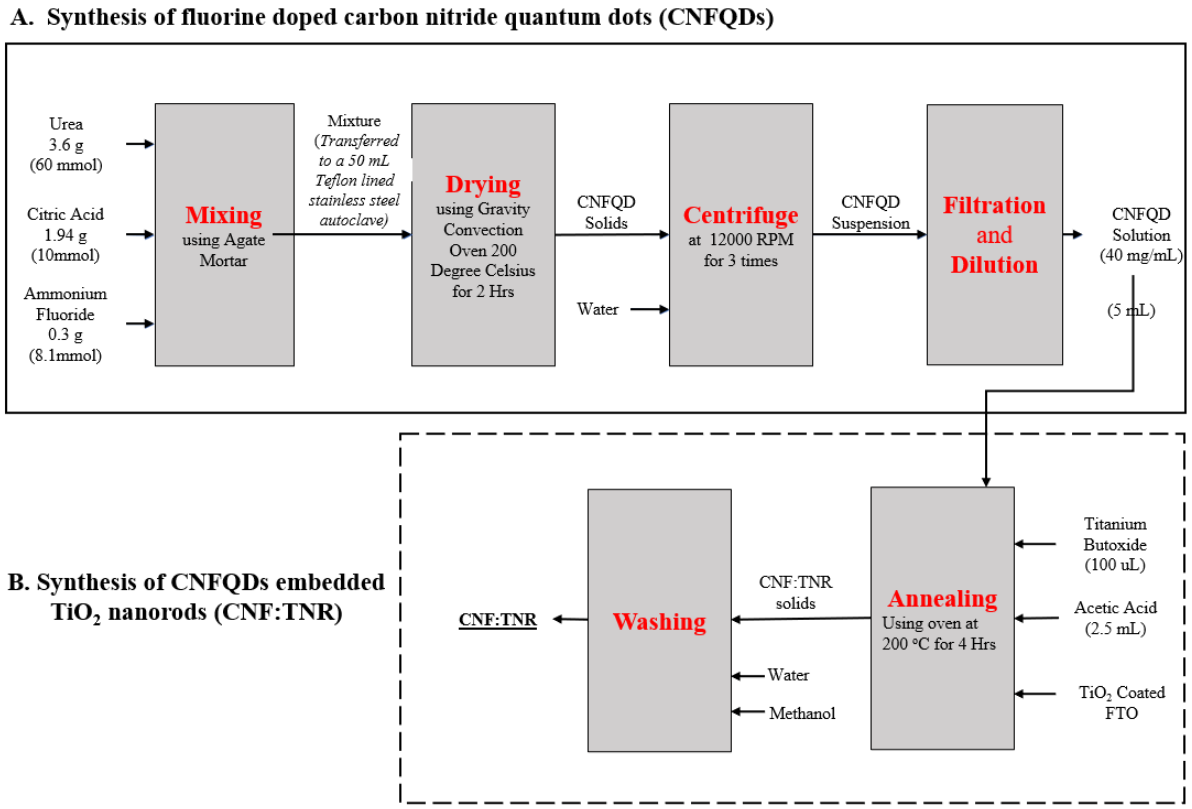

Figure B15: Flowchart of the synthesis of TNR and CNF:TNR

B1:B. Flowchart of the synthesis of g-C_3N_4-S and g-C_3N_4/BiOI photocatalysts

The flowchart is prepared by adapting the method explained by Kumar et al. [64, 65]. The synthesis of the photocatalysts is used to design the system for the fabrication of photocatalytic cells for mass-scale production.

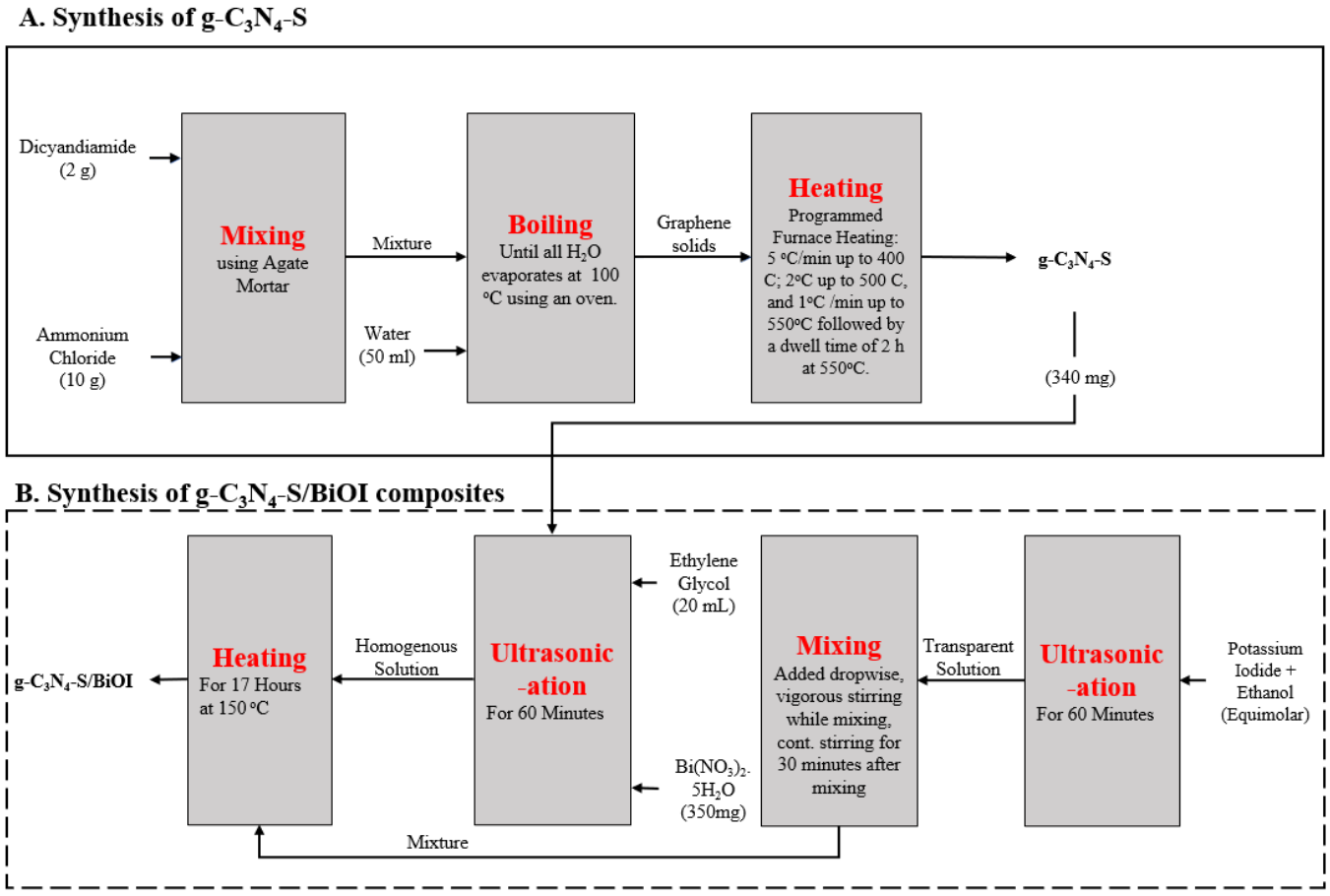

Figure B16- Flowchart of the synthesis of g-C3N4-S and g-C3N4/BiOI

B2: Fabrication and process design

Section S2 lists all the processes required for the fabrication of photocatalysts for mass production. Processes such as stirring and cleaning systems are not critical for the overall system and hence are considered supportive in nature and are in white boxes. Processes such as ultrasonic coating, calcination, and annealing govern the overall production capacity of the facility in terms of cells per day and hence are important to the system. These are part of the critical path of the process. For every process, the critical path is highlighted and the time duration for each activity is given to find the key process in the critical path.

v. Fabrication of TNR

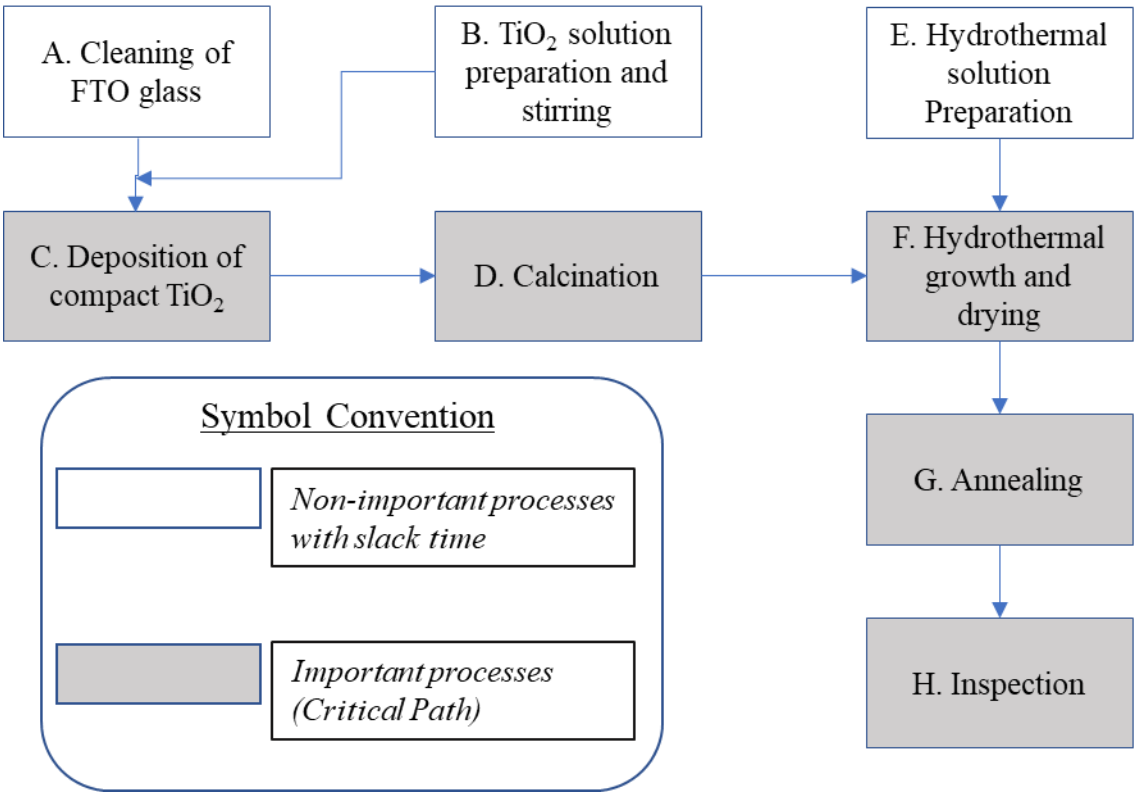

Figure B17- Layout for the process design and fabrication of TNR

Table B25- Process parameter description for TNR

Component series	Component Name	Process Name	Process Duration
A	Ultrasonic cleaning system	Cleaning of FTO glass	30 minutes
B	Stirrer	TiO_2 solution preparation and stirring	8 Hours
C	Ultrasonic coating system	Deposition of compact TiO_2	30 Seconds
D	Large walk-in furnace-I	Calcination	30 Minutes
E	Preparation of hydrothermal solution	Hydrothermal solution preparation	2 Hours
F	Large walk-in furnace-II	Hydrothermal growth and drying	1 Hour
G	Large walk-in furnace-III	Annealing	4 hours
H	Testing table	Inspection	15 Minutes

vi. Fabrication of CNF:TNR

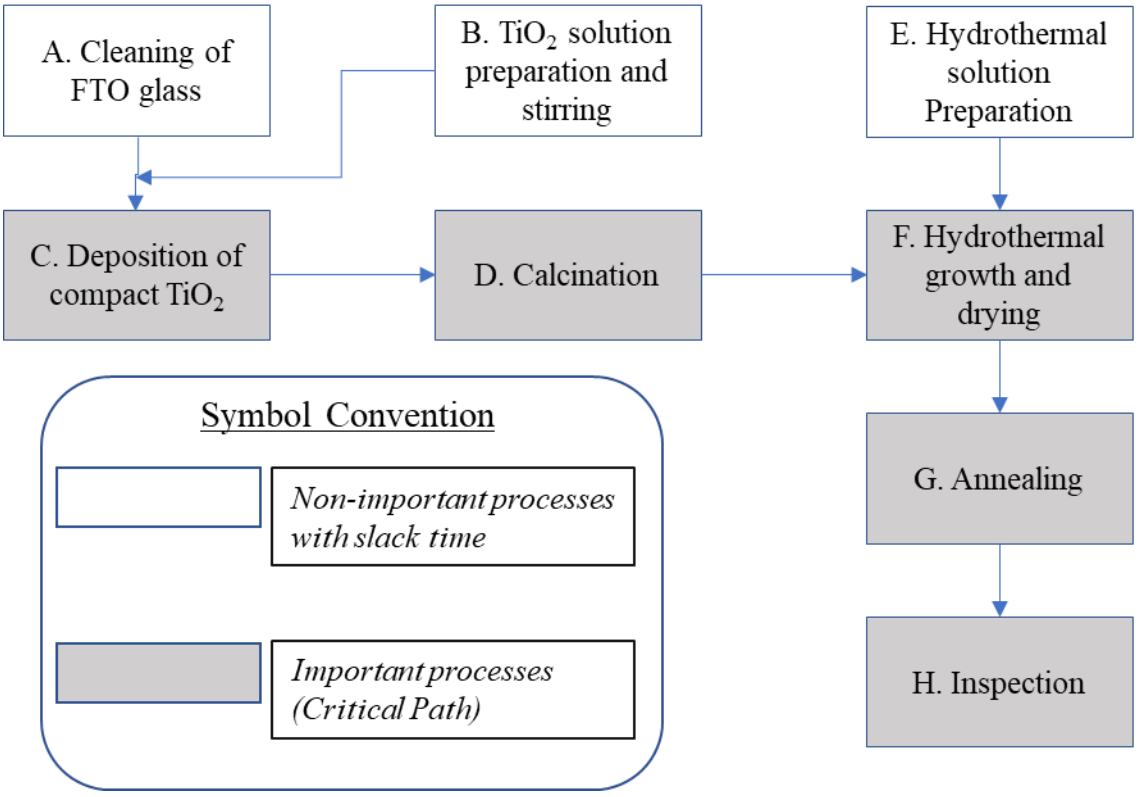

Figure B18- Layout for the process design and fabrication of CNF TNR

Table B26- Process parameter description for CNF: TNR

Component series	Component Name	Process Name	Process Duration
A	Ultrasonic Cleaning System	Cleaning of FTO Glass	30 Minutes
B	Stirrer	TiO_2 solution preparation and stirring	8 Hours
C	Ultrasonic coating system	Deposition of compact TiO_2	30 Seconds
D	Large walk-in furnace-I	Calcination	30 Minutes
E	Preparation of hydrothermal solution	Hydrothermal solution preparation	2 Hours
F	Large walk-in furnace-II	Hydrothermal growth and drying	1 Hour
G	Large walk-in furnace-III	Annealing	4 hours
H	Testing table	Inspection	15 Minutes
I	Gravity convection oven	Carbon nitride mixture preparation	2 Hours
J	Centrifuge	CNFQD suspension preparation	15 Minutes
K	Filtration and dilution	CNFQD solution preparation	2 Hours

vii. Fabrication of g-C_3N_4-Ss

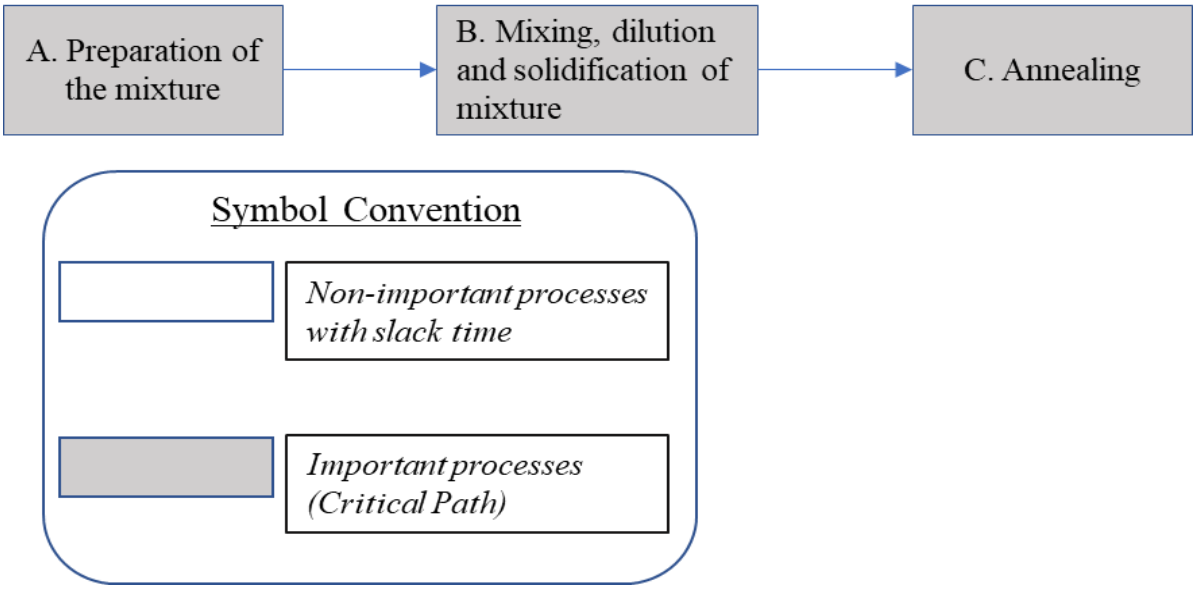

Figure B19- Layout for the process design and fabrication of g-C3N4-S

Table B27- Process parameter description for g-C3N4-Ss

Component series	Component Name	Process Name	Process Duration
A	Agate mortar	Preparation of the mixture	5 Minutes
B	Solidification	Mixing, dilution and solidification of the mixture	15 Minutes
C	Large walk-in furnace	Annealing	5 Hours

viii. Fabrication of g-C_3N_4/BiOI

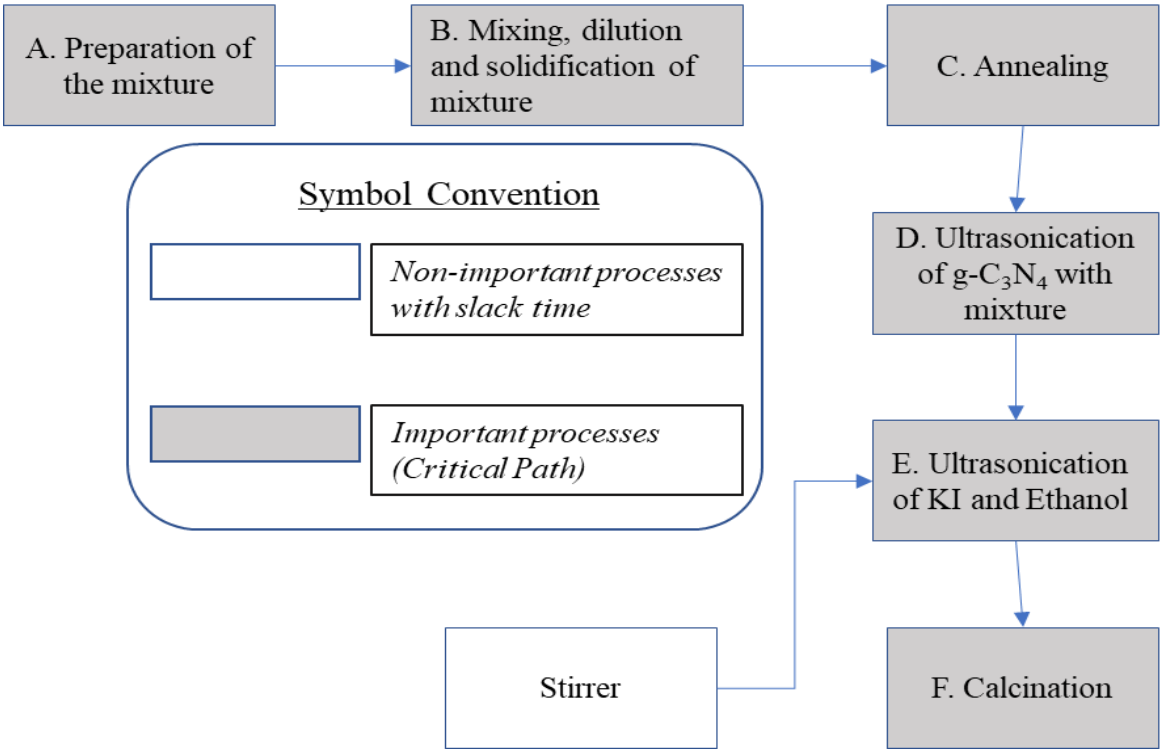

Figure B20- Layout for the process design and fabrication of g-C3N4/BiOI

Table B28- Process parameter description of g-C3N4/BiOI

Component series	Component Name	Process Name	Process Duration
A	Agate Mortar	Preparation of the mixture	5 Minutes
B	Solidification	Mixing, dilution and solidification of the mixture	15 Minutes
C	Large walk-in furnace-I	Annealing	5 Hours
D	Ultrasonication-I	Ultrasonication of g-C_3N_4 with the mixture	1 Hour
E	Ultrasonication-II	Ultrasonication of KI and Ethanol	30 Minutes
F	Stirrer	Mixing the solution	1 Hour
G	Large walk-in furnace-II	Calcination	14 Hours

B3: Equipment sizing

Below is the list of equipment available commercially for unit operations of the system. The power vs capacity relationship clarifies that power and capacity are not linearly dependent. Depending on the number of cells to be produced, appropriate equipment is selected to optimize power consumption. This directly impacts the LCOH. In this study, a facility capacity of 5000 cells per day is assumed. The cycle time for each piece of equipment in overall photocatalyst fabrication is noted. The closest equipment to the capacity of 5000 cells (or more) is selected.

Table B29- Equipment for process design

Applicable to TNRs and CNF: TNR				Process: Spray Coating	
Power (W)	**Volume (cm^3)**	**Time per cell (min)**	**Cost ($/No.)**	**Capacity (No. of cells)**	**Source**
3500	400	0.5	25000	102	Alibaba.com[161]
5000	1750	0.5	50000	448	Alibaba.com [162]
8000	2500	0.5	65000	640	Alibaba.com [163]
11000	3240	0.5	78000	829	Alibaba.com [164]
110000	120000	0.5	300000	30720	Alibaba.com [165]
Applicable to TNRs and CNF: TNR				Process: Calcination (Furnace)	
Power (W)	**Volume (cm^3)**	**Time per cell (min)**	**Cost ($/No.)**	**Capacity (No. of cells)**	**Source**
15000	468300	30	12000	681	Alibaba.com [166]
40000	2456400	30	48000	3573	Alibaba.com [167]
950000	30000000	30	250000	43636	Alibaba.com [168]
210000	57600000	30	400000	83782	Alibaba.com [169]
Applicable to TNRs and CNF: TNR				Process: Drying + HT growth (Furnace)	
Power (W)	**Volume (cm^3)**	**Time per cell (min)**	**Cost ($/No.)**	**Capacity (No. of cells)**	**Source**
15000	468300	60	12000	341	Alibaba.com [166]

39000	2456400	60	48000	1786	Alibaba.com [167]
950000	24000000	60	275000	17455	Alibaba.com [168]
210000	134750000	60	600000	98000	Alibaba.com [169]
Applicable to TNRs and CNF: TNR				Process: Annealing (Furnace)	
Power (W)	**Volume(cm^3)**	**Time per cell (min)**	**Cost ($/No.)**	**Capacity (No. of cells)**	**Source**
15000	468300	240	12000	85	Alibaba.com [166]
39000	2456400	240	48000	447	Alibaba.com [167]
950000	30000000	240	250000	5455	Alibaba.com [168]
210000	134750000	240	550000	24500	Alibaba.com [169]
Applicable to CNF:TNR				Process: Oven Heating (Gravity Convection Oven*)	
Power (W)	**Volume(cm^3)**	**Time per cell (min)**	**Cost ($/No.)**	**Capacity (No. of cells)**	**Source**
15000	3328000	240	25000	4538	Alibaba.com [170]
18000	4032000	240	25650	5498	Alibaba.com [171]
20000	18050000	240	70000	24614	Alibaba.com [172]
**The convection oven can work overnight and hence have a lead of 8 hrs.*					
Applicable to g-C_3N_4-S				Process: Solidification (Furnace)	
Power (W)	**Volume(cm^3)**	**Time per cell (min)**	**Cost ($/No.)**	**Capacity (No. of cells)**	**Source**
15000	468300	15	12000	1362	Alibaba.com [166]
39000	2456400	15	48000	7146	Alibaba.com [167]
950000	30000000	15	250000	87273	Alibaba.com [168]
210000	57600000	15	400000	167564	Alibaba.com [169]
Applicable to g-C_3N_4-S				Process: Annealing (Furnace)	
Power (W)	**Volume(cm^3)**	**Time per cell (min)**	**Cost ($/No.)**	**Capacity (No. of cells)**	**Source**
15000	468300	300	12000	68	Alibaba.com [166]

39000	2456400	300	48000	357	Alibaba.com [167]
950000	30000000	300	250000	4364	Alibaba.com [168]
210000	134750000	300	550000	20533	Alibaba.com [169]
Applicable to g-C_3N_4/BiOI				Process: Ultrasonication of Carbon nitride	
Power (W)	**Volume(cm^3)**	**Time per cell (min)**	**Cost ($/No.)**	**Capacity (No. of cells)**	**Source**
1500	25	60	6000	1800	Alibaba.com [173]
2250	50	60	12000	3600	Alibaba.com [173]
3000	300	60	72000	21600	Alibaba.com [173]
Applicable to g-C_3N_4/BiOI				Process: Ultrasonication of KI+Ethanol	
Power (W)	**Volume(cm^3)**	**Time per cell (min)**	**Cost ($/No.)**	**Capacity (No. of cells)**	**Source**
1500	25	30	8000	2400	Alibaba.com [173]
2250	50	30	16000	4800	Alibaba.com [173]
3000	300	30	96000	28800	Alibaba.com [173]
Applicable to g-C_3N_4/BiOI				Process: Calcination (Furnace)	
Power (W)	**Volume(cm^3)**	**Time per cell (min)**	**Cost ($/No.)**	**Capacity (No. of cells)**	**Source**
15000	2341500	1020	12000	100	Alibaba.com [166]
39000	12282000	1020	48000	525	Alibaba.com [167]
950000	150000000	1020	250000	6417	Alibaba.com [168]
210000	480000000	1020	450000	20535	Alibaba.com [169]

B4: Material cost for cell production

For mass-scale hydrogen production, the laboratory fabrication of cells in this study is scaled up to produce 5 tonnes of hydrogen per day. The cell manufacturing facility is assumed to have an output capacity of 5000 cells per day based on the equipment adapted for the process. Depending on the hydrogen production capacity, each photocatalyst type will need a different number of cells to produce the same amount of hydrogen (5 tonnes per day). For example, TNR has lower productivity than CNF: TNR. So, to produce the same amount of hydrogen in a specific given time, more cells are needed for TNR than for CNF: TNR and the material needed to produce those cells will vary as well.

Output: 5 tonnes per day, capacity: 5000 cells per day

Table B30- Material extraction inventory for TNR

Process	Material	Amount (Gram/Unit)	Total amount (Tons)	Cost (USD/Tonne)	Total cost (USD)
Material for Electrodes	Pt	0.13	1.17	500000	334880.7
	Ag	0.08	0.71	416000	170322.4
Material for Cell Body	PVC	0.52	4.48	1350	3472.4
	Glass (PVC Coat)	0.05	0.45	1350	347.2
Ancillary Materials	PTFE	5	43.3	45450	79052.4
	Water	100	86.5	327	162627.0
	KOH	60.5	52.3	34	10222.3
Photocatalyst Material	$Ti(C_4H_9O)_4$	0.9	7.4	20000	84680.3
	Acetic Acid	2.6	22.7	500	6516.3
	FTO	10.0	86.5	20	993.9

Table B31- Material extraction inventory for CNF:TNR

Process	Material	Amount (Gram/Unit)	Total amount (Tons)	Cost (USD/Tonne)	Total cost (USD)
Material for Electrodes	Pt	0.13	57.41	500000	334880.7
	Ag	0.08	35.10	416000	170322.4
Material for Cell Body	PVC	0.52	220.49	1350	3472.4
	Glass (PVC Coat)	0.05	22.05	1350	347.2
Ancillary Materials	PTFE	5	2130.0	45450	79052.4
	Water	100	4260.0	327	162627.0
	KOH	60.5	2577.3	34	10222.3
Photocatalyst Material	$Ti(C_4H_9O)_4$	0.9	363.0	20000	84680.3
	Acetic Acid	2.6	1117.2	500	6516.3
	FTO	10.0	4260.0	20	993.9
	Urea	3.6	1533.60	320	4007.4
	NH4F	0.3	127.80	51900	54162.6
	Citric Acid	1.94	826.44	3782	25523.1

Table B32- Material extraction inventory for g-C3N4-S

Process	Material	Amount (Gram/Unit)	Total amount (Tons)	Cost (USD/Tonne)	Total cost (USD)
Material for Electrodes	Pt	0.13	57.41	500000	334880.7
	Ag	0.08	35.10	416000	170322.4
Material for Cell Body	PVC	0.52	220.49	1350	3472.4
	Glass (PVC Coat)	0.05	22.05	1350	347.2

Ancillary Materials	PTFE	5	2130.00	45450	79052.4
	Water	100	42600.00	327	162627.0
	Na_2SO_4	50	21300.00	1440	250463.0
Photocatalyst Material	Dicyandiamide	2	852.00	30000	208719.1
	NH4Cl	10	4260.00	624	21706.8
	FTO	10.0	4260.0	20	993.9

Table B33- Material extraction inventory for g-C3N4/BiOI

Process	Material	Amount (Gram/Unit)	Total amount (Tons)	Cost (USD/Tonne)	Total cost (USD)
Material for Electrodes	Pt	0.13	57.41	500000	334880.7
	Ag	0.08	35.10	416000	170322.4
Material for Cell Body	PVC	0.52	220.49	1350	3472.4
	Glass (PVC Coat)	0.05	22.05	1350	347.2
Ancillary Materials	PTFE	5	2130.00	45450	79052.4
	Water	100	42600.00	327	162627.0
	Na_2SO_4	50	21300.00	1440	250463.0
Photocatalyst material	Dicyandiamide	2	852.00	30000	208719.1
	NH_4Cl	10	4260.00	624	21706.8
	Bismuth nitrate	10.0	4260.00	20	993.9
	Ethylene glycol	2.2	948.28	1300	100665.2
	FTO	10.0	4260.00	20	993.9
	KI	5	2130.00	29500	513101.2

B5: Utility cost details

The fabrication process of the photocatalytic cell is based on the system design shown in S3. Using the cycle time for each process, we calculated every piece of equipment's energy consumption in the production of 5000 cells per day. The use factor is the percentage of the total power rating that is used by every piece of equipment. This gives the amount of energy consumed. The power consumption is based on the equipment selected from B3 for the 5000 cells per day capacity of the facility. We used Canadian electricity and natural gas costs for commercial businesses as rates to calculate the cost of use. This is in line with Alberta's average, and the electricity and natural gas prices are $0.09/kWh and $0.016/MJ, respectively [148].

Table B34- Utility cost details for TNR

Activity	Machine	Power (W)	Number of equipment used	Hours of use	Operating time per day (s)	Electricity use (kWh)
Sonication of FTO glass	Ultrasonic cleaner	7200	1	2	7200	3.8
TiO2 solution preparation and stirring	Stirrer	590	1	8	28800	4.72
Deposition of compact TiO2	Ultrasonic coating system	110000	1	1	1875	57.29
Calcination	Heating Oven I	40000	1	4	32400	141.69
Preparation of the hydrothermal (HT) soln	Tank I	-	-		-	-
HT growth	Furnace II	39000	1	3	11755	74.25
Annealing	Furnace III	950000	1	16	16200	3973.05
Testing	Testing table	1200	2	8	64800	43.2

Table B35- Utility cost details for CNF: TNR

Activity	Machine	Power (W)	Number of equipment used	Hours of use	Operating time per day (s)	Electricity use (kWh)
Sonication of FTO glass	Ultrasonic cleaner	7200	1	0.5	1800	0.9

TiO_2 solution preparation and stirring	Stirrer	590	1	1	28800	4.72
Deposition of compact TiO_2	Ultrasonic coating system	120000	1	10	37500	1250
Calcination	Furnace I	950000	1	7	32400	3365.16
Preparation of the hydrothermal (HT) soln	Tank I	-	-		-	-
HT growth & Drying of the nanorods	Furnace II	210000	1	3	11755	399.83
Annealing	Furnace III	210000	1	16	16200	878.25
Preparation of CNFQD solids	Gravity Convection Oven	20000	5	24	86400	2068.97
Preparation of CNFQD solution	Centrifuge	6600	5	8	28800	132.00
Testing	Testing table	11000	1		64800	198

Table B36- Utility cost details for g-C3N4-S

Activity	Machine	Power (W)	Number of equipment used	Hours of use	Operating time per day (s)	Electricity use (kWh)
Mixture preparation	Centrifuge	950000	1	12	42281	5578.69
Mixture annealing	Gravity Convection Oven	210000	1	16	57600	2896.55
Testing	Testing table	500	1		64800	9

Table B37- Utility cost details for g-C3N4/BiOI

Activity	Machine	Power (W)	Number of equipment used	Hours of use	Operating time per day (s)	Electricity use (kWh)
Mixture preparation	Centrifuge	950000	1	6	21140.	2789.3
Mixture annealing	Furnace III	210000	1	16	16200	878.2
Ultrasonication of C_3N_4 Mixture	Ultrasonic coating system	3000	3	4	16000	40
Ultrasonication of KI mixture	Ultrasonic coating system	3000	2	3	12000	20
Stirring and mixing	Stirrer	590	1	4	28800	4.72
Annealing of the mixture	Furnace II	210000	1	8	28800	979.5
Testing	Testing table	500	1		64800	9

B6: A. Calculation for labour cost

Table B38- Labour cost for all four pathways

i. TNR				
Activity	**Equipment/ shift**	**No. of production hours**	**Production hours 1**	**Production hours 2**
		12 - 8 a.m.	8 a.m. - 4 p.m.	4 p.m. - 12 a.m.
Sonication of FTO glass	Ultrasonic cleaner	0.5	0.5	1
TiO_2 solution preparation and stirring	Stirrer	0.5	0.5	0
Deposition of compact TiO_2	Ultrasonic coating system	7.5	7.5	0
Calcination	Furnace I	0	5	5
HT growth & drying of the nanorods	Furnace II	0	5	5
Annealing	Furnace III	0	5	5
Panel assembly	Laminator	0	3	3
Cleaning staff	-	0	2	2
Testing	Testing table	0	2	2
Total number of workers = 62				
Floor manager	1	40000	Project coordinator equivalent - Canada, updated 20th Feb 2020	
Floor supervisor	2	80000	Project coordinator equivalent - Canada, updated 20th Feb 2020	
R & D	1	44000	Research scientist	
Factory manager	1	69,000	Operations manager equivalent	
Shift length (hours)	8			
Labour cost/hour	18	Canadian average		
Total labour cost/day	8928			
Final labour cost	2350460	0.7 factor to convert to USD		
Salaries of engineers/year	0	Already accounted		
The total cost of labour/salaries	**2350460**	**USD/per project**		

ii. CNF: TNR				
Activity	**Equipment/ shift**	**No production hours**	**Production hours 1**	**Production hours 2**
		12 - 8 a.m.	8 a.m. - 4 p.m.	4 p.m. - 12 a.m.
Sonication of FTO glass	Ultrasonic cleaner	0.5	0.5	1
TiO_2 solution preparation and stirring	Stirrer	0.5	0.5	0
Carbon nitride Mixture preparation	Agate Mortar	0	1	0
CNFQD Suspension preparation	Furnace I	1	1	1
CNFQD Solution preparation	Centrifuge	5	5	5
Deposition of compact TiO_2	Ultrasonic coating system	7.5	7.5	0
Calcination	Furnace I	0	5	5
HT growth & Drying of the nanorods	Furnace II	0	5	5
Annealing	Furnace III	0	5	5
Panel Assembly	laminator	0	3	3
Cleaning staff	-	0	2	2
Testing	Testing table	0	2	2
Total number of workers = 81				
Floor Manager	1	40000	Project coordinator equivalent - Canada, updated 20th Feb 2020	
Floor Supervisor	1	40000	Project coordinator equivalent - Canada, updated 20th Feb 2020	
R & D	1	44000	Research Scientist	
Factory Manager	1	69,000	Operations manager equivalent	
Labour cost/ year	2992780	0.7 factor to convert to USD		
Salaries of engineers/year	0	Already accounted		
The total cost of labour/ salaries	**2992780**	**USD/Per project**		
iii. g-C_3N_4-S				

Activity	Equipment/ shift	No production hours	Production hours 1	Production hours 2
		12 - 8 a.m.	8 a.m. - 4 p.m.	4 p.m. - 12 a.m.
Preparation of mixture	Agate Mortar	0	1	0
Solidification of the mixture	Furnace I	0	0.5	0
Annealing of the mixture	Furnace II	0	16	8
Panel Assembly	laminator	0	6	6
Cleaning staff	-	0	2	2
Testing	Testing table	0	2	2
Total number of workers = 45.5				
Floor Manager	1	40000	Project coordinator equivalent - Canada, updated 20th Feb 2020	
Floor Supervisor	2	80000	Project coordinator equivalent - Canada, updated 20th Feb 2020	
R & D	1	44000	Research Scientist	
Factory Manager	1	69,000	Operations manager equivalent	
Labour cost/ year	1768340	0.7 factor to convert to USD		
Salaries of engineers/year	0	Already accounted		
The total cost of labour/ salaries	**1768340**	**USD/Per project**		
iv. BiOI/g-C3N4-S				

Activity	**Equipment/ shift**	**No production hours**	**Production hours 1**	**Production hours 2**
		12 - 8 a.m.	8 a.m. - 4 p.m.	4 p.m. - 12 a.m.
Preparation of mixture	Agate Mortar	0	1	0
Solidification of the mixture	Furnace I	0	1.5	0.75
Annealing of the mixture	Furnace II	0	16	8
Ultrasonication of C_3N_4 Mixture	Ultrasonic coating system	0	2	0
Ultrasonication of KI mixture	Ultrasonic coating system	0	1	1
Stirring and mixing	Stirrer	1	0	0
Annealing of the mixture	Furnace II	1	10	5
Panel Assembly	laminator	0	3	3
Cleaning staff	-	0	2	2
Testing	Testing table	0	2	2
Total number of workers = 62.25				
Floor Manager	1	40000	Project coordinator equivalent - Canada, updated 20th Feb 2020	
Floor Supervisor	2	80000	Project coordinator equivalent - Canada, updated 20th Feb 2020	
R & D	1	44000	Research Scientist	
Factory Manager	1	69,000	Operations manager equivalent	
Labour cost/ year	2359280	0.7 factor to convert to USD		
Salaries of engineers/year	0	Already accounted		
The total cost of labour/ salaries	**2359280**	**USD/Per project**		

B6: B. Calculation for building (facility) cost

Table B39- Building costs for all four pathways.

i.	TNR			
Sl. No	**Equipment**	**Floor space (cm or m)**	**Area (m^2)**	**Comments / Reference**
1	Ultrasonic cleaner	200 x 100 cm	6	See section S3.
2	Stirrer	32.5 x 21.5 cm	0.14	See section S3.
3	Ultrasonic coating system	3 x 10 x 20 m	600	See section S3.
4	Walk-in furnace I	12 x 1.15 x1.78 m	25	See section S3.
5	Walk-in furnace II	12 x 1.15 x 1.78 m	25	See section S3.
6	Furnace III	50 x 3 x 2 m	300	See section S3.
7	Testing table	3 x 3 x 10 m	90	See section S3.
8	Washrooms	3 x 500 x 300 cm	45	Exceeds 25 employees; 2 toilets for the same gender and 1 if the other sex is also employed as per Canadian standards [175]
9	Dining area		15	Estimate
10	Change rooms		15	Estimate
11	Office & Storage		50	Estimate
	Total floorspace (excluding 8,9,10,11)		1045.27	m^2
	Overall floor space		3260.80	m^2
	Building cost/m^2		376.6	US$/ m^2
	Total building cost		1228018.7	US$
	Depreciation period		20	years
	Maintenance		6140.09	USD/year
	Depreciation amount per year		61400.9	USD/year
	Total building rent per year		**67541.03**	**$/year**

ii.	CNF: TNR			
Sl. No	**Equipment**	**Floor space**	**Area (m^2)**	**Reference**
1	Ultrasonic cleaner	200 x 100 cm	6	See section S3.
2	Stirrer	32.5 x 21.5 cm	0.14	See section S3.
3	Ultrasonic coating system	3 x 10 x 20 m	600	See section S3.
4	Walk-in furnace I	12 x 1.15 x1.78 m	25	See section S3.
5	Walk-in furnace II	12 x 1.15 x 1.78 m	25	See section S3.
6	Furnace III	50 x 3 x 2 m	300	See section S3.
7	Gravity convection oven	2.4 x 1.72 x 3.02	12.47	See section S3.
8	Suspension Preparation	4000 cm^3	2.00	See section S3.
9	Testing table	3 x 3 x 10	90	See section S3.
10	Washrooms	3 x 500 x 300 cm	45	Exceeds 25 employees; 2 toilets for the same gender and 1 if the other sex is also employed as per Canadian standards [175]
11	Dining area		15	Estimate
12	Change rooms		15	Estimate
13	Office & Storage		50	Estimate
	Total floor space (excluding 10,11,12,13)		1059.73	m^2
	Overall floor space		3304.20	m^2
	Building cost/m^2		376.6	US$/ m^2
	Total building cost		1244363.106	US$
	Depreciation period		20	years
	Maintenance		6221.8	USD/year
	Depreciation amount per year		62218.1	USD/year
	Total building rent per year		**68439.9**	**$/year**

iii.	$g\text{-}C_3N_4$			
Sl. No	**Equipment**	**Floor space**	**Area (m^2)**	**Reference**
1	Centrifuge	2 x 1.05 x 2.23	4.683	See section S3.
2	Gravity convection heater	50 x 3 x 2	300.00	See section S3.
3	Testing table	3 x 3 x 10	90	See section S3.
4	Washrooms	3 x 500 x 300 cm	45	exceeds 25 employees, 2 toilets for the same gender and 1 if the other sex is also employed as per Canadian standards [175]
5	Dining area		15	Estimate
6	Change rooms		15	Estimate
7	Office & Storage		50	Estimate
	Total floorspace (excluding 4,5,6,7)		394.7	m^2
	Overall floor space		1309.0	m^2
	Building cost/m^2		376.6	US$/ m^2
	Total building cost		492987.9	US$
	Depreciation period		20.0	years
	Maintenance		2464.9	USD/year
	Depreciation amount per year		24649.4	USD/year
	Total building rent per year		**27114.3**	**$/year**

iv.	$BiOI$ / $g\text{-}C_3N_4$-S			
Sl. No	**Equipment**	**Floor space**	**Area (m^2)**	**Reference**
1	Centrifuge	2 x 1.05 x 2.23	4.7	See section S3.

2	Gravity convection heater	50 x 3 x 2	300.0	See section S3.
3	Ultrasonic coating system	5	15.0	See section S3.
4	Ultrasonic coating system	5	5.0	See section S3.
5	Stirrer	32.5 x 21.5 cm	0.1	See section S3.
6	Furnace	50 x 3 x 2	300.0	See section S3.
7	Testing table	3 x 3 x 10	90.0	Equipment details
8	Washrooms	3 x 500 x 300 cm	45.0	exceeds 25 employees, 2 toilets for same-gender and 1 if the other sex is also employed as per Canadian standards [175]
9	Dining area		15.0	Estimate
10	Change rooms		15.0	Estimate
11	Office & Storage		50.0	Estimate
	Total floorspace (excluding 8,9,10,11)		714.8	m^2
	Overall floor space		2269.5	m^2
	Building cost/m^2	376.6	376.6	US$/ m^2
	Total building cost		854682.0	US$
	Depreciation period		20.0	years
	Maintenance		4273.4	USD/year
	Depreciation amount per year		42734.1	USD/year
	Total building rent per year		**47007.51**	**$/year**

B7: Hydrogen produced per photocatalytic cell considering laboratory and real conditions

Kumar et al.'s current densities were used [25, 26] under no bias condition (no external electricity supply). The current is produced by the area of heterojunction. Multiplying the two gives the current produced in each case. This current is then used to quantify the amount of hydrogen produced under an artificial solar simulator (AM 1.5G).

When the setup is scaled to a larger photocatalytic cell, the area of heterojunction increases. This results in higher hydrogen production. Now, solar to hydrogen efficiency is assumed to be 0.2 to 1.2%. When scaled to real Alberta insolation of 4500 MJ/m^2 or 150 W/m^2 [174].

Table B40.1- Hydrogen production from laboratory conditions

Case	Current density	Area of heterojunction	Current = CD*area	Time	Charge = Q = I*t	Number of moles	Mass of H_2 produced
Unit	mA/cm^2	cm^2	Ampere	Seconds	Coulomb	n= Q/Zf	g/day
TNR	0.1	14.06	0.0014	3600	5.06	2.62346E-05	0.0013
CNF: TNR-4h	0.36	14.06	0.005	3600	18.22	9.44447E-05	0.0045
g-C3N4-S	0.13	14.06	0.002	3600	6.58	3.4105E-05	0.0016
BiOI/g-C3N4-S	0.39	14.06	0.005	3600	19.74	0.000102315	0.0049

Table B17.2- Hydrogen production in real conditions by one photocatalytic cell

Photocatalyst	Assumed Efficiency	Input	Output	Output	Output H_2	Number of cells needed for 5 tonnes per day	Area Needed for the facility
	%	W/m^2	W/m^2	J/Day/m^2	G/Day/Cell		km^2
TNR	0.24	150	0.36	12960	0.11	46296296.30	60.2
CNF:TNR-4h	0.4	150	0.6	21600	0.18	27777777.78	36.1
g-C3N4-S	0.18	150	0.27	9720	0.08	61728395.06	80.2
BiOI/g-C3N4-S	1.2	150	1.8	64800	0.54	9259259.26	12.0

Number of electrons (Z) = 2, Faraday's constant (F) = 96485, H_2 CV value: 138 MJ/Kg

B8: Hydrogen operating facility costs

Steel is needed as a structure for panels to rest on. Aluminum is needed to connect the components in the frame. and Glass cover and polystyrene are needed on the top to protect the panel from impacts or accidents during operation. The amount needed for each was adapted from Sathre et al. [37].

1. Cost of panel installation material

Table B18- Inventory for panel assembly

Material	Amount/m^2	Unit	Amount/panel	Unit	Cost	$/panel
Aluminum	0.8	kg	5.43	kg/panel	13.58	13.58
Steel frame	1.5	kg	10.19	kg/panel	5.09	5.09
Polystyrene	0.133	kg	0.90	kg/panel	0.63	0.63
Glass	0.32	kg	2.17	kg/panel	1.74	1.74

2. Cost of panel acquisition (production)

	Value	Unit/Remark
Cost per panel	146	$/panel (from cash flow analysis)
Number of panels to be installed	7822	TNR
	2173	CNF: TNR-4h
	6017	g-C3N4-S
	2006	BiOI/g-C3N4-S
Capital cost for panels (USD)	864500	TNR
	268984	CNF: TNR-4h
	796362	g-C3N4-S
	340329	BiOI/g-C3N4-S

Table B41- Panel acquisition cost

2. Cost of panel installation

After panel fabrication, it needs to be placed in a particular direction for operation. Since these panels are very similar to solar panels, we derived the installation cost from the solar panel installation cost.

Table B42- Panel installation cost

	Value	Unit	Remarks
Cost of fabrication	1.034	0.77 for converting AUD to USD	[176]
Cost of installation	1.435	USD	[177]
Ratio (installation: fabr.)	0.4		

Hence cost of installation	345800	USD	TNR
	107593	USD	CNF: TNR
	318545	USD	g-C3N4-S
	136132	USD	g-C3N4-S/BiOI

3. Cost of supplies

Table 43- Cost of supplies in the hydrogen production field

	Capacity	**Unit**	**No.**	**Cost**	**Total**		**Remarks**
Pumps (H_2O)	100	hp	5	10000	50000	USD	[118]
Vacuum Pump (H_2+O_2)	650	RPM	5	*6254*	31270	USD	[119]
Compressor	75	HP	2.5	50000	125000	USD	[120]
Pipes (including installation)	3911	m	1	15	58667	USD	TNR
	1086	m	1	15	16296	USD	CNF: TNR
	3009	m	1	15	45129	USD	g-C3N4-S
	1003	m	1	15	15043	USD	g-C3N4-S/BiOI
The average life span of pumps and compressors is 15 years, which is the same as the life of the facility, so no replacement is included.							
Total fixed supply cost		264937	USD		TNR		
		222566	USD		CNF: TNR		
		251399	USD		g-C3N4-S		
		221313	USD		g-C3N4-S/BiOI		
Recurring cost							
Cost of operation of all equipment	720	HP	536760	Watts	319737	USD/ year	
Maintenance	10% of fixed cost				340364	USD/ year	

4. Cost of land

Table B44- Cost of land for the hydrogen production facility

	Rate	376.6	US$/m^2		
Area of facility	0.5	km^2	1988468	USD	TNR
	0.1	km^2	552352	USD	CNF: TNR
	0.4	km^2	1529591	USD	g-C3N4-S
	0.1	km^2	509864	USD	g-C3N4-S/BiOI
Fixed aggregated cost	3463706	USD	TNR		
	1151496	USD	CNF: TNR		
	2895896	USD	g-C3N4-S		
	1207637	USD	g-C3N4-S/BiOI		
Recurring cost	340364	USD/year			